On the use of car observations to evaluate and improve road weather forecasting

Geophysical Institute,
University of Bergen

Henrik Larsen
Supervisor: Thomas Spengler

Thesis for Masters degree (MSc)
at the University of Bergen

2023

Contents

1 Introduction **1**

2 Method **4**
2.1 Instruments 4
2.1.1 InterMet iMet-XQ2 4
2.1.2 S+S Regeltechnik HTF 100 Pt100 4
2.2 Variability testing 4
2.2.1 Sensitivity to car speed and position of instrument 6
2.3 Car Measurements for model comparisons and variability while driving . 9
2.4 External Data 11
2.4.1 Netatmo data 11
2.4.2 Model data 11
2.5 Statistics 13

3 Variability testing **15**
3.1 Static variability 15
3.1.1 Sheltered sensors 15
3.1.2 Exposed sensors 17
3.2 Car-mounted sensor variability 18
3.2.1 Stationary heating 18
3.2.2 Acceleration and movement 19
3.2.3 Variability while driving 21

4 Model Comparison **24**
4.1 Analysis 24
4.1.1 Haugesund 28.09.2022 22:00 UTC 24
4.1.2 Haugesund 29.09.2022 04:00 UTC 26
4.1.3 Haugesund 29.09.2022 10:00 UTC 27
4.1.4 Haugesund 29.09.2022 16:00 UTC 29
4.1.5 Haugesund 18.11.2022 23:00 UTC 30
4.1.6 Haugesund statistics 32
4.1.7 Bergen 20.01.2023 23:00 UTC 34
4.1.8 Bergen 21.01.2023 11:00 UTC 35
4.1.9 Bergen 26.01.2023 23:00 UTC 36
4.1.10 Bergen 27.02.2023 11:00 UTC 38
4.1.11 Bergen 27.02.2023 23:00 UTC 39
4.1.12 Bergen 28.02.2023 11:00 UTC 41
4.1.13 Bergen 28.02.2023 23:00 UTC 42
4.1.14 Bergen 01.03.2023 11:00 UTC 44
4.1.15 Bergen 01.03.2023 23:00 UTC 45
4.1.16 Bergen statistics 47
4.2 Forecast validation 51
4.2.1 Haugesund forecasts for 28.09.2022 22:00 UTC 51

4.2.2 Haugesund Forecasts for 29.09.2022 10:00 UTC 54
4.2.3 Forecast Results Haugesund 58
4.2.4 Forecasts for Bergen 20.01.2023 23:00 UTC 64
4.2.5 Forecasts for Bergen 21.01.2023 11:00 UTC 67
4.2.6 Forecast Results Bergen 71

5 Discussion **79**
5.1 Benchmarking 79
5.2 Analysis 79
5.3 Forecast 80
5.4 Future use of RWS and observation products 81

6 Summary and Conclusion **84**

List of Figures

1.1 Example forecast by the Roadsurf model, driving difficulty displayed as traffic light colors (*Kangas et al.*, 2015) . . . 1
1.2 Map overview of official and Netatmo weather stations in the UK (*Coney et al.*, 2022), main colorbar indicating number of stations per $20km^2$, and secondary mini-colorbar showing population . . . 3

2.1 Boxed instrument setup on the GFI tower's roof, with iMets placed inside the junction box . . . 5
2.2 Garden instrument setup in front of the GFI, iMets on the fence, and reference instrument on the mast behind, this is an example, with the same setup as the benchmark, but fewer iMets . . . 5
2.3 Map of the northern section of the NAF practice facility, blue route: 10km/h-30km/h, red route:40km/h-50km/h, ref: (*Google Inc*, n.d.a) . . . 6
2.4 Instrument mounts used at NAF practice facility, left: iMet mounted on the roof rack, right: iMet mounted on the bottom . . . 8
2.5 Instrument mounts used at the proof of concept trial and roof mount for main runs for the Haugesund route, left: car overview, top right: roof mount, bottom right: iMet mounted on bottom . . . 8
2.6 Trial route around Northern Karmøy, starting/stopping at Gunnarshaug South buss stop (*Google Inc*, n.d.b) . . . 9
2.7 Main car observation routes, left: Haugesund-Haukås-Aksdal ref: (*Google Inc*, n.d.b), right:Bergen-Northern Os ref: (*Google Inc*, n.d.c) . . . 10
2.8 Data assimilation flow chart for AROME-MetCoOp, by *Müller et al.* (2017), illustrating the surface and upper-air data assimilation process to obtain the analysis. . . . 11
2.9 Illustration of the processes calculated by the SURFEX model (*CNRM*, 2023) . . . 12

3.1 Temperature variability between the iMets compared to the reference temperature for 07.09.2022, top: temperature in $°C$, bottom: temperature anomaly between iMets and reference in $°C$ . . . 15
3.2 Temperature variability between the iMets compared to the reference temperature for 12.11.2022, top: temperature in $°C$, bottom: temperature anomaly between iMets and ensemble in $°C$ . . . 16
3.3 Temperature variability between the iMets compared to the reference PT100 sensor for 16.09.2022, top: temperature [$°C$], bottom: temperature anomaly between iMets and PT100 [$°C$] . . . 17
3.4 Test runs for the temperature variability of car-mounted iMets, instruments mounted on the roof and near the bottom of the car, including asphalt and gravel ground materials. . . . 18
3.5 Average temperature variability ensembles for different surfaces and mount points . . . 19

3.6 Shows the temperature evolution on the roof while the vehicle accelerates from a standstill, with temperature in the top plot and speed in the lower plot. . . . 20
3.7 Shows the temperature evolution on the shaded lower front while the vehicle accelerates from a standstill, with temperature in the top plot and speed in the lower plot. . . . 20
3.8 Spatial temperature plots for day and nighttime trial runs, including roof and engine went mount points, top row: roof measurements, daytime on the left, and nighttime on the right, bottom row, intake vent measurements same layout as the top row. Observations from 29.09.2022. . . . 21
3.9 Time series comparison of roof mounting and lower engine vent mounting for day and evening conditions, 29.09.2022 . . . 23

4.1 Model bias from iMet(points) and Netatmo(triangles) to the MEPS 1km post-processed model (left), and MEPS 2,5km model (right), represented by mesh grids over a map tile, Netatmo observations are averaged by grid cell, time: 28.09.2022 22Z. Map tiles by Stamen Design, under CC BY 3.0. Data by OpenStreetMap, under ODbL. . . . 25
4.2 Model bias from iMet(points) and Netatmo(triangles) to the MEPS 1km post-processed model (left), and MEPS 2,5km model (right), represented by mesh grids over a map tile, observations are averaged by grid cell, time: 28.09.2022 22Z. Map tiles by Stamen Design, under CC BY 3.0. Data by OpenStreetMap, under ODbL. . . . 25
4.3 Model bias from iMet(points) and Netatmo(triangles) to the MEPS 1km post-processed model (left), and MEPS 2,5km model (right), represented by mesh grids over a map tile, Netatmo observations are averaged by grid cell, time: 29.09.2022 04Z. Map tiles by Stamen Design, under CC BY 3.0. Data by OpenStreetMap, under ODbL. . . . 26
4.4 Model bias from iMet(points) and Netatmo(triangles) to the MEPS 1km post-processed model (left), and MEPS 2,5km model (right), represented by mesh grids over a map tile, observations are averaged by grid cell, time: 29.09.2022 04Z. Map tiles by Stamen Design, under CC BY 3.0. Data by OpenStreetMap, under ODbL. . . . 27
4.5 Model bias from iMet(points) and Netatmo(triangles) to the MEPS 1km post-processed model (left), and MEPS 2,5km model (right), represented by mesh grids over a map tile, Netatmo observations are averaged by grid cell, time: 29.09.2022 10Z. Map tiles by Stamen Design, under CC BY 3.0. Data by OpenStreetMap, under ODbL. . . . 28
4.6 Model bias from iMet(points) and Netatmo(triangles) to the MEPS 1km post-processed model (left), and MEPS 2,5km model (right), represented by mesh grids over a map tile, observations are averaged by grid cell, time: 29.09.2022 10Z. Map tiles by Stamen Design, under CC BY 3.0. Data by OpenStreetMap, under ODbL. . . . 28
4.7 Model bias from iMet(points) and Netatmo(triangles) to the MEPS 1km post-processed model (left), and MEPS 2,5km model (right), represented by mesh grids over a map tile, Netatmo observations are averaged by grid cell, time: 29.09.2022 16Z. Map tiles by Stamen Design, under CC BY 3.0. Data by OpenStreetMap, under ODbL. . . . 29
4.8 Model bias from iMet(points) and Netatmo(triangles) to the MEPS 1km post-processed model (left), and MEPS 2,5km model (right), represented by mesh grids over a map tile, observations are averaged by grid cell, time: 29.09.2022 16Z. Map tiles by Stamen Design, under CC BY 3.0. Data by OpenStreetMap, under ODbL. . . . 30

4.9 Model bias from iMet(points) and Netatmo(triangles) to the MEPS 1km post-processed model (left), and MEPS 2,5km model (right), represented by mesh grids over a map tile, Netatmo observations are averaged by grid cell, time: 18.11.2022 23Z. Map tiles by Stamen Design, under CC BY 3.0. Data by OpenStreetMap, under ODbL 31
4.10 Model bias from iMet(points) and Netatmo(triangles) to the MEPS 1km post-processed model (left), and MEPS 2,5km model (right), represented by mesh grids over a map tile, observations are averaged by grid cell, time: 18.11.2022 23Z. Map tiles by Stamen Design, under CC BY 3.0. Data by OpenStreetMap, under ODbL 31
4.11 Model bias from iMet(points) and Netatmo(triangles) to the MEPS 1km post-processed model (left), and MEPS 2,5km model (right), represented by mesh grids over a map tile, Netatmo observations are averaged by grid cell, time: 20.01.2023 23Z. Map tiles by Stamen Design, under CC BY 3.0. Data by OpenStreetMap, under ODbL. 34
4.12 Model bias from iMet(points) and Netatmo(triangles) to the MEPS 1km post-processed model (left), and MEPS 2,5km model (right), represented by mesh grids over a map tile, all observations are averaged by grid cell, time: 20.01.2023 23Z. Map tiles by Stamen Design, under CC BY 3.0. Data by OpenStreetMap, under ODbL. 35
4.13 Model bias from iMet(points) and Netatmo(triangles) to the MEPS 1km post-processed model (left), and MEPS 2,5km model (right), represented by mesh grids over a map tile, Netatmo observations are averaged by grid cell, time: 21.01.2023 11Z. Map tiles by Stamen Design, under CC BY 3.0. Data by OpenStreetMap, under ODbL. 35
4.14 Model bias from iMet(points) and Netatmo(triangles) to the MEPS 1km post-processed model (left), and MEPS 2,5km model (right), represented by mesh grids over a map tile, all observations are averaged by grid cell, time: 21.01.2023 11Z. Map tiles by Stamen Design, under CC BY 3.0. Data by OpenStreetMap, under ODbL. 36
4.15 Model bias from iMet(points) and Netatmo(triangles) to the MEPS 1km post-processed model (left), and MEPS 2,5km model (right), represented by mesh grids over a map tile, Netatmo observations are averaged by grid cell, time: 26.01.2023 23Z. Map tiles by Stamen Design, under CC BY 3.0. Data by OpenStreetMap, under ODbL. 37
4.16 Model bias from iMet(points) and Netatmo(triangles) to the MEPS 1km post-processed model (left), and MEPS 2,5km model (right), represented by mesh grids over a map tile, all observations are averaged by grid cell, time: 26.01.2023 23Z. Map tiles by Stamen Design, under CC BY 3.0. Data by OpenStreetMap, under ODbL. 37
4.17 Model bias from iMet(points) and Netatmo(triangles) to the MEPS 1km post-processed model (left), and MEPS 2,5km model (right), represented by mesh grids over a map tile, Netatmo observations are averaged by grid cell, time: 27.02.2023 11Z. Map tiles by Stamen Design, under CC BY 3.0. Data by OpenStreetMap, under ODbL. 38
4.18 Model bias from iMet(points) and Netatmo(triangles) to the MEPS 1km post-processed model (left), and MEPS 2,5km model (right), represented by mesh grids over a map tile, all observations are averaged by grid cell, time: 27.02.2023 11Z. Map tiles by Stamen Design, under CC BY 3.0. Data by OpenStreetMap, under ODbL. 39
4.19 Model bias from iMet(points) and Netatmo(triangles) to the MEPS 1km post-processed model (left), and MEPS 2,5km model (right), represented by mesh grids over a map tile, Netatmo observations are averaged by grid cell, time: 27.02.2023 23Z. Map tiles by Stamen Design, under CC BY 3.0. Data by OpenStreetMap, under ODbL. 40

4.20 Model bias from iMet(points) and Netatmo(triangles) to the MEPS 1km post-processed model (left), and MEPS 2,5km model (right), represented by mesh grids over a map tile, all observations are averaged by grid cell, time: 27.02.2023 23Z. Map tiles by Stamen Design, under CC BY 3.0. Data by OpenStreetMap, under ODbL. 40
4.21 Model bias from iMet(points) and Netatmo(triangles) to the MEPS 1km post-processed model (left), and MEPS 2,5km model (right), represented by mesh grids over a map tile, Netatmo observations are averaged by grid cell, time: 28.02.2023 11Z. Map tiles by Stamen Design, under CC BY 3.0. Data by OpenStreetMap, under ODbL. 41
4.22 Model bias from iMet(points) and Netatmo(triangles) to the MEPS 1km post-processed model (left), and MEPS 2,5km model (right), represented by mesh grids over a map tile, all observations are averaged by grid cell, time: 28.02.2023 11Z. Map tiles by Stamen Design, under CC BY 3.0. Data by OpenStreetMap, under ODbL. 42
4.23 Model bias from iMet(points) and Netatmo(triangles) to the MEPS 1km post-processed model (left), and MEPS 2,5km model (right), represented by mesh grids over a map tile, Netatmo observations are averaged by grid cell, time: 28.02.2023 23Z. Map tiles by Stamen Design, under CC BY 3.0. Data by OpenStreetMap, under ODbL. 43
4.24 Model bias from iMet(points) and Netatmo(triangles) to the MEPS 1km post-processed model (left), and MEPS 2,5km model (right), represented by mesh grids over a map tile, All observations are averaged by grid cell, time: 28.02.2023 23Z. Map tiles by Stamen Design, under CC BY 3.0. Data by OpenStreetMap, under ODbL. 43
4.25 Model bias from iMet(points) and Netatmo(triangles) to the MEPS 1km post-processed model (left), and MEPS 2,5km model (right), represented by mesh grids over a map tile, Netatmo observations are averaged by grid cell, time: 01.03.2023 11Z. Map tiles by Stamen Design, under CC BY 3.0. Data by OpenStreetMap, under ODbL. 44
4.26 Model bias from iMet(points) and Netatmo(triangles) to the MEPS 1km post-processed model (left), and MEPS 2,5km model (right), represented by mesh grids over a map tile, all observations are averaged by grid cell, time: 01.03.2023 11Z. Map tiles by Stamen Design, under CC BY 3.0. Data by OpenStreetMap, under ODbL. 45
4.27 Model bias from iMet(points) and Netatmo(triangles) to the MEPS 1km post-processed model (left), and MEPS 2,5km model (right), represented by mesh grids over a map tile, Netatmo observations are averaged by grid cell, time: 01.03.2023 23Z. Map tiles by Stamen Design, under CC BY 3.0. Data by OpenStreetMap, under ODbL. 46
4.28 Model bias from iMet(points) and Netatmo(triangles) to the MEPS 1km post-processed model (left), and MEPS 2,5km model (right), represented by mesh grids over a map tile, all observations are averaged by grid cell, time: 01.03.2023 23Z. Map tiles by Stamen Design, under CC BY 3.0. Data by OpenStreetMap, under ODbL. 46
4.29 Model bias from iMet(points) and Netatmo(triangles) to the MEPS 1km post-processed model (left), and MEPS 2,5km model (right), represented by mesh grids over a map tile, observations are averaged by grid cell, time: 28.09.2022 18Z+4H. Map tiles by Stamen Design, under CC BY 3.0. Data by OpenStreetMap, under ODbL. 51
4.30 Model bias from iMet(points) and Netatmo(triangles) to the MEPS 1km post-processed model (left), and MEPS 2,5km model (right), represented by mesh grid over a map tile, observations are averaged by grid cell, time: 28.09.2022 12Z+10H. Map tiles by Stamen Design, under CC BY 3.0. Data by OpenStreetMap, under ODbL. 52

4.31 Model bias from iMet(points) and Netatmo(triangles) to the MEPS 1km post-processed model (left), and MEPS 2,5km model (right), represented by mesh grid over a map tile, observations are averaged by grid cell, time: 28.09.2022 06Z+16H. Map tiles by Stamen Design, under CC BY 3.0. Data by OpenStreetMap, under ODbL. 53
4.32 Model bias from iMet(points) and Netatmo(triangles) to the MEPS 1km post-processed model (left), and MEPS 2,5km model (right), represented by mesh grid over a map tile, observations are averaged by grid cell, time: 28.09.2022 00Z+22H. Map tiles by Stamen Design, under CC BY 3.0. Data by OpenStreetMap, under ODbL. 54
4.33 Model bias from iMet(points) and Netatmo(triangles) to the MEPS 1km post-processed model (left), and MEPS 2,5km model (right), represented by mesh grid over a map tile, observations are averaged by grid cell, time: 29.09.2022 06Z+4H. Map tiles by Stamen Design, under CC BY 3.0. Data by OpenStreetMap, under ODbL. 55
4.34 Model bias from iMet(points) and Netatmo(triangles) to the MEPS 1km post-processed model (left), and MEPS 2,5km model (right), represented by mesh grid over a map tile, observations are averaged by grid cell, time: 29.09.2022 00Z+10H. Map tiles by Stamen Design, under CC BY 3.0. Data by OpenStreetMap, under ODbL. 56
4.35 Model bias from iMet(points) and Netatmo(triangles) to the MEPS 1km post-processed model (left), and MEPS 2,5km model (right), represented by mesh grid over a map tile, observations are averaged by grid cell, time: 28.09.2022 18Z+16H. Map tiles by Stamen Design, under CC BY 3.0. Data by OpenStreetMap, under ODbL. 57
4.36 Model bias from iMet(points) and Netatmo(triangles) to the MEPS 1km post-processed model (left), and MEPS 2,5km model (right), represented by mesh grid over a map tile, observations are averaged by grid cell, time: 28.09.2022 12Z+22H. Map tiles by Stamen Design, under CC BY 3.0. Data by OpenStreetMap, under ODbL. 58
4.37 Model bias from iMet(points) and Netatmo(triangles) to the MEPS 1km post-processed model (left), and MEPS 2,5km model (right), represented by mesh grids over a map tile, observations are averaged by grid cell, time: 20.01.2023 18Z+5H. Map tiles by Stamen Design, under CC BY 3.0. Data by OpenStreetMap, under ODbL. 64
4.38 Model bias from iMet(points) and Netatmo(triangles) to the MEPS 1km post-processed model (left), and MEPS 2,5km model (right), represented by mesh grids over a map tile, observations are averaged by grid cell, time: 20.01.2023 12Z+11H. Map tiles by Stamen Design, under CC BY 3.0. Data by OpenStreetMap, under ODbL. 65
4.39 Model bias from iMet(points) and Netatmo(triangles) to the MEPS 1km post-processed model (left), and MEPS 2,5km model (right), represented by mesh grids over a map tile, observations are averaged by grid cell, time: 20.01.2023 6Z+17H. Map tiles by Stamen Design, under CC BY 3.0. Data by OpenStreetMap, under ODbL. 66

4.40 Model bias from iMet(points) and Netatmo(triangles) to the MEPS 1km post-processed model (left), and MEPS 2,5km model (right), represented by mesh grids over a map tile, observations are averaged by grid cell, time: 20.01.2023 00Z+23H. Map tiles by Stamen Design, under CC BY 3.0. Data by OpenStreetMap, under ODbL. 67
4.41 Model bias from iMet(points) and Netatmo(triangles) to the MEPS 1km post-processed model (left), and MEPS 2,5km model (right), represented by mesh grids over a map tile, observations are averaged by grid cell, time: 21.01.2023 06Z+5H. Map tiles by Stamen Design, under CC BY 3.0. Data by OpenStreetMap, under ODbL. 68
4.42 Model bias from iMet(points) and Netatmo(triangles) to the MEPS 1km post-processed model (left), and MEPS 2,5km model (right), represented by mesh grids over a map tile, observations are averaged by grid cell, time: 21.01.2023 00Z+11H. Map tiles by Stamen Design, under CC BY 3.0. Data by OpenStreetMap, under ODbL. 69
4.43 Model bias from iMet(points) and Netatmo(triangles) to the MEPS 1km post-processed model (left), and MEPS 2,5km model (right), represented by mesh grids over a map tile, observations are averaged by grid cell, time: 20.01.2023 18Z+17H. Map tiles by Stamen Design, under CC BY 3.0. Data by OpenStreetMap, under ODbL. 70
4.44 Model bias from iMet(points) and Netatmo(triangles) to the MEPS 1km post-processed model (left), and MEPS 2,5km model (right), represented by mesh grids over a map tile, observations are averaged by grid cell, time: 20.01.2023 12Z+23H. Map tiles by Stamen Design, under CC BY 3.0. Data by OpenStreetMap, under ODbL. 71

5.1 Snapshot from Vegær (RWF), green dots are observation stations, the color over the roads is the estimated temperature with red corresponding to $10°C$ or higher, temperature ranges are divided into 7-degree intervals for values between $-10°C$ and $10 \circ C$, precise values for each section is given if click on *Statens Vegvesen* (2022). 82

1 Introduction

Roads serve as the fundamental infrastructure for modern logistics and transportation, facilitating essential daily commutes and the efficient delivery of goods and services (*Nurmi et al.*, 2013). However, adverse weather conditions, including snow, rain, ice, and wind, often affect them, causing delays and accidents (*El Faouzi et al.*, 2010). Road weather forecasting (RWF) has the potential to mitigate these problems by providing timely weather information and prediction (*Kangas et al.*, 2015). An accurate RWF product would be of great societal value as it could lower road maintenance costs during winter by employing preventative measures (*Karsisto et al.*, 2017).

RWF (Road Weather Forecast) is a forecast product that provides information on the variables that affect road conditions, such as temperature, precipitation, and the chance of frost (*Kangas et al.*, 2015). RWF is based on numerical weather prediction models and observational data and has been proven effective by several surveys through historical road weather data comparisons (*Karsisto and Lovén*, 2019) (*Karsisto et al.*, 2017). The models are designed to help road users and authorities make informed decisions about road safety and enable preventative maintenance to reduce the risk of accidents (*Kangas et al.*, 2015). Figure 1.1 shows an example forecast produced by the Roadsurf model (*Kangas et al.*, 2015).

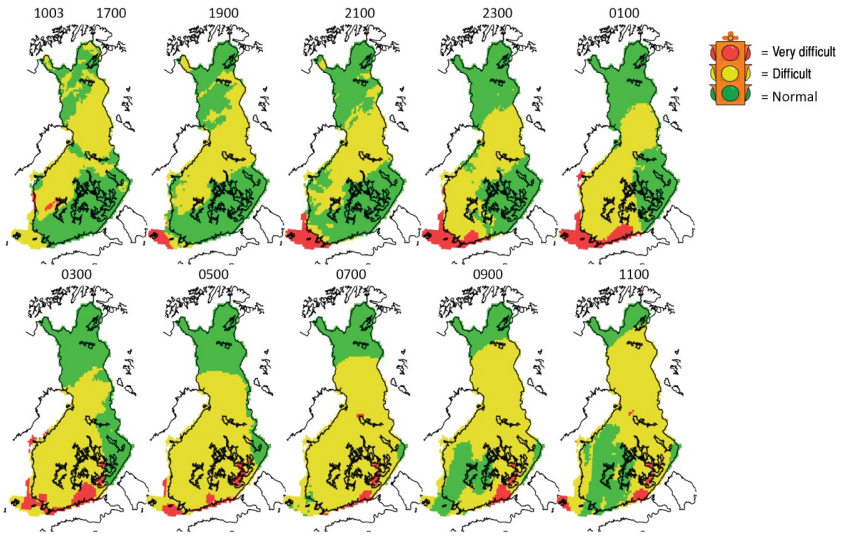

Figure 1.1: Example forecast by the Roadsurf model, driving difficulty displayed as traffic light colors (Kangas et al., 2015)

Road weather models (RWM) are often one-dimensional and are traditionally designed to run for singular locations, resulting in less computationally demanding models, that can be run in a more timely manner (*Kangas et al.*, 2015). However, relying on model results from single stations can be unreliable if the results are used to cover larger areas, as variations in road type and traffic amount can have a major impact on local conditions (*Kangas et al.*, 2015). Some newer RWMs have the capability to be run over several points, or even entire countries, such as the RoadSurf model developed

by the Finnish Meteorological Institute (*Kangas et al.*, 2015). Examples of operational RWF models can be found in several countries, notably, countries that are affected by freezing conditions during winter, such as the Netherlands with the RWM model from the Royal Netherlands Meteorological Institute (*Karsisto et al.*, 2017), and the METRo model used in Canada (*Crevier and Delage*, 2001).

The importance of RWMs and RWFs cannot be understated as there are surveys detailing the correlation between accidents on the road and poor driving conditions (*Nurmi et al.*, 2013). The availability of reliable forecasts could reduce the risk of accidents by informing the public about dangerous conditions, enabling people to make informed decisions when accessing the driving conditions. Additionally, it is much cheaper to deploy preventative measures like salt before it freezes, as it takes significantly more salt to melt the ice if it is already formed (*Karsisto et al.*, 2017). Likewise, there is a large potential for savings by adopting route-based forecasting, as it could make it easier to distinguish which routes need salting, as some sections of road are more liable to freezing conditions than others (*Chapman and Thornes*, 2011).

Road conditions are strongly impacted by local variations such as changes in topography, vegetation, traffic, and nearby man-made structures(*Bell et al.*, 2022). These variations can be found at scales that are unresolved in typical NWP or road weather models, as microscale variations require denser observation networks to capture and are computationally demanding to model, requiring higher horizontal model resolutions for the processes to be resolved (*Chapman and Thornes*, 2011). Even with spatially and temporally dense observation, there is still an issue of representability, as temperatures can vary significantly across a few meters of the roadway (*Chapman and Thornes*, 2011).

Increasing the number of observations can help to resolve small-scale temperature differences, but expanding the official observation networks can be expensive (*Hintz et al.*, 2019). Crowdsourced data provides a possible solution to this problem, opening several new avenues for opportunistic data collection, including private weather stations, car observations, bus observation, and indirect measurements like phone battery temperature (*Hintz et al.*, 2019) & (*Bell et al.*, 2022). While data sources like private weather stations and vehicular observations are of lower quality they can still be useful given proper quality control during the data assimilation, especially for areas with few or no official weather stations (*Nipen et al.*, 2020).

This new source of data is especially useful for post-processing of the NWP and creating nowcasts, as post-processing often relies on observation from official weather stations, which tends to be limited, especially considering high-resolution model grids of 2.5km or lower (*Nipen et al.*, 2020). Post-processing can be used to improve the output of the NWP model, enabling corrections for known biases, integration of updated observations, and even downscaling of the base model output to include more detail in the forecast (*Müller et al.*, 2017). An example of station coverage in the UK is shown in fig 1.2, where there is a distinct difference between official station coverage and Netatmo station coverage, particularly in densely populated areas.

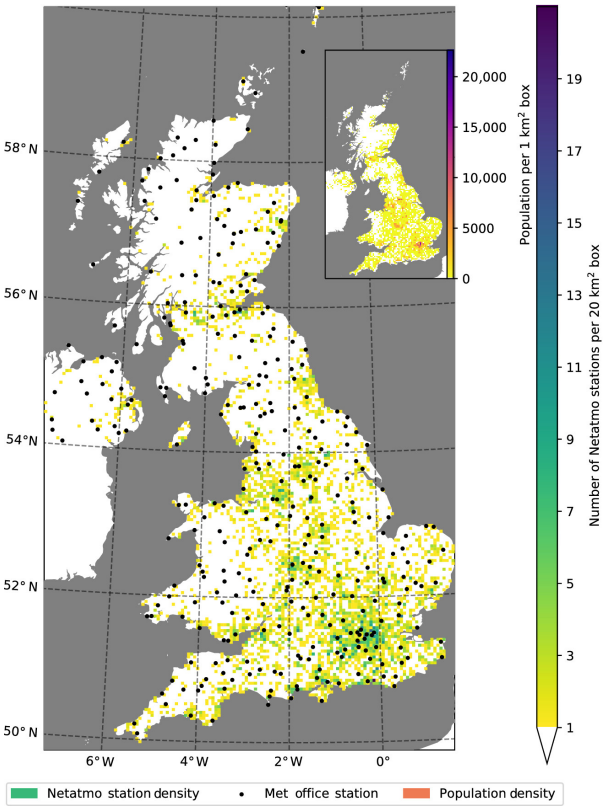

Figure 1.2: Map overview of official and Netatmo weather stations in the UK (Coney et al., 2022), main colorbar indicating number of stations per $20km^2$*, and secondary mini-colorbar showing population*

In this thesis, I will investigate the performance of the operational forecast model AROME-MetCoOp (*Müller et al.*, 2017) across two regions in Norway and assess the use of car observations in reference to the model, and Netatmo weather stations (*Netatmo*). Both the stock 2.5km model and the post-processed 1.0km model supplied by the Norwegian Meteorological Institute (Met Norway) will be evaluated. The comparison between the car observations and Netatmo observations will investigate whether these private stations are representable for road conditions. Finally, I will investigate the usefulness of spatially and/or temporally dense observations for use in RWF, and nowcasting products.

2 Method

2.1 Instruments

2.1.1 InterMet iMet-XQ2

The InterMet iMet-XQ2 (iMet) is a battery-powered lightweight temperature, humidity, and pressure sensor with a GPS receiver designed to be used on drones. It features a five-hour battery and storage for 15 hours of operation using a sampling rate of 1hz, battery, and storage capacity depending on sampling frequency. Temperature is measured through an exposed bead transistor resulting in a fast 1-second response time, but making it highly vulnerable to damage by moisture, as the circuitry is exposed. Specifications are listed below in table 2.1

Table 2.1: Excerpt from manufacturers specifications for iMet-XQ2 (InterMet International Met Systems, 2021)

Operating parameters		**Temperature Sensor**		**GPS**	
Battery life	5-6 hours	Type	Bead thermistor	Type	Ublox CAM-M8
Data storage	16Mb Flash Memory	Range	-90 to 50 C	Vertical accuracy	12m
Data transfer	USB	Response Time	1s at 5m/s flow	Response Time	1s
Sampling Rate	1hz	Accuracy	±0.3 degC		
Size/weight	126x58, 60g	Resolution	0.01degC		

2.1.2 S+S Regeltechnik HTF 100 Pt100

The S+S Regeltechnik HTF 100 Pt100 is a temperature sensor used on the ITAS automatic weather station in the Met-Garden by the Geophysical Institute (*UiB*, 2016). It is a reliable high-resolution temperature sensor set to sample at 1hz, with data exported once per hour. The instrument is covered by a sun screen to reduce the heating effect of insolation.

Table 2.2: Specifications for S+S Regeltechnik HTF 100 Pt100 temperature sensor (UiB, 2016)

Meassurement	**Range**	**Resolution**	**accuracy**	**Unit**
Air temperature	-50 to 180	0.1	N/A	[$^{\circ}C$]

2.2 Variability testing

One in an insulated box, out of direct sunlight and wind, and the other exposed to the elements. The boxed setup was tested on the roof of the tower at the Geophysical Institute (GFI) at the University of Bergen (UiB). The exposed test setup occurred in front of the GFI (Met-garden), with the sensors zip-tied to the fence (fig:2.2), while the rooftop sensors were placed in an instrument junction box (fig: 2.1).

Instruments were left running for 4-5 hours, or until they ran out of battery, depending on the specific device, as some had been modified with larger batteries. The sampling frequency was set to 1hz for all tests. Due to high sampling frequency and large datasets,

the static variability data, collected at the GFI, was resampled to 60 seconds through a rolling mean to match the frequency of the comparative instruments.

This line of testing allowed us to determine the bias and precision of the portable sensors (iMets), both in terms of how they related to each other and environmental factors such as wind and changes in cloud cover. Additionally, the boxed experiment was retested later to investigate sensor drift over time.

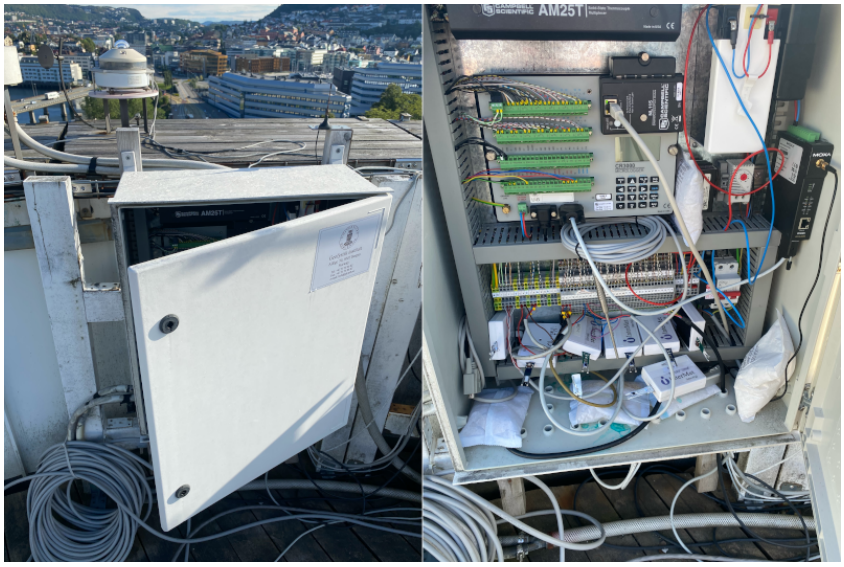

Figure 2.1: Boxed instrument setup on the GFI tower's roof, with iMets placed inside the junction box

Figure 2.2: Garden instrument setup in front of the GFI, iMets on the fence, and reference instrument on the mast behind, this is an example, with the same setup as the benchmark, but fewer iMets

2.2.1 Sensitivity to car speed and position of instrument

We performed tests to assess the impact of instrument placement and how they were affected by insolation, stationary, acceleration, and movement, as well as different surface materials. The tests were split between two cars, one white and the other dark blue. Due to availability, most trials were conducted on the latter.

Due to limitations posed by the instrument and time limitations, the testing is centered around daytime testing, focusing on sunny conditions. The effect of heating during short-term stops was tested by driving around a circuit, taking a one-minute stop between each lap, and simulating the impact of a short traffic stop. Laps were divided into speed brackets (10km/h, 20km/h,30km/h,40km/h, and 50km/h), with each speed bracket being tested five times. All brackets were tested at the NAF practice circuit at Sotra. Due to occupancy and traffic, the 10-30km/h brackets and 40-50km/h brackets were tested on different circuit parts. The different paths are shown in figure 2.3, with the blue track used for the 10km/h-30km/h and the red used for the 40km/h-50km/h tests.

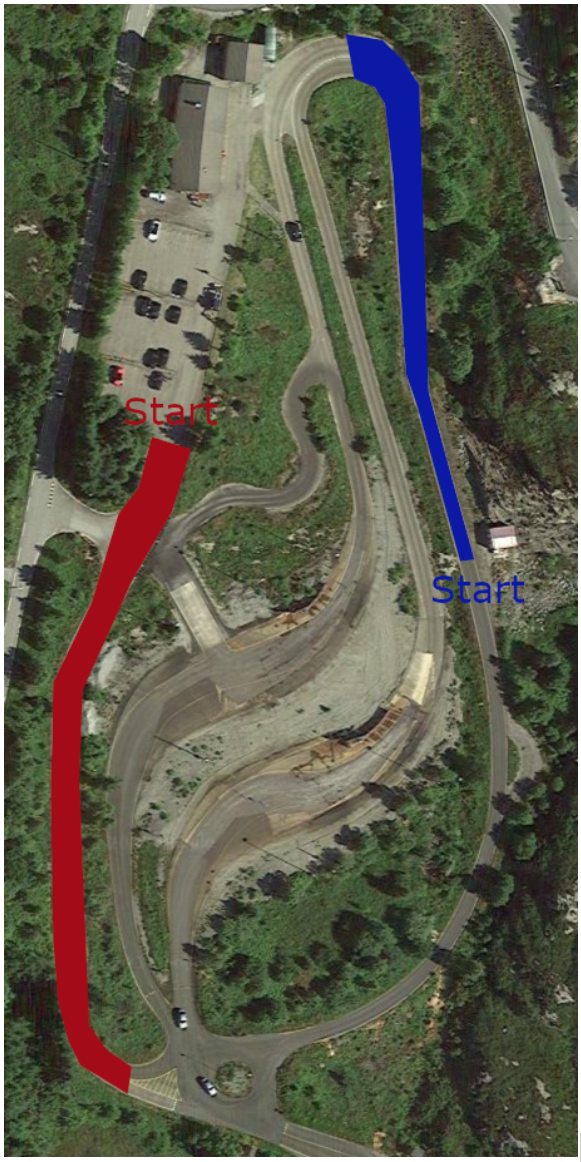

[H]

Figure 2.3: Map of the northern section of the NAF practice facility, blue route: 10km/h-30km/h, red route:40km/h-50km/h, ref: (Google Inc, n.d.a)

The 10-30km/h brackets were tested on a shorter stretch of the circuit, with short stops on a dark gravel patch next to the road between the runs, while the 40-50km/h brackets had a short on an asphalt surface.

Two iMets were used for the experiment, one mounted on a roof rack, referred to as roof, and the other near the bottom of the car on the lower engine intake, referred to as bottom. Mounting points are shown in figure 2.4

The sensitivity to the surface and movement tests, from the NAF practice circuit at Sotra, kept their native sampling frequency due to their shorter run times. The nature of the tests and surrounding traffic made it impractical to rely on lap times, especially considering there was no place to stop at the end of the testing areas. The sensitivity and movement test at the NAF circuit

utilized the geodetic distance derived from the Haversine formula to estimate speed from changes in longitude, latitude, and time, combined with spatial boundaries to identify the lap times.

$$a = \sin^2\left(\frac{\Delta\phi}{2}\right) + \cos(\phi_1) \cdot \cos(\phi_2) \cdot \sin^2\left(\frac{\Delta\lambda}{2}\right) \tag{2.1}$$

$$c = 2 \cdot \text{atan2}\left(\sqrt{a}, \sqrt{1-a}\right) \tag{2.2}$$

$$d = R \cdot c \tag{2.3}$$

where $\Delta\phi$ and $\Delta\lambda$ are the change in latitude and longitude, ϕ_1 and ϕ_2 are the latitudes of starting and end position, R is the radius of the earth, a is the haversine of the angular separation between the points, c is the angular distance in radians, and d is the final distance between the two points on the surface of the sphere.

Each lap was set to start when acceleration was detected, however, due to inaccuracy in the GPS signal resulting in short erroneous accelerations when stationary, filtering was needed. A simple clipping filter was used to set every value below 1 km/h to zero, while a Hampel filter was used to remove larger outliers, caused by larger jumps in the GPS location.

$$M_j = \text{median}_j(x_j) \tag{2.4}$$

$$MAD_j = \text{median}_j\left(|x_j - M_j|\right) \tag{2.5}$$

$$y_i = \begin{cases} x_i & \text{if } |x_i - M_j| \leq k \times MAD_j \\ M_j & \text{otherwise} \end{cases} \tag{2.6}$$

where y_i is the filtered value of the ith data point in the time series, x_i is the original value of the ith data point, $median_j(x_j)$ is the median value of the data points within the window centered at the jth data point, and $MAD_j(x_j)$ is the median absolute deviation of the data points within the window centered at the jth data point. The k is a tuning parameter determining the threshold for outlier detection and is set to 3, to remove outliers larger than 1 km/h while the vehicle is stationary, and outliers caused by drifting of the GPS signal while moving. The resulting speed, time, and coordinates were used as lap limiters and identifiers.

Figure 2.4: Instrument mounts used at NAF practice facility, left: iMet mounted on the roof rack, right: iMet mounted on the bottom

Figure 2.5: Instrument mounts used at the proof of concept trial and roof mount for main runs for the Haugesund route, left: car overview, top right: roof mount, bottom right: iMet mounted on bottom

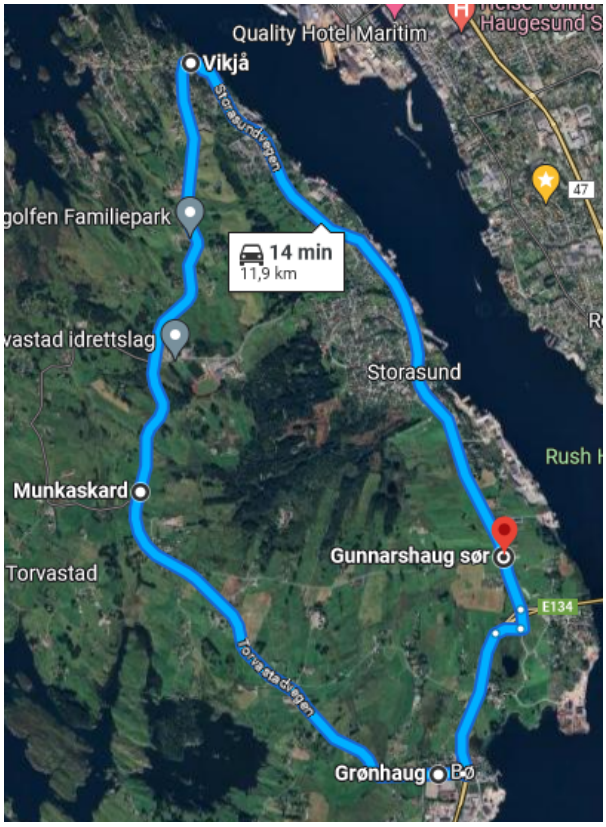

Figure 2.6: Trial route around Northern Karmøy, starting/stopping at Gunnarshaug South buss stop (Google Inc, n.d.b)

2.3 Car Measurements for model comparisons and variability while driving

First, there was a proof of concept trial including two iMets using the white car with the configuration above (fig: 2.5), driving around a short loop of Northern Karmøy (approximately 20 minutes), with tests including both daytime and late evening measurements. The route is shown in fig 2.6. Data gathering for the primary datasets was conducted along two routes. The first route was a loop between Haugesund-Haukås-Aksdal and the second between Bergen and Northern Os along the old E-39 (fig: 2.7).

The first route was tested in a six-hourly fashion for 24 hours, each run taking approximately one hour, with an extra midnight run driven later. While the Bergen route was driven in a twelve-hourly manner, each run took around 30 minutes. Each route is depicted in fig 2.7, with driving times in table 2.3.

Rooftop instruments collect all data gathered on these routes due to roadway moisture concerns and results from the trial run. Additionally, all runs in the Haugesund were performed in a white car, while runs in the Bergen region used a dark blue car.

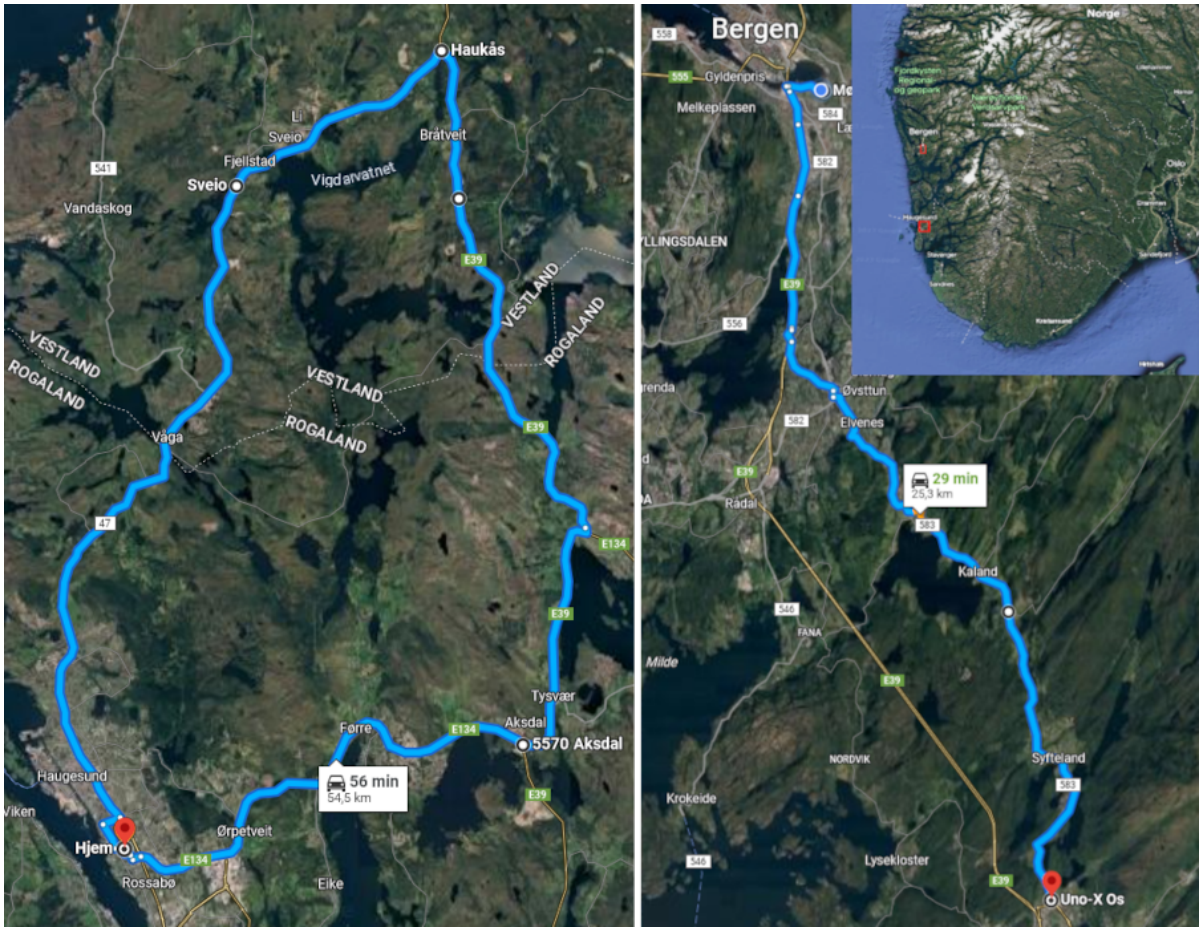

Figure 2.7: Main car observation routes, left: Haugesund-Haukås-Aksdal ref: (Google Inc, n.d.b), right:Bergen-Northern Os ref: (Google Inc, n.d.c)

Table 2.3: Driving times for main routes depicted in fig2.7, all times in UTC

Location	Date	Start	Stop	Duration
Haugesund	28.09.2022	22:00	23:00	60 min
Haugesund	29.09.2022	04:00	4:57	57 min
Haugesund	29.09.2022	10:00	10:56	56 min
Haugesund	29.09.2022	16:00	16:57	57 min
Haugesund	18.11.2022	23:00	23:55	55 min
Bergen	20.01.2023	23:00	23:33	33 min
Bergen	21.01.2023	11:00	11:32	32 min
Bergen	26.01.2023	23:00	23:32	32 min
Bergen	27.02.2023	11:00	11:33	33 min
Bergen	27.02.2023	23:00	23:32	32 min
Bergen	28.02.2023	11:00	11:32	32 min
Bergen	28.02.2023	23:00	23:32	32 min
Bergen	01.03.2023	11:00	11:33	33 min
Bergen	01.03.2023	23:00	23:32	32 min

2.4 External Data

2.4.1 Netatmo data

The project was granted access to Netatmo observations through Met-Norway, for the areas and timeslots of the car runs. Netatmo weather stations are small privately owned weather stations commonly found in residential areas(*Netatmo*). The stations are connected to the internet and can provide real-time weather monitoring to their users, including temperature, humidity, wind, and precipitation (*Netatmo*). Additionally, Met-Norway integrates Netatmo data into the observation product used in the post-processing for the 1.0km model ((*Nipen et al.*, 2020)), providing spatially dense observations in densely populated areas. As a result, they also make for an interesting comparison to car observations, as official RWS are few and far between, providing a poor basis for comparison.

2.4.2 Model data

AROME-MetCoOp is a high-resolution NWP model with a 2.5km horizontal resolution, utilizing an ensemble prediction system (*Müller et al.*, 2017). The model was originally a cooperative effort between the Norwegian Meteorological Institute (Met Norway) and the Swedish Meteorological Institute and Hydrological Institute (*Müller et al.*, 2017) but has been joined by several other countries including Finland and Denmark (*Meteorologisk Institutt*, n.d.). The model is built on the French AROME model and optimized for the Nordic regions, with 6-hourly forecasts for the main cycle updating atmospheric and land surface variables at (00,06,12,18 UTC) producing a 66-hour forecast, and intermediate cycles at (03,09,15,21 UTC) producing a shorter three-hour forecast (*Müller et al.*, 2017).

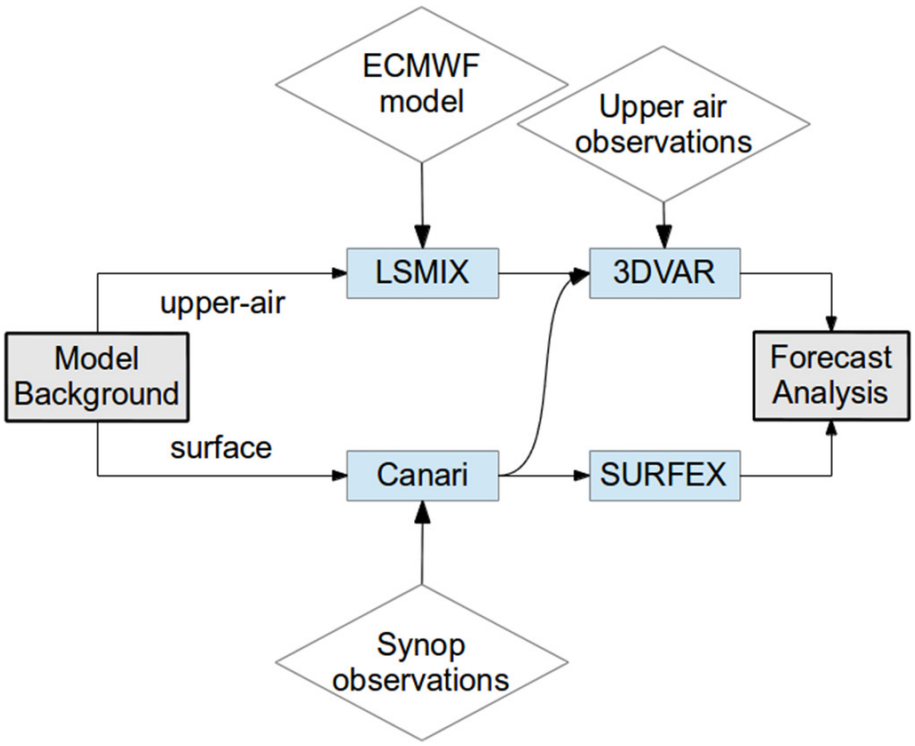

Figure 2.8: Data assimilation flow chart for AROME-MetCoOp, by Müller et al. (2017), illustrating the surface and upper-air data assimilation process to obtain the analysis.

The surface model uses the SURFEX model for atmosphere-surface and surface-soil interactions (fig: 2.9), where all surface processes are described as one-dimensional processes (*Müller et al.*, 2017) & (*CNRM*, 2023). ECOCLIMAP2 is used to define the land surface parameters, initializing soil, vegetation, and atmosphere transfer schemes(*Müller et al.*, 2017). Surface data assimilation is performed by CANARI (Code d'Analyze Nécessaire à ARPEGE pour ses Rejets et son Initialization), using two-meter temperature and relative humidty to adjust surface temperature, soil temperature, and moisture fields, by use of optimal interpolation (*Müller et al.*, 2017). T_{2m} and RH_{2m} is supplied by the regional observation networks.

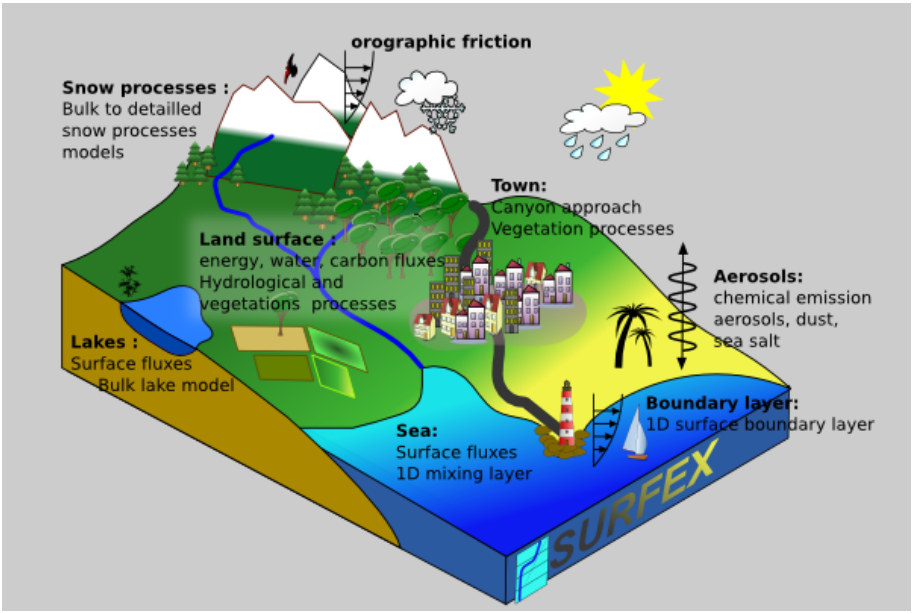

Figure 2.9: Illustration of the processes calculated by the SURFEX model (CNRM, 2023)

The upper-air data assimilation uses the mixing of large-scale information (LSMIX) (*Müller et al.*, 2017) from the european center for medium range forecasting integrated forecasting system (ECMWF-IFS), and 3DVAR data assimilation (*Müller et al.*, 2017), which calculates errors from a previous forecast run and compares the data to observations identifying differences and creates a cost function. Initial conditions are iteratively adjusted to minimize the cost function, giving the analysis, which represents the best estimate of the atmospheric conditions (*Fisher*, 2001). The assimilation process for surface and upper-air assimilations is illustrated in figure 2.8.

Met Norway utilizes a modified version of the MEPS 2.5km model that downscales the control run temperature to a 1km horizontal resolution and applies bias corrections from a 1.0km temperature analysis (*Meteorologisk institutt*, 2021). This helps to minimize errors from the NWP model output and enables regular adjustments to the output without requiring a complete re-run of the main NWP model, which typically takes several hours to run, allowing the post-processed forecast product to be updated hourly (*Nipen et al.*, 2020). However, the 1.0km post-processed model does not use the improved ground tiling product used in the main 2.5km model (SURFEX), instead relying on a coarser surface tile setup, likely leading to model biases near lakes(*Nypen*, 2023).

Model data was downloaded from Met-Norway originating from the AROME-MetCoOp model and distributed through the Met-Norway THREDDS server (*Norwegian Meteorological Institute*, n.d.). This project uses data from the MetCoOp ensemble prediction system (MEPS), specifically the deterministic 2.5km model runs(MEPS25), and the analysis and forecast runs from the 1.0km post-processed model product (MEPSPP) described in section 1.

Analysis/closest forecast

Observations are unfiltered and matched to their grid cells using a nearest neighbor lookup function, precisely the KdTree function in the SciPy spatial package. Returning the indexes and distances to the nearest point on the model mesh grid allows for averaging all observations inside each grid cell, resulting in the grid-averaged product, which resembles the scale of the parent model with one value for each grid cell. The process is repeated for the Netatmo observations, adding a cutoff filter to account for inaccurate data from misplaced stations. Said filter uses a cutoff threshold of ± 3 degrees of the max/min values of the iMet observations.

Due to differences in forecast times, and available model products, the 1km post-processed model product uses the analysis, which starts simultaneously with the car runs. In comparison, the 2,5km product uses the closest preceding forecast, which varies between 1-2 hours lead time depending on daylight savings time.

All car runs use model data corresponding to the run's start time; it is assumed that there is little or no change in the forecast products over the individual test runs.

Forecasts

The Forecast comparisons use the same method as the analysis but adjusted to compare the forecasts from t-5 hours, t-11 hours, t-17 hours, and t-23hours, with lead time referring to hours before the car observations. I utilized the six hourly forecasts for the 2,5km and 1km products to investigate the whole observation and grid-averaged products, including the Netatmo observations.

2.5 Statistics

General statistics will be calculated for all relevant datasets, including extreme values, mean bias error(MBE), standard deviation(StDev), and root mean square error (RMSE), with equations listed below:

The

$$\mathrm{MBE} = \frac{1}{n}\sum_{i=1}^{n}(x_i - y_i) \tag{2.7}$$

where n is the number of observations, x_i is the forecasted value, and y_i is the observed value. The MBE measures the average difference between the forecasted and observed values, indicating the direction and extent of the bias in the models.

The mean absolute error is defined as

$$\text{MAE} = \frac{1}{n}\sum_{i=1}^{n}|x_i - y_i| \tag{2.8}$$

where n is the number of observations, x_i is the forecasted value, and y_i is the observed value. The MAE measures the average absolute difference between the forecasted and observed values, indicating the magnitude of the bias in the models.

The standard deviation is defined as

$$\text{StDev} = \sqrt{\frac{1}{n-1}\sum_{i=1}^{n}(x_i - \bar{x})^2} \tag{2.9}$$

where n is the number of observations, x_i is the i-th value, and $\bar{x}$ is the mean of the values. The StDev measures the spread of data points around the mean, indicating the variability or precision of the measurements.

The root mean square error is defined as

$$\text{RMSE} = \sqrt{\frac{1}{n}\sum_{i=1}^{n}(x_i - y_i)^2} \tag{2.10}$$

where n is the number of observations, x_i is the forecasted value, and y_i is the observed value. The RMSE measures the difference between forecasted and observed values, considering both the direction and extent of the difference. It is a commonly used metric for evaluating the accuracy of predictive models.

3 Variability testing

3.1 Static variability

3.1.1 Sheltered sensors

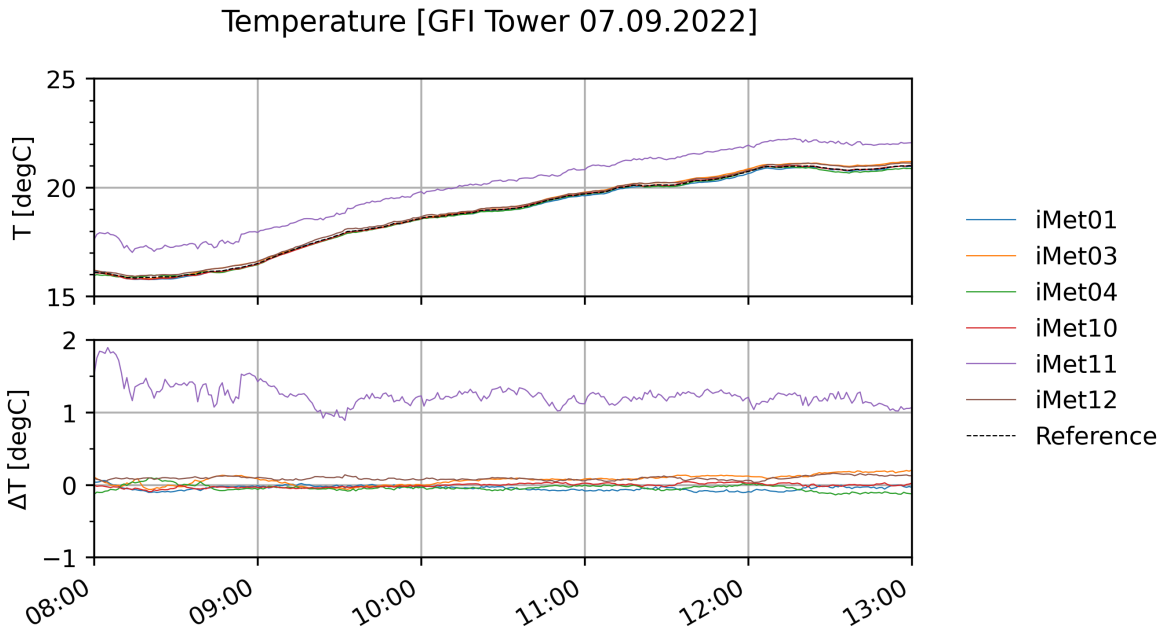

Figure 3.1: Temperature variability between the iMets compared to the reference temperature for 07.09.2022, top: temperature in °C, bottom: temperature anomaly between iMets and reference in °C

The first experiment, conducted at 08:00-13:00 UTC 07.09.2022, showed slight variation between the instruments, except iMet11 being around 1 degree warmer than the rest. Furthermore, iMet11 has more significant variability seemingly caused by signal noise and bad calibration, resulting in a consistent difference from the other iMets (fig: 3.1). It is clear from the temperature anomaly shown in the lower half of the figure, consisting of the difference between the individual sensors to the ensemble of the sensors (the reference), excluding outliers, that the majority of the sensors have a very low bias.

From table 3.1, it is shown that the bias and RMSE of the instruments are less than $\pm 0.10°C$ for all the devices except iMet11, with the StDev staying consistently between all sensors ($\leq 0.05°C$). N/A values show instruments missing or broken during the current test but available/fixed for later trials.

Table 3.1: iMet temperature statistics for 07.09.2022 for the sheltered instrument setup

Instrument	StDev	Bias	RMSE
iMet01	$1.76°C$	$-0.05°C$	$0.067°C$
iMet03	$1.82°C$	$0.07°C$	$0.097°C$
iMet04	$1.76°C$	$-0.05°C$	$0.068°C$
iMet05	N/A	N/A	N/A
iMet06	N/A	N/A	N/A
iMet10	$1.79°C$	$-0.01°C$	$0.035°C$
iMet11	$1.78°C$	$1.23°C$	$1.243°C$
iMet12	$1.77°C$	$0.09°C$	$0.093°C$
average	$1.78°C$	$0.21°C$	$0.267°C$
ensemble	$1.77°C$		

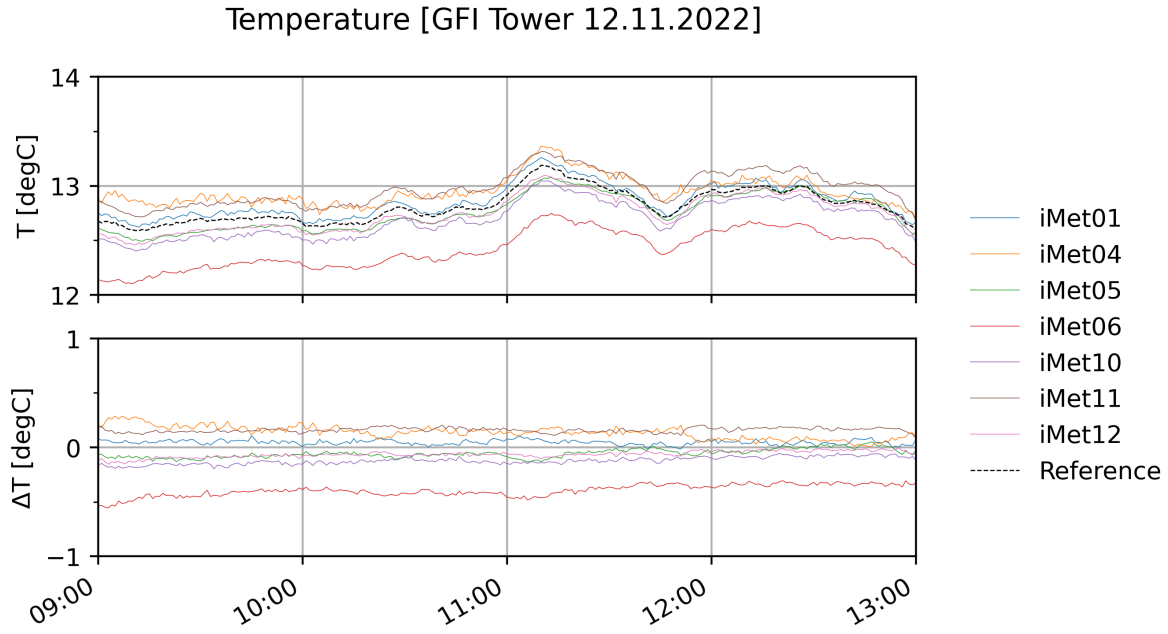

Figure 3.2: Temperature variability between the iMets compared to the reference temperature for 12.11.2022, top: temperature in °C, bottom: temperature anomaly between iMets and ensemble in °C

The second experiment, conducted at 09:00-13:00 UTC 12.11.2022, shows less total variability for the individual sensors (fig: 3.2), with the reduction coinciding with a more stable ambient temperature brought on by cloudy weather. Once again, there is an outlier, this time iMet06 with a bias of $-0.40°C$ (tab 3.2). Interestingly iMet11 now has a much-reduced bias, suggesting external factors might be at play.

In contrast to iMet11, there is an increase in mean bias, with a marginal rise in mean RMSE and a sharp increase in StDev. Furthermore, table 3.2 includes bias drift showing less than $0.20°C$ difference for instruments included in both tests, excluding iMet11, which had a much higher difference of $-1.07°C$. Three devices were excluded from the bias drift calculations, where drift is the change in bias over two boxed instrument tests, as a; they were not available for both tests (iMets 5-6), or b; they were damaged between or during one of the tests.

Table 3.2: iMet temperature statistics for 12.11.2022 for the sheltered instrument setup

Instrument	StDev	Bias	RMSE	Bias Drift
iMet01	$0.16°C$	$0.05°C$	$0.057°C$	$0.10°C$
iMet03	N/A	N/A	N/A	N/A
iMet04	$0.14°C$	$0.14°C$	$0.162°C$	$0.19°C$
iMet05	$0.16°C$	$-0.05°C$	$0.070°C$	N/A
iMet06	$0.17°C$	$-0.40°C$	$0.399°C$	N/A
iMet10	$0.17°C$	$-0.12°C$	$0.128°C$	$-0.11°C$
iMet11	$0.16°C$	$0.16°C$	$0.164°C$	$-1.07°C$
iMet12	$0.17°C$	$-0.06°C$	$0.071°C$	$-0.15°C$
average	$0.16°C$	$-0.04°C$	$0.150°C$	$-0.21°C$
ensemble	$0.15°C$			

3.1.2 Exposed sensors

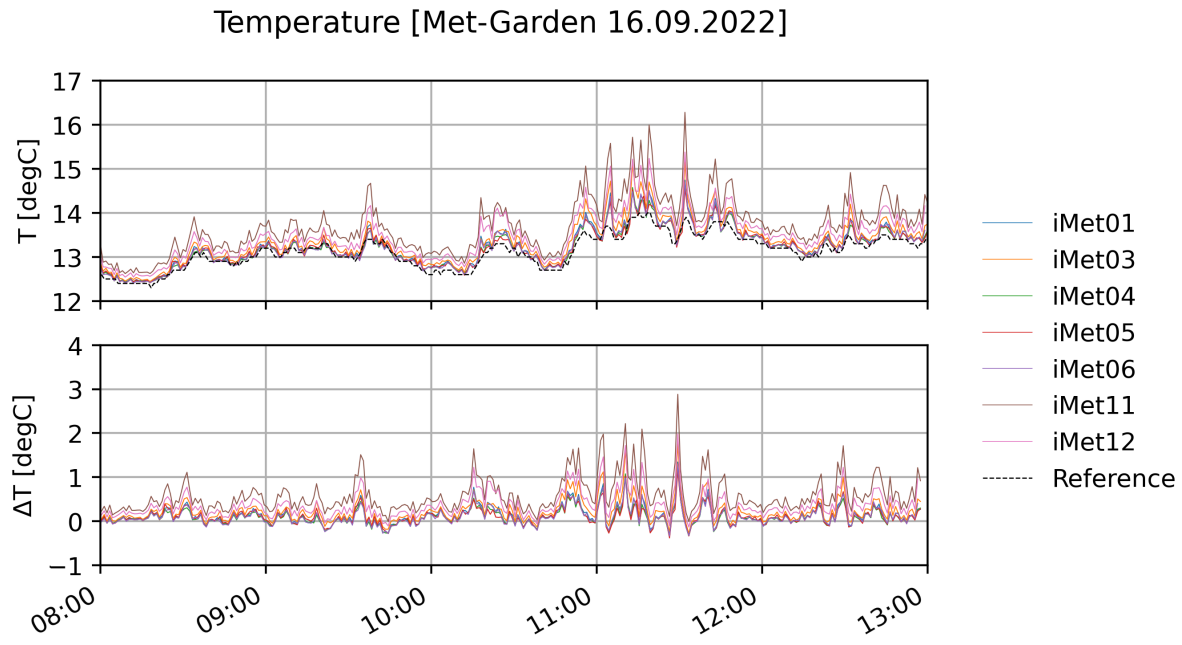

Figure 3.3: Temperature variability between the iMets compared to the reference PT100 sensor for 16.09.2022, top: temperature [°C], bottom: temperature anomaly between iMets and PT100 [°C]

Figure 3.3 shows an entirely different result from the sheltered sensors, with the test taking place at 08:00-13:00 UTC 16.09.2022 with windy semi-overcast conditions. While the iMets were fully exposed to the elements, except for some fence shading, the reference instrument had a sun shield, causing lower overall temperatures and leading to positive biases for all sensors, as shown in table 3.3. The figure also indicates distinctive peaking, likely due to sunlight briefly piercing the clouds.

As expected, the peaks and differences between the reference and the iMets increase the bias compared to the sheltered setup, especially when excluding the outliers. The standard deviation ranges from $0.45°C$ to $0.70°C$, and the RMSE between $0.27°C$ and

$0.82°C$, where even the lowest value is higher than the mean in tables 3.1-3.2 in section 3.1.2.

Table 3.3: iMet temperature statistics for 16.09.2022 for the exposed instrument setup

Instrument	StDev	Bias	RMSE
iMet01	$0.47°C$	$0.13°C$	$0.303°C$
iMet03	$0.53°C$	$0.23°C$	$0.411°C$
iMet04	$0.45°C$	$0.10°C$	$0.270°C$
iMet05	$0.45°C$	$0.11°C$	$0.276°C$
iMet06	$0.47°C$	$0.11°C$	$0.284°C$
iMet11	$0.70°C$	$0.59°C$	$0.820°C$
iMet12	$0.57°C$	$0.37°C$	$0.544°C$
average	$0.52°C$	$0.23°C$	$0.415°C$
PT100	$0.38°C$		

3.2 Car-mounted sensor variability

3.2.1 Stationary heating

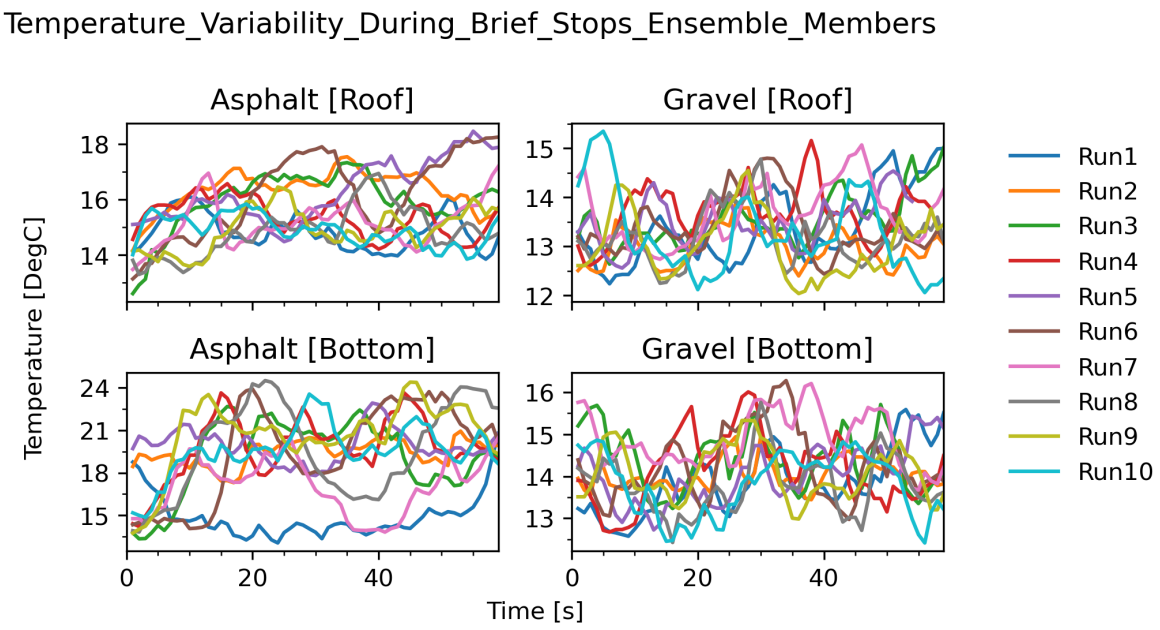

Figure 3.4: Test runs for the temperature variability of car-mounted iMets, instruments mounted on the roof and near the bottom of the car, including asphalt and gravel ground materials.

Figure 3.4 illustrates the temperature variability for a stationary vehicle, including readings from the shaded lower front section of the car and the roof. It includes ten test runs, for each plot, showcasing considerable variability with some notable outliers. The best example of such an outlier is in the lower left section, where there is a dotted blue line with clearly anomalous behavior. Its temperature stays close to its equivalent roof temperature.

The variability can be more easily investigated by looking at the test runs in figure 3.5, where we can see a more distinctive pattern revealing discrete heating patterns while stationary on an asphalt surface, with a more complicated evolution on a gravel surface. Temperature drops are recorded when parking on a gravel surface next to the road, remaining relatively stable, except for a brief maximum at around the 30-second marker, which incidentally is near the local minimum of the bottom mount over asphalt.

The hump detected at the 30-second marker for the gravel surface is likely due to air from the road being pushed over by passing cars, as the traffic around the circuit was quite consistent, with one car passing by for each test run.

Due to missing data values caused by faulty GPS readings, some test runs can be up to 5 seconds delayed.

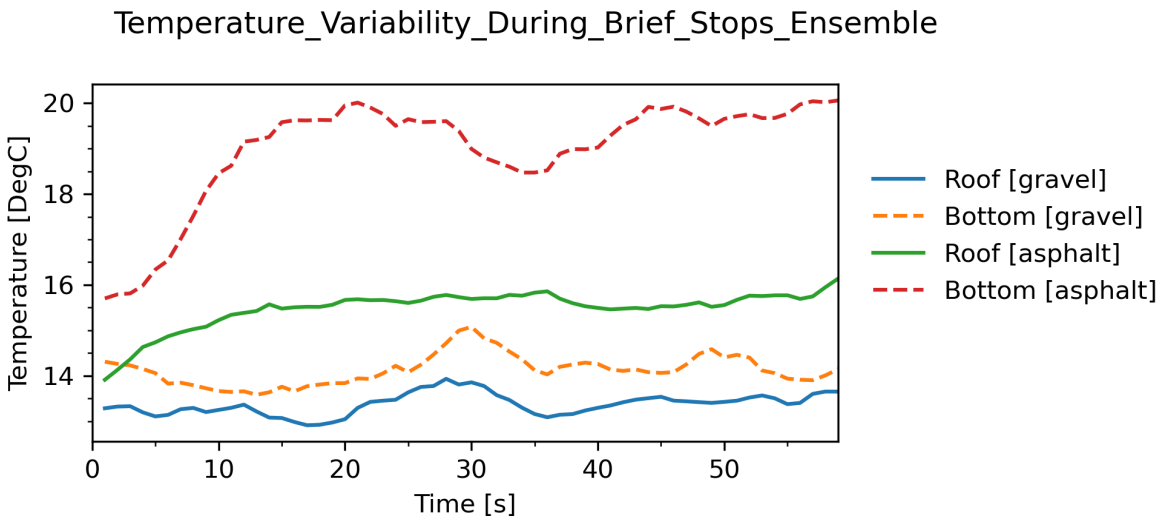

Figure 3.5: Average temperature variability ensembles for different surfaces and mount points

3.2.2 Acceleration and movement

Examining the information in figures 3.6-3.7, it is apparent that accelerating or moving the vehicle can have a profound impact on the temperature registered by the sensors as surrounding air displaces the air around the car. Such a process generally implies a cooling effect on the vehicle, but this is not always the case.

The bottom readings over gravel increase in temperature for up to 9 seconds, perhaps unsurprisingly after the investigation of stationary heating showing a significantly stronger temperature increase over time for asphalt than gravel (section 3.2.1). In fact, this difference in heat emitted by the surface makes it harder to diagnose differences in temperature for the surfaces, as the difference in starting temperature is around $4°C$. Making it more likely to cool as the surrounding air is pulled toward the car.

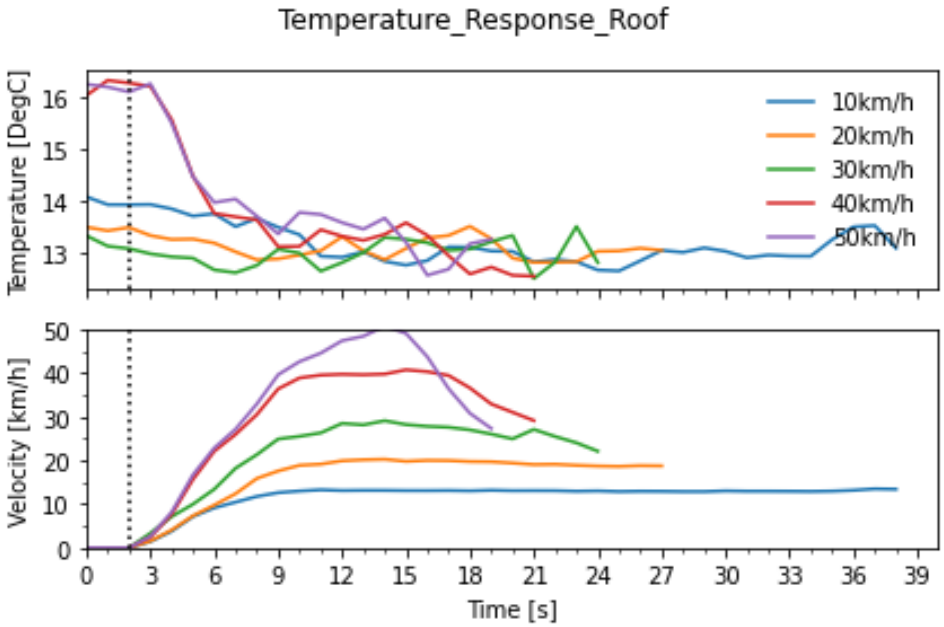

Figure 3.6: Shows the temperature evolution on the roof while the vehicle accelerates from a standstill, with temperature in the top plot and speed in the lower plot.

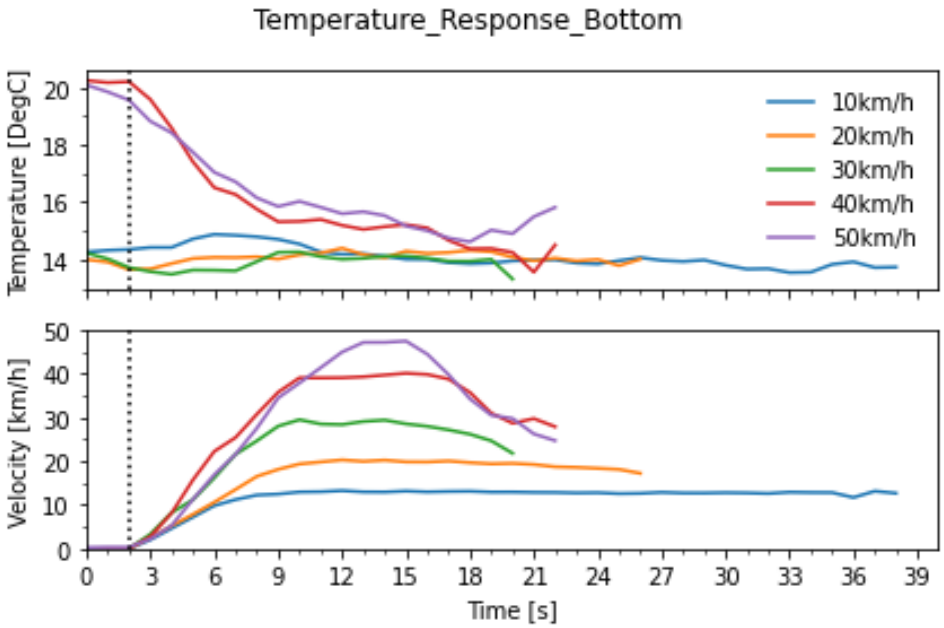

Figure 3.7: Shows the temperature evolution on the shaded lower front while the vehicle accelerates from a standstill, with temperature in the top plot and speed in the lower plot.

Figures 3.6-3.7 contain the temperature response while accelerating/moving, with the temperature evolution in the top plot and speeds in the lower field. Figures are divided into Roof and Bottom, respectively.

The roof has smaller temperature differences between the asphalt and gravel surface, although still notable at around two degrees. Both gravel and asphalt surfaces show a decline in temperature, and an increase in variability when the temperature nears $13°C$.

Increases in variability could be caused by changes in direct sunlight and wind exposure, or by passing through sections of warm air caused by areas of increased surface albedo, like darker patches of asphalt, or areas with less ventilation (near trees).

While the gravel surface produces mixed results when accelerating, the asphalt keeps to a predictable cooling pattern. Reducing consistently between speeds of 10-30km/h, until it gets closer to the ambient temperature of $13 - 14°C$.

3.2.3 Variability while driving

Figure 3.8 contains measurements from a car's roof and bottom with the vehicle having a silver-white color. With measurements spanning daytime, 13:00-13:22 UTC, and evening, 20:00-20:26 UTC. The upper row contains roof measurements, with the lower row containing the lower engine intake measurements, and time increases from left to right. The area covers Northern Karmøy, part of an island just west of Haugesund, Rogaland.

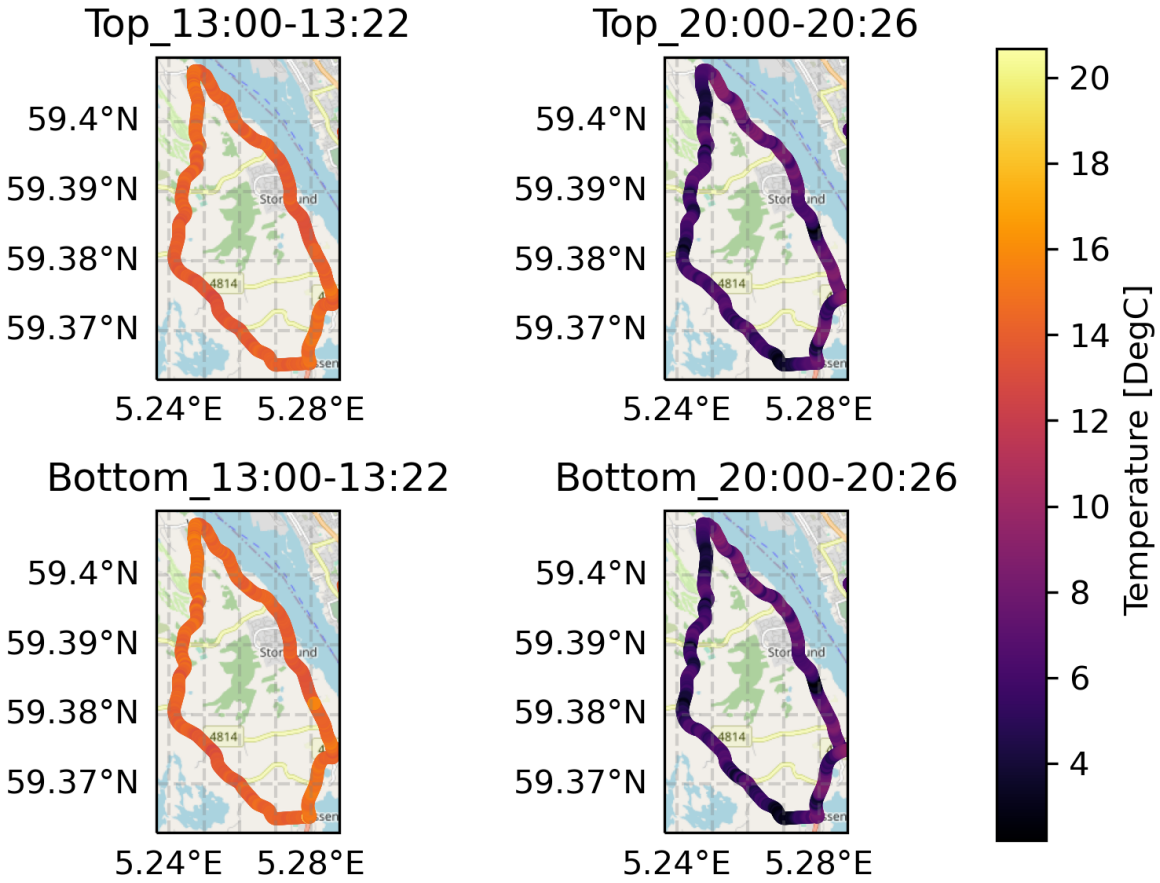

Figure 3.8: Spatial temperature plots for day and nighttime trial runs, including roof and engine went mount points, top row: roof measurements, daytime on the left, and nighttime on the right, bottom row, intake vent measurements same layout as the top row. Observations from 29.09.2022.

The figure illustrates that the instrument is sensitive enough to register local temperature differences with sufficient response times and that the GPS can reliably place the GPS coordinates on the road. Furthermore, it confirms small localized areas with significant temperature drops during the evening and regions with higher temperatures than surrounding areas.

This is expanded in figure 3.9, where the data is presented as a time series, including the drive to the test route, which contains interesting heating data as there a many small-scale temperature-variations that would not be resolved in a weather model. Daytime observation concurs with the results of sections 3.2.1-3.2.2, with heat building up faster on the bottom sensor, although it shows that the difference between the roof and bottom is minimal while driving. In the evening, they mostly equalize, albeit with a slight reversal of the daytime situation. The roof is slightly warmer than the engine vent, except when the vehicle is stationary.

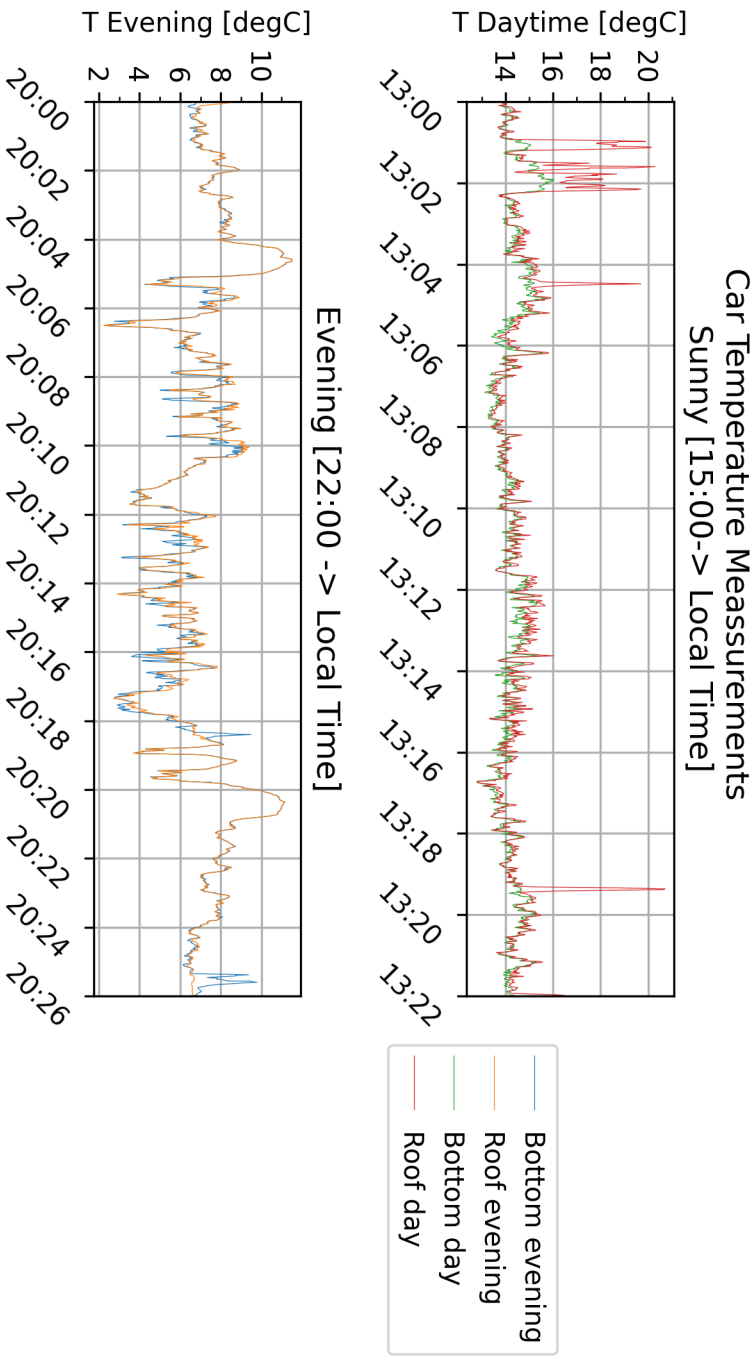

Figure 3.9: Time series comparison of roof mounting and lower engine vent mounting for day and evening conditions, 29.09.2022

4 Model Comparison

4.1 Analysis

4.1.1 Haugesund 28.09.2022 22:00 UTC

The first set of results shown in fig 4.1 & 4.2 shows a partition in model bias between the northern and southern section of the test area, visible in both the iMet and Netatmo datasets. The area to the south and southwest holds the major population centers, with Haugesund situated in the southwestern corner and suburbs sprawling in every direction. However, the suburb population is denser on the eastern side of Haugesund than on the Northern side, and there is more traffic passing through due to two major roads passing through (E39 & E134).

The MEPS 1.0km product fits better to the observations, which is unsurprising as the Netatmo data is used in the post-processing (*Meteorologisk Institutt*, 2018). However, some selection/wetting algorithms are used as they are not treated equally. A vetting process was also conducted on these datasets as they are commercially available private weather stations; they are not always ideally placed, leading to inaccurate readings. However, assessing which readings are valid without other observations can be challenging, as there can be a significant degree of natural variation even in a single grid cell.

As for the temperature bias, the model is around two degrees Celsius warmer in the northern half of the post-processed domain, with an exception to the west just above the midpoint, which is up to 4-5 degrees too cold, which is worse than the result from the 2.5km model. The 2.5km model has a bias of around 3-4 degrees in the northern half. For the southern section, it is a bit more chaotic. Still, the temperature anomaly generally decreases from the 2.5km to the 1.0km model, except for the area just east of Haugesund, which is notably warmer. The grid averaging in fig 4.2 gives the same pattern but reduces the peak temperatures by 1-2 degrees.

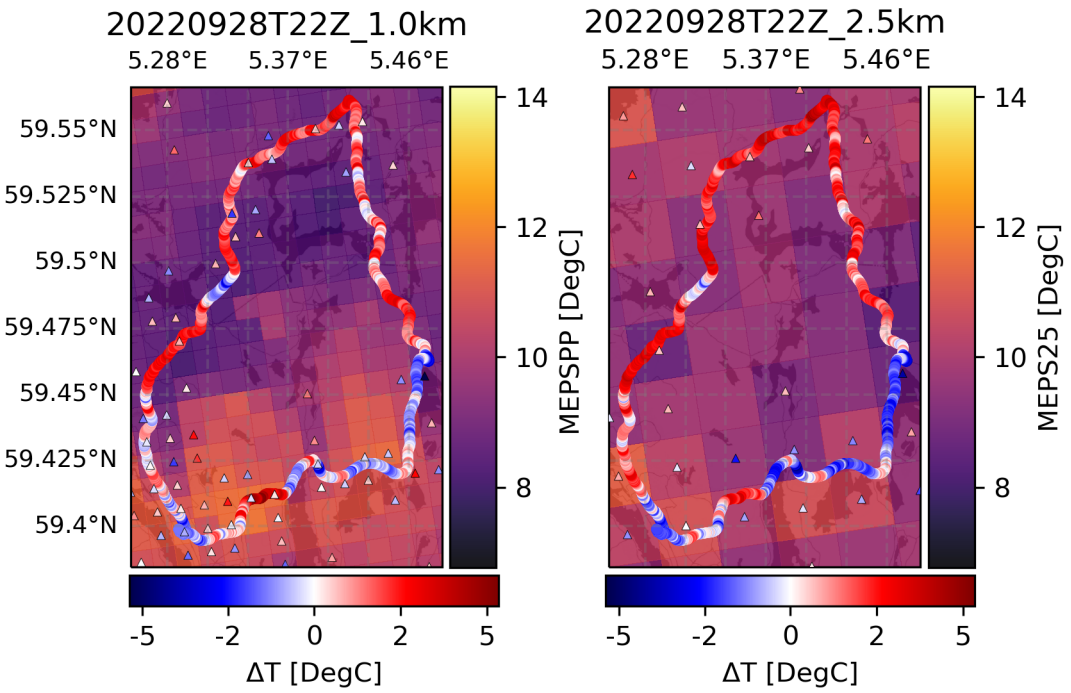

Figure 4.1: Model bias from iMet(points) and Netatmo(triangles) to the MEPS 1km post-processed model (left), and MEPS 2,5km model (right), represented by mesh grids over a map tile, Netatmo observations are averaged by grid cell, time: 28.09.2022 22Z. Map tiles by Stamen Design, under CC BY 3.0. Data by OpenStreetMap, under ODbL.

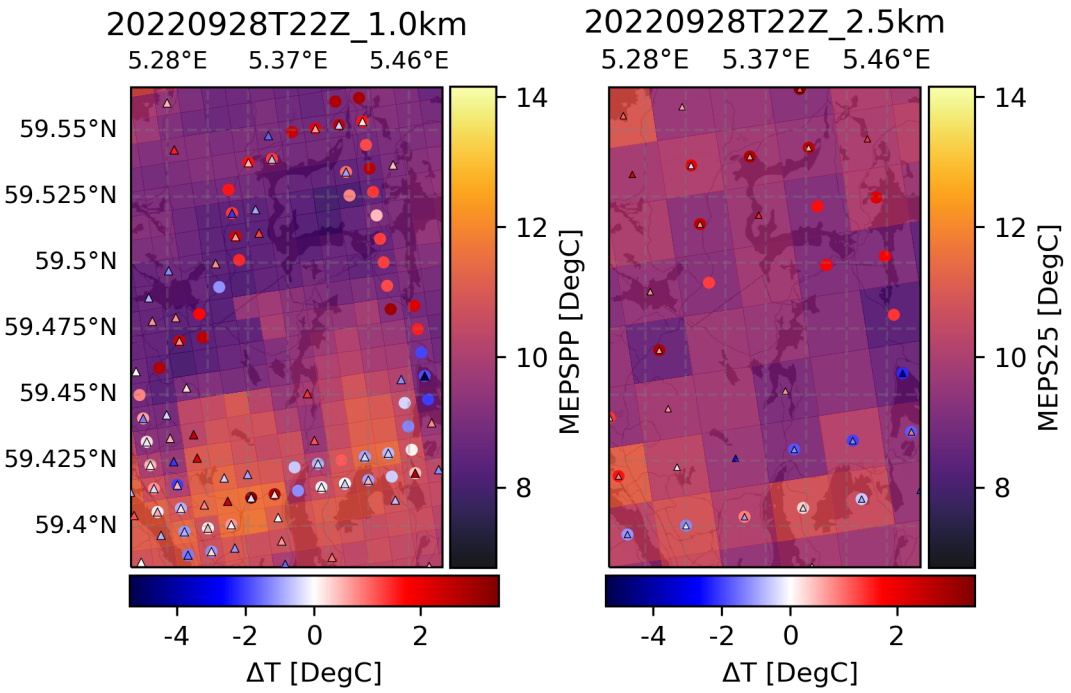

Figure 4.2: Model bias from iMet(points) and Netatmo(triangles) to the MEPS 1km post-processed model (left), and MEPS 2,5km model (right), represented by mesh grids over a map tile, observations are averaged by grid cell, time: 28.09.2022 22Z. Map tiles by Stamen Design, under CC BY 3.0. Data by OpenStreetMap, under ODbL.

4.1.2 Haugesund 29.09.2022 04:00 UTC

Figures 4.3 & 4.4 give the same general temperature distribution albeit with more uniform temperature differences, i.e., less variation in temperature difference within the northern/southern region. The exceptions noted in section 4.1.1, namely the cold bias around the domain midpoint to the west, and the warm section east of Haugesund, have all but disappeared or at least strongly diminished. Additionally, the models' temperatures have decreased, unsurprisingly, as 04:00 UTC is 06:00 local time, about 1.5 hours before sunrise, being near the diurnal minimum under stable conditions.

As a result, the gridded mean staying around $\pm 1°C$, with outliers around $\pm 3°C$ for the observations. Precise statistics can be found in table 4.1. While the results have less variation, it is interesting that the Netatmo data in the northern half are less consistent with the iMet, especially in the northwestern quadrant of the 2.5km grid. The Netatmo stations report that the model is too cold while previously having the same sign and roughly the same values as the iMet.The southern section shows near identical values for the 2.5km model, with a strong cold bias.

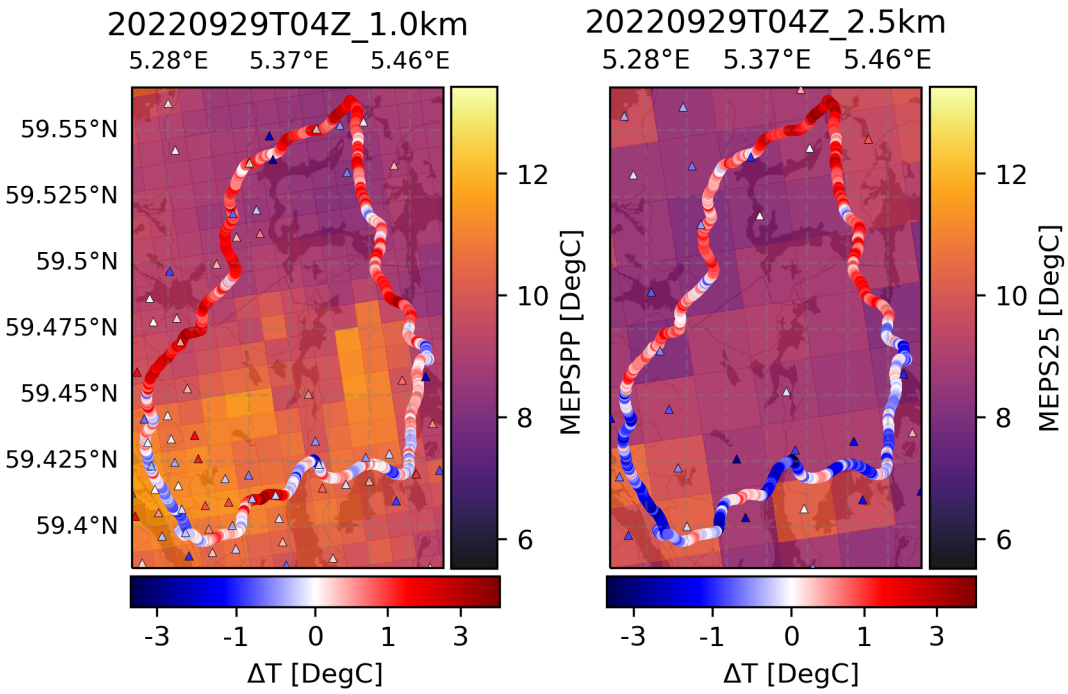

Figure 4.3: Model bias from iMet(points) and Netatmo(triangles) to the MEPS 1km post-processed model (left), and MEPS 2,5km model (right), represented by mesh grids over a map tile, Netatmo observations are averaged by grid cell, time: 29.09.2022 04Z. Map tiles by Stamen Design, under CC BY 3.0. Data by OpenStreetMap, under ODbL.

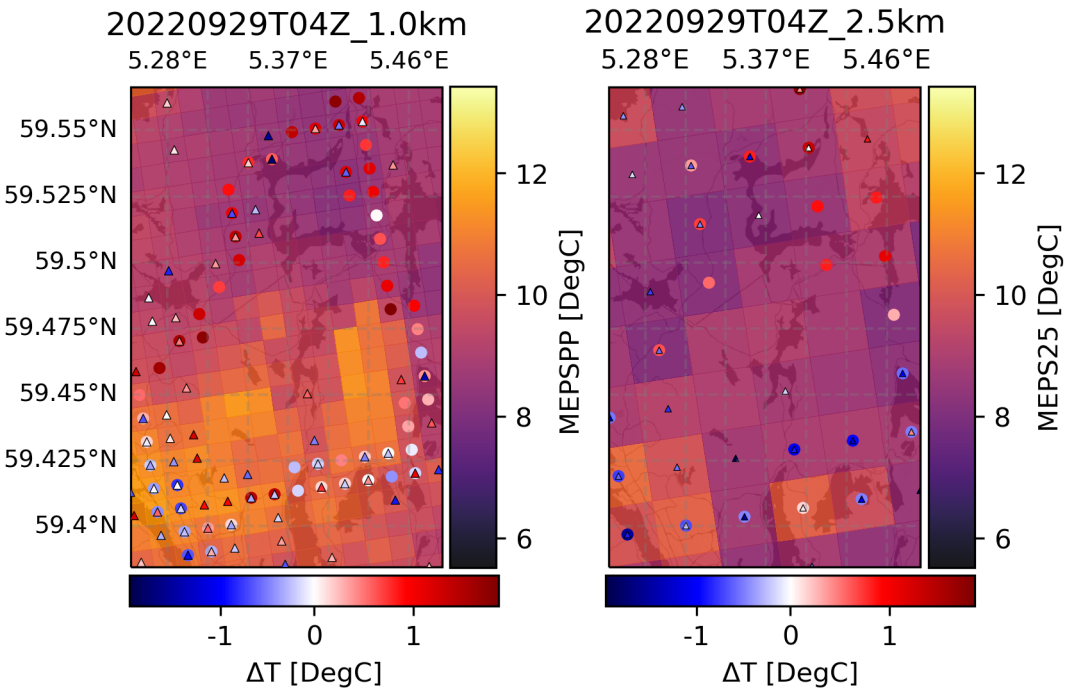

Figure 4.4: Model bias from iMet(points) and Netatmo(triangles) to the MEPS 1km post-processed model (left), and MEPS 2,5km model (right), represented by mesh grids over a map tile, observations are averaged by grid cell, time: 29.09.2022 04Z. Map tiles by Stamen Design, under CC BY 3.0. Data by OpenStreetMap, under ODbL.

4.1.3 Haugesund 29.09.2022 10:00 UTC

The midday run shows a much more mixed result between the Netatmo stations and the iMet, where the model is heavily biased according to the iMet readings, showing that the model is too cold over the road (figs: 4.5 & 4.6). However, there is more variation in the Netatmo data, specifically in the 1.0km product, where there is less of a discernable bias pattern. Do note that the color bar does not have equally spaced ticks for positive and negative values, as the max and min values are -8.0 and 2.2, respectively. When averaged over larger grid cells, it is apparent that the model bias is predominantly negative, as the Netatmo data averaged to the 2.5km grid cells shows a similar tendency to that of the iMet.

There is also a discernable improvement from the 2.5km model to the 1.0km model, lessening the overall negative bias and resulting in much better results for the road measurements, with the mean bias being reduced by around $1.5°C$. The mean model bias with respect to the Netatmo data was also reduced by nearly $2.0°C$, but this is less impressive considering the Netatmo values are more spread between positive and negative values, resulting in a lower average.

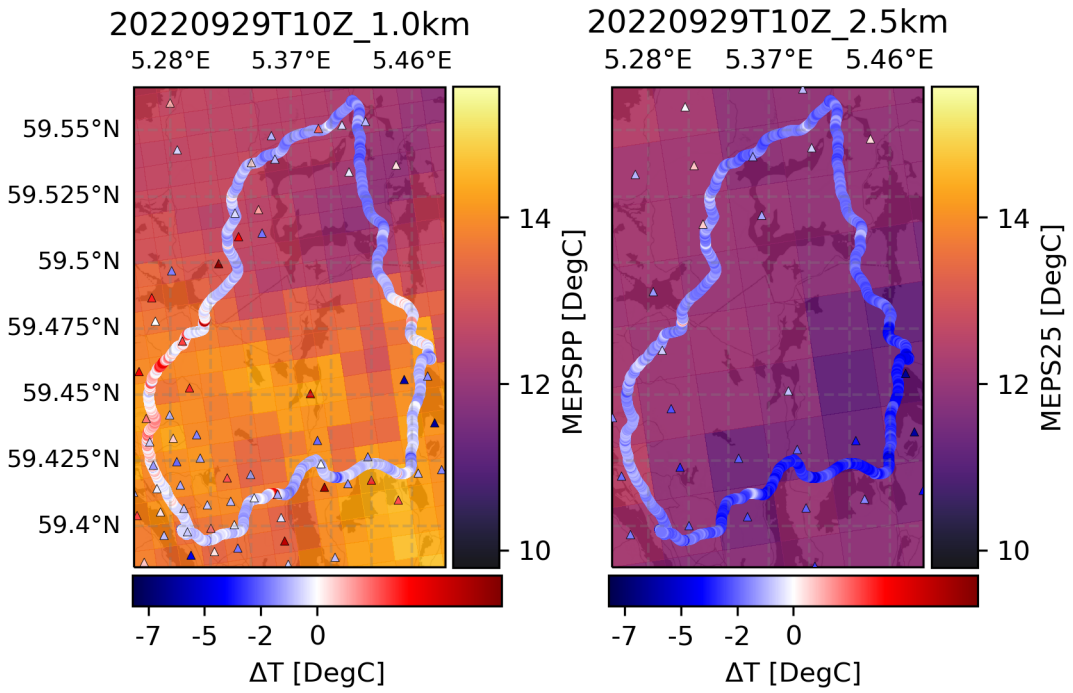

Figure 4.5: Model bias from iMet(points) and Netatmo(triangles) to the MEPS 1km post-processed model (left), and MEPS 2,5km model (right), represented by mesh grids over a map tile, Netatmo observations are averaged by grid cell, time: 29.09.2022 10Z. Map tiles by Stamen Design, under CC BY 3.0. Data by OpenStreetMap, under ODbL.

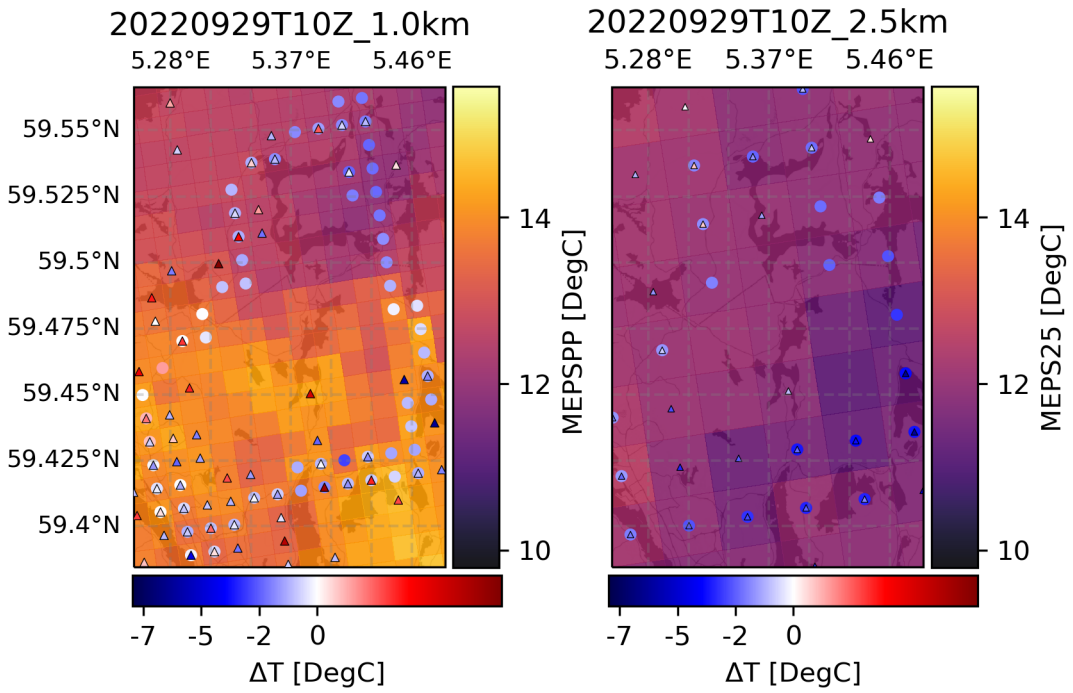

Figure 4.6: Model bias from iMet(points) and Netatmo(triangles) to the MEPS 1km post-processed model (left), and MEPS 2,5km model (right), represented by mesh grids over a map tile, observations are averaged by grid cell, time: 29.09.2022 10Z. Map tiles by Stamen Design, under CC BY 3.0. Data by OpenStreetMap, under ODbL.

4.1.4 Haugesund 29.09.2022 16:00 UTC

The early evening run is almost precisely opposite from the midday run (figs: 4.7 & 4.8), with iMet values showing that the model is too warm for the roads. Interestingly the 2.5km model seems to outperform the 1.0km model from the iMet perspective, likely due to the Netatmo stations implying that the 2.5km model is too cold, resulting in a post-processing adjustment. Again, the result is likely impacted by the diurnal cycle as sundown was around 19:30, which means that the run was taken between 1.5h to 0.5h before sundown. The resulting sun angle, topography, and vegetation likely impact the 2.5km and 1.0km model data, contributing to the overall warm bias. Full statistics are shown in table 4.1.

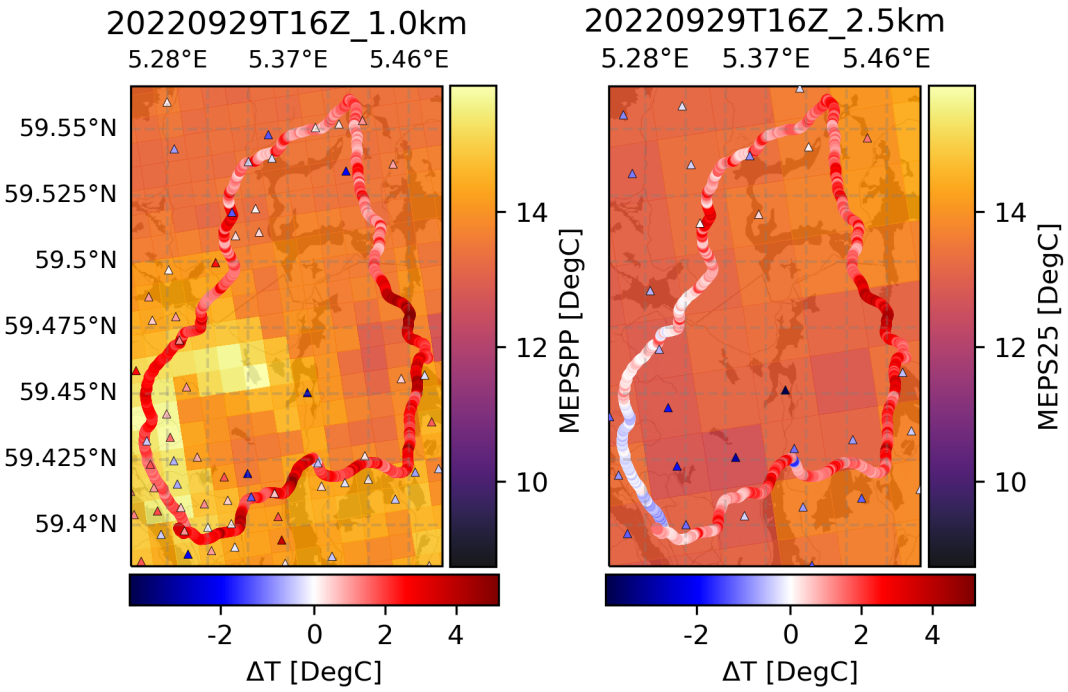

Figure 4.7: Model bias from iMet(points) and Netatmo(triangles) to the MEPS 1km post-processed model (left), and MEPS 2,5km model (right), represented by mesh grids over a map tile, Netatmo observations are averaged by grid cell, time: 29.09.2022 16Z. Map tiles by Stamen Design, under CC BY 3.0. Data by OpenStreetMap, under ODbL.

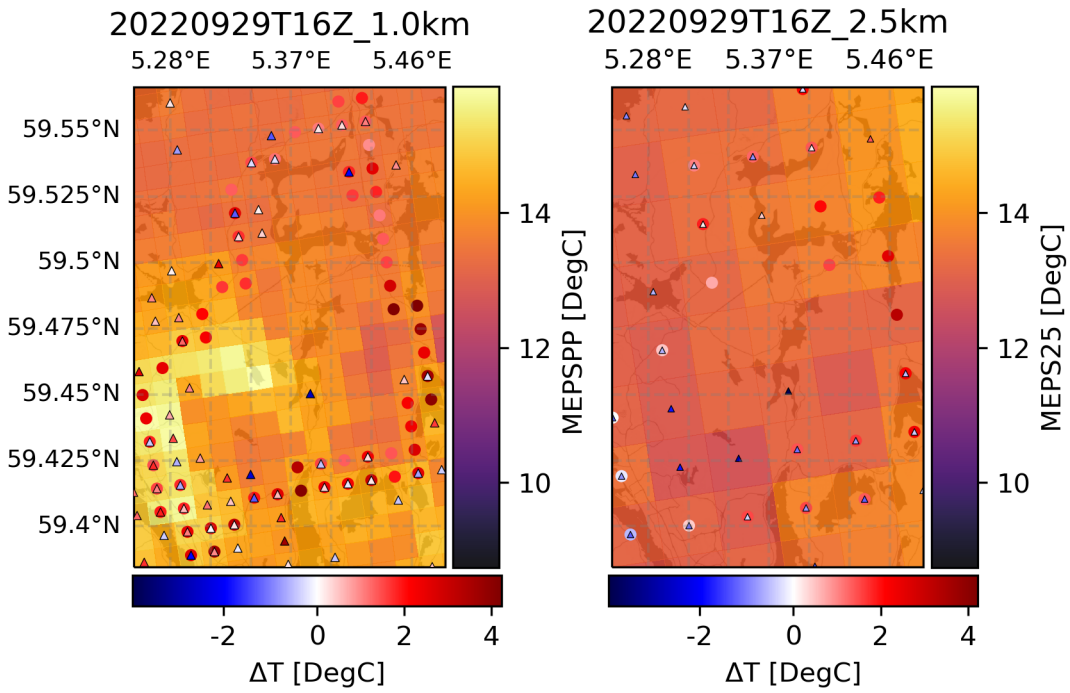

Figure 4.8: Model bias from iMet(points) and Netatmo(triangles) to the MEPS 1km post-processed model (left), and MEPS 2,5km model (right), represented by mesh grids over a map tile, observations are averaged by grid cell, time: 29.09.2022 16Z. Map tiles by Stamen Design, under CC BY 3.0. Data by OpenStreetMap, under ODbL.

4.1.5 Haugesund 18.11.2022 23:00 UTC

The last run of the Haugesund route was driven later in autumn on 18.11.2022 and had a more distinct temperature anomaly distribution. The 2.5km model shows a predominantly cold bias, which differs from the previous evening example in section4.1.1. However, daylight savings ended earlier in the month, resulting in a later starting time in UTC, fewer daylight hours, and less environmental heating.

The post-processing for the 1.0km data has been rather effective at lessening the bias, which is especially apparent when looking at the gridded averages in fig 4.10. The mean gridded bias for the iMet changes sign from $-0.922°C$ to $0.208°C$, while the Netatmo mean bias changes from $-0.503°C$ to $-0.182°C$ (table 4.1). Again, some of the reduction of the mean bias is likely due to the increased frequency of sign changes introduced to the bias in the post-processed product and not necessarily due to the smaller bias.

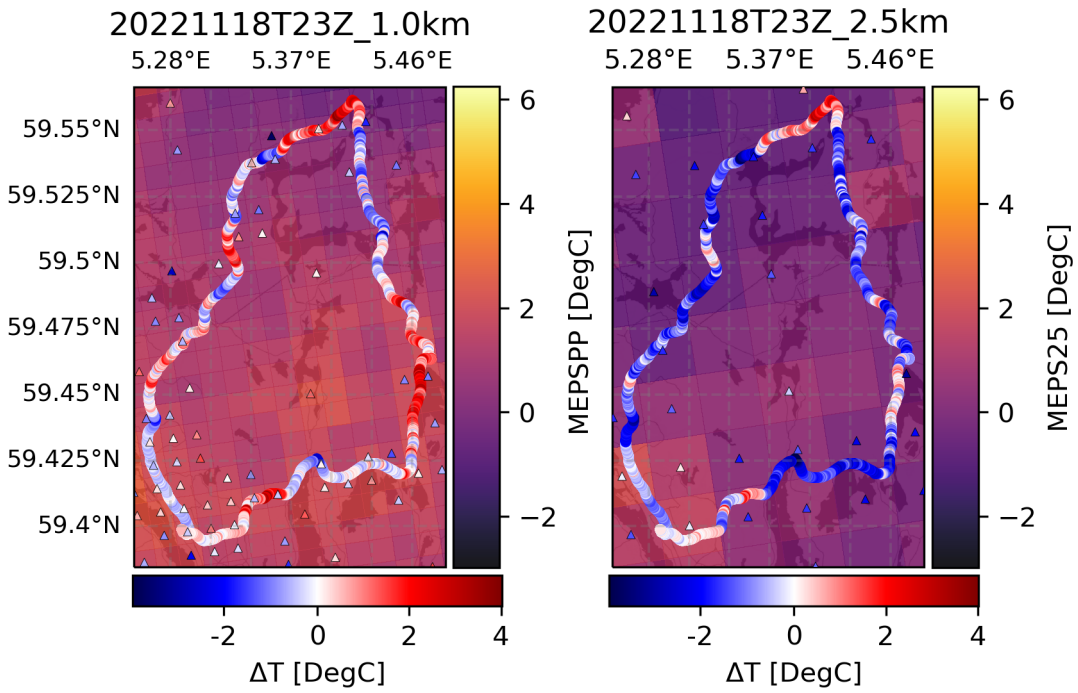

Figure 4.9: Model bias from iMet(points) and Netatmo(triangles) to the MEPS 1km post-processed model (left), and MEPS 2,5km model (right), represented by mesh grids over a map tile, Netatmo observations are averaged by grid cell, time: 18.11.2022 23Z. Map tiles by Stamen Design, under CC BY 3.0. Data by OpenStreetMap, under ODbL

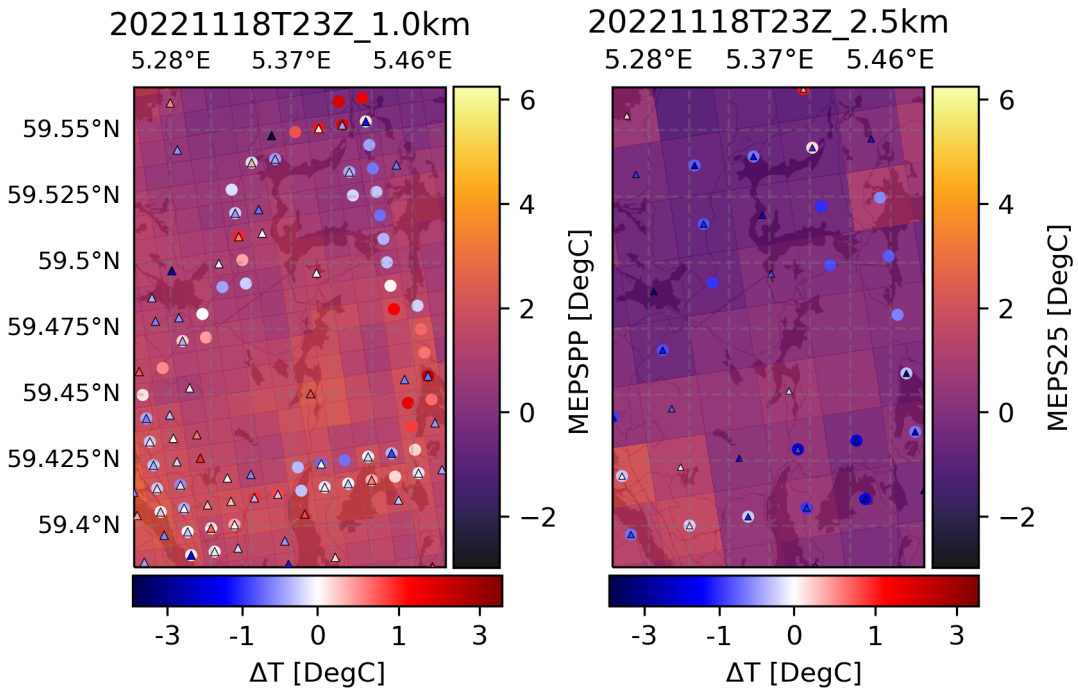

Figure 4.10: Model bias from iMet(points) and Netatmo(triangles) to the MEPS 1km post-processed model (left), and MEPS 2,5km model (right), represented by mesh grids over a map tile, observations are averaged by grid cell, time: 18.11.2022 23Z. Map tiles by Stamen Design, under CC BY 3.0. Data by OpenStreetMap, under ODbL

4.1.6 Haugesund statistics

Looking at the observation runs in table 4.1, there is a decrease in the MSE and RMSE for most runs when going from 2.5km to 1.0 km, the drop is not universal, but it is apparent when taking the mean errors for all runs. Additionally, the standard deviation is reduced for all runs, perhaps unsurprisingly, as the 2.5km product has lower minimums for all runs and higher maximums for most runs, with a majority of negative biases in the 2.5km product and all but one positive for the 1.0km product.

Similarly, the Netatmo stations highlight the 2.5km model data have a mean bias that is entirely negative for all runs, but keep in mind that the pure Netatmo values are not plotted. Moving on to the 1.0km data, the mean bias is still negative for the majority of the runs, albeit much smaller in magnitude, which is to be expected as these Netatmo observations are used in the post-processing. Standard deviation is comparable with the 2.5km model, albeit slightly higher on average, likely due to the minimums being lower across all runs and the maximums being comparable in value. MSE and RMSE show a similar pattern with the standard deviation, where the averaged errors overall runs are slightly higher, albeit by a minimal amount.

The grid averaged values for the iMet and Netatmo observations give minimum, and maximum values of lesser magnitude, which is to be expected as averaging will reduce the outliers for grid cells with multiple Netatmo/iMet readings. They also show an increase in the mean bias for all but the last run for the 1.0km iMet readings and are overall equivalent for the 2.5km model. Mean model bias relating to Netatmo observations is of lesser magnitude with gridded averages for the 2.5km model and similar magnitude for the 1.0km model. For the RMSE, the gridded means reduced the average error by 17% for the 1.0km model RMSE and 18% for the 2.5km model RMSE (tab: 4.1).

Table 4.1: Temperature anomaly statistics between MEPS 1.0km and 2.5km datasets to iMet and Netatmo observations, including gridded averages, for the Haugesund route.

MEPS - iMet											
Datetime	Min 1.0	Min 2.5	Max 1.0	Max 2.5	Bias 1.0	Bias 2.5	Stdev 1.0	Stdev 2.5	MSE 1.0	MSE 2.5	RMSE 1.0	RMSE 2.5
20220928T22Z	-4.382	-4.713	5.333	4.953	0.456	0.470	1.779	2.141	3.372	4.806	1.836	2.192
20220929T04Z	-2.321	-3.505	3.810	3.821	0.689	-0.082	1.194	1.418	1.901	2.017	1.379	1.420
20220929T10Z	-6.604	-8.199	2.337	0.782	-0.988	-2.567	0.938	1.001	1.856	7.589	1.362	2.755
20220929T16Z	-0.659	-1.691	5.198	4.634	2.192	1.110	0.891	1.148	5.598	2.550	2.366	1.597
20221118T23Z	-2.948	-3.940	4.019	3.388	1.055	-0.877	1.055	1.113	1.160	2.007	1.077	1.417
MEPS - Netatmo												
20220928T22Z	-6.903	-6.178	4.800	4.258	-0.025	-0.262	1.226	1.440	1.504	2.142	1.226	1.464
20220929T04Z	-2.588	-3.701	5.953	4.973	0.031	-0.813	1.029	1.248	1.060	2.219	1.029	1.490
20220929T10Z	-8.319	-10.194	5.586	3.720	-0.754	-2.616	1.937	2.081	4.319	11.175	2.078	3.343
20220929T16Z	-3.919	-4.809	4.098	2.787	0.116	-0.939	1.413	1.461	2.010	3.015	1.418	1.736
20221118T23Z	-4.853	-5.816	4.754	4.536	-0.121	-0.526	1.043	1.381	1.101	2.184	1.049	1.478

MEPS - grid averaged iMet												
Datetime	Min 1.0	Min 2.5	Max 1.0	Max 2.5	Bias 1.0	Bias 2.5	Stdev 1.0	Stdev 2.5	MSE 1.0	MSE 2.5	RMSE 1.0	RMSE 2.5
20220928T22Z	-2.054	-2.256	3.467	3.528	0.688	1.055	1.472	1.784	2.640	4.296	1.625	2.073
20220929T04Z	-1.192	-2.296	2.791	3.063	0.813	0.345	1.043	1.374	1.749	2.007	1.323	1.417
20220929T10Z	-2.944	-3.818	0.424	-1.533	-1.111	-2.563	0.750	0.749	1.797	7.131	1.341	2.670
20220929T16Z	0.953	-0.542	4.231	3.291	2.224	1.384	0.823	0.918	5.625	2.758	2.372	1.661
20221118T23Z	-1.095	-2.219	2.555	1.592	0.208	-0.922	0.911	0.897	0.873	1.654	0.934	1.286
MEPS - grid averaged Netatmo												
20220928T22Z	-5.381	-4.207	3.078	3.469	-0.064	-0.142	1.097	1.251	1.208	1.586	1.099	1.259
20220929T04Z	-2.588	-2.952	2.345	2.203	-0.043	-0.669	0.866	1.050	0.752	1.549	0.867	1.245
20220929T10Z	-7.960	-6.437	2.237	1.245	-0.721	-2.419	1.591	1.596	3.051	8.400	1.747	2.898
20220929T16Z	-3.793	-3.939	3.684	2.444	0.084	-0.630	1.177	1.107	1.391	1.623	1.180	1.274
20221118T23Z	-3.697	-3.048	3.412	2.673	-0.182	-0.503	0.924	1.276	0.886	1.882	0.941	1.372

4.1.7 Bergen 20.01.2023 23:00 UTC

The evening of January 20^{th}, 2023 (figs: 4.11 & 4.12), shows a decent correlation between the iMet measurements and the model data, particularly for the northern half of the domain. The southern section shows a strong, warm bias in the 2.5km model, primarily corrected in the 1.0km model. While the bias is mainly corrected, a small area remains with a solid warm bias, perhaps due to the gap in the Netatmo coverage, preventing corrections during the post-processing for the 1.0km model. The magnitude of the bias is interesting, as there is a significant difference of up to $9.2°C$ in the 2.5km model and $6.4°C$ in the 1.0km model, as shown in table 4.2, which could cause issues if the temperature was closer to the freezing point.

Similarly, the Netatmo observations near the car route have warm biases in the 2.5km model and are more mixed in the 1.0km model. However, the bias generally becomes negative/more negative further away from the road, especially on the western side. This change might be due to the proximity of the ocean causing a warmer ambient temperature by heat exchange, as the ocean typically does not freeze. Furthermore, it is noteworthy that the topography around the southern half of the route is generally dominated by north-south facing valleys, potentially inducing cold pools along sections of/along the road. Bodies of water are present along the route, but due to the low temperature, most freshwater lakes and slow-flowing rivers are likely frozen. Keep in mind that the 1.0km model does not resolve lakes, which is likely a contributing factor to the cold biases found near the lake at the center of the domain, relating to the Netatmo stations (fig: 4.12).

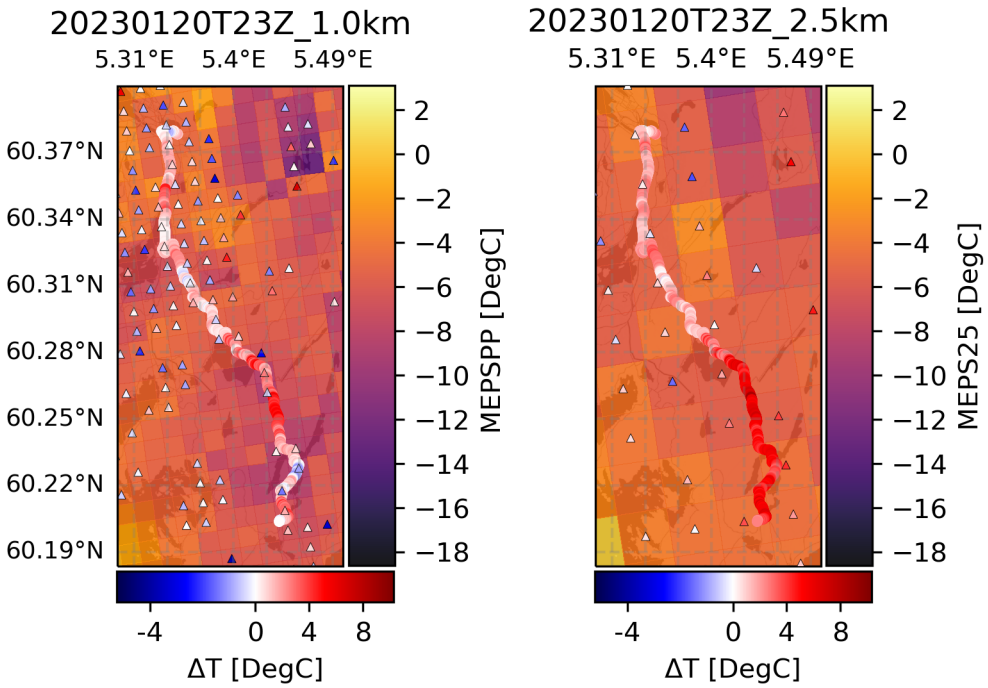

Figure 4.11: Model bias from iMet(points) and Netatmo(triangles) to the MEPS 1km post-processed model (left), and MEPS 2,5km model (right), represented by mesh grids over a map tile, Netatmo observations are averaged by grid cell, time: 20.01.2023 23Z. Map tiles by Stamen Design, under CC BY 3.0. Data by OpenStreetMap, under ODbL.

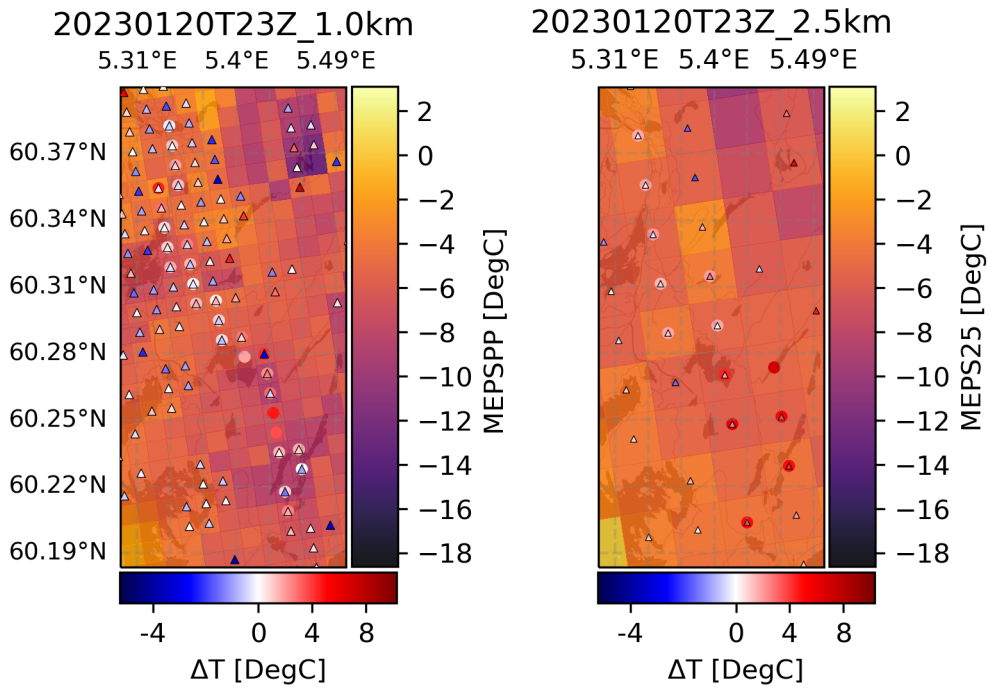

Figure 4.12: Model bias from iMet(points) and Netatmo(triangles) to the MEPS 1km post-processed model (left), and MEPS 2,5km model (right), represented by mesh grids over a map tile, all observations are averaged by grid cell, time: 20.01.2023 23Z. Map tiles by Stamen Design, under CC BY 3.0. Data by OpenStreetMap, under ODbL.

4.1.8 Bergen 21.01.2023 11:00 UTC

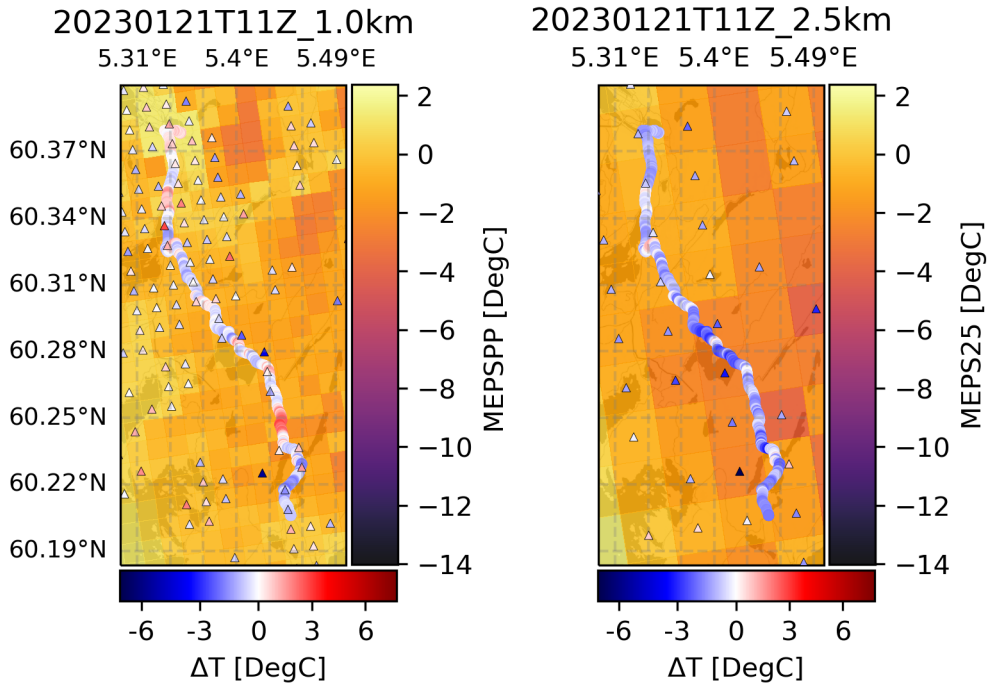

Figure 4.13: Model bias from iMet(points) and Netatmo(triangles) to the MEPS 1km post-processed model (left), and MEPS 2,5km model (right), represented by mesh grids over a map tile, Netatmo observations are averaged by grid cell, time: 21.01.2023 11Z. Map tiles by Stamen Design, under CC BY 3.0. Data by OpenStreetMap, under ODbL.

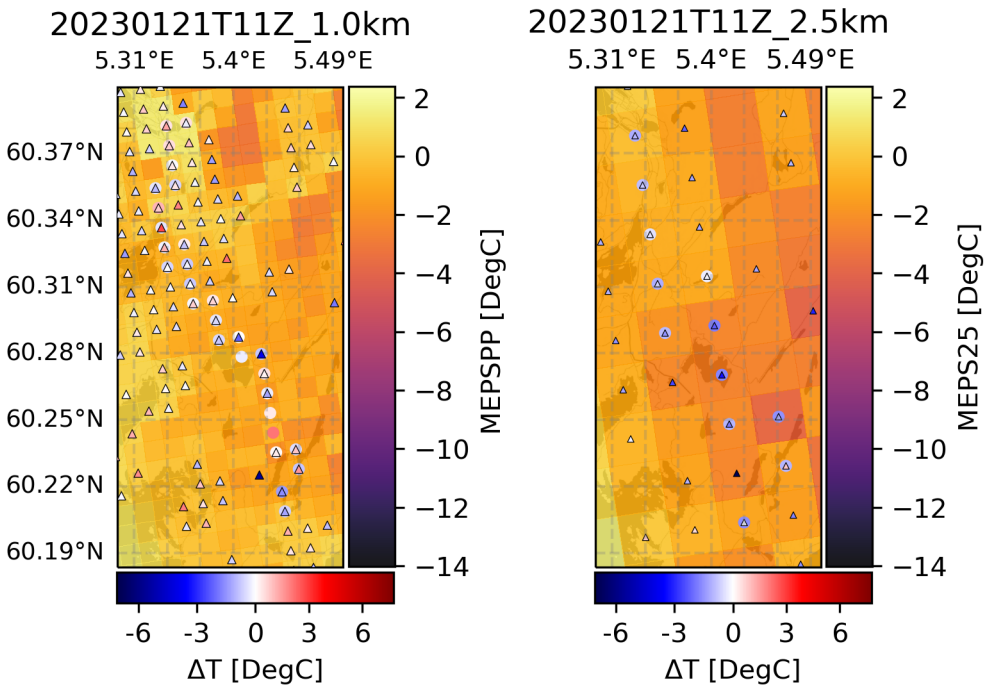

Figure 4.14: Model bias from iMet(points) and Netatmo(triangles) to the MEPS 1km post-processed model (left), and MEPS 2,5km model (right), represented by mesh grids over a map tile, all observations are averaged by grid cell, time: 21.01.2023 11Z. Map tiles by Stamen Design, under CC BY 3.0. Data by OpenStreetMap, under ODbL.

Around midday of January 21^{st}, 2023 (figs: 4.13 & 4.14), the bias has reversed and weakened in magnitude. The 2.5km model is almost exclusively negatively biased, which is again primarily corrected by the observations in the 1.0km model. The strongest bias in the 2.5km model is found near the middle of the domain, next to a large body of water. In comparison, the most significant anomaly is located in the southern area for the 1.0km model (fig: 4.13).

Interestingly, the post-processing performed in the 1.0km product fits better with the iMet measurements than the Netatmo observations for the lake, as mentioned earlier in section 4.1.7. Remember that the Netatmo measurements are grid averaged and are likely further away from the water. Overall, the Netatmo and iMet measurements indicate an accurate analysis, as there is little model bias in the domain, potentially helped by the stable conditions, resulting in less temperature variability.

4.1.9 Bergen 26.01.2023 23:00 UTC

The evening of January 26^{th}, 2023 (figs: 4.15 & 4.16), shows a similar bias to the analysis at 26.01.2022, 23:00 (section 4.1.7), but with a smaller magnitude. Biases are mostly positive for the road measurements and mixed for Netatmo observations hovering around $-2°C$ to $2°C$ for most areas, with a mostly negative bias in the northern domain, south of the city center. The car observations are more stable causing a consistent weak warm bias in the models throughout the domain, with the warmest anomaly at the lake in the center of the domain(fig: 4.15). Grid-averaged iMet values are similar to the gridded Netatmo counterparts close to the road, albeit reporting a weak warm model bias instead of the weak cold bias that is prevalent from the Netatmo data (fig: 4.16).

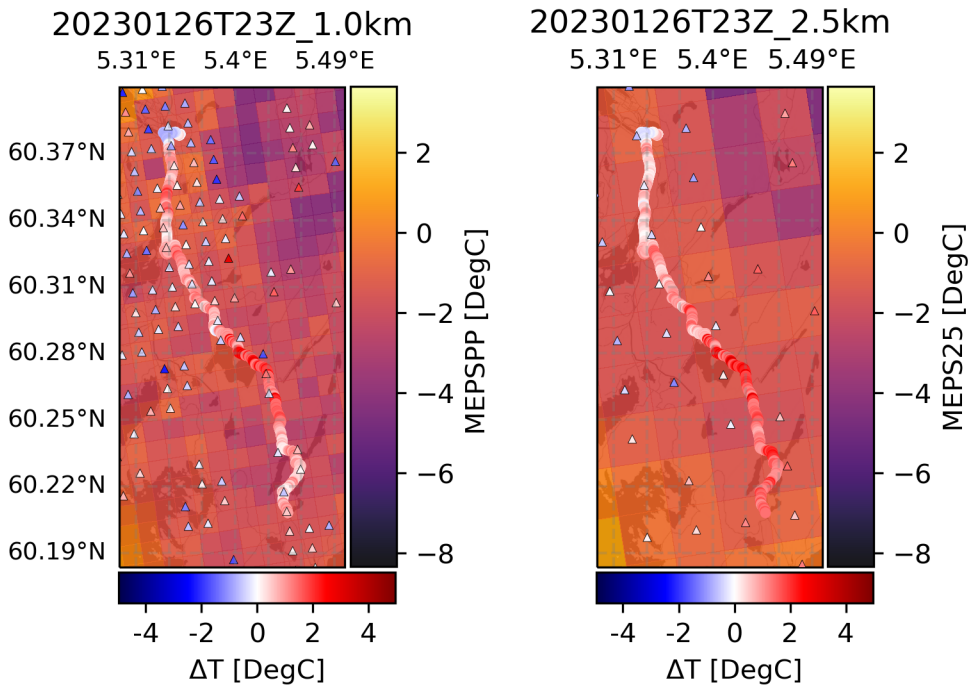

Figure 4.15: Model bias from iMet(points) and Netatmo(triangles) to the MEPS 1km post-processed model (left), and MEPS 2,5km model (right), represented by mesh grids over a map tile, Netatmo observations are averaged by grid cell, time: 26.01.2023 23Z. Map tiles by Stamen Design, under CC BY 3.0. Data by OpenStreetMap, under ODbL.

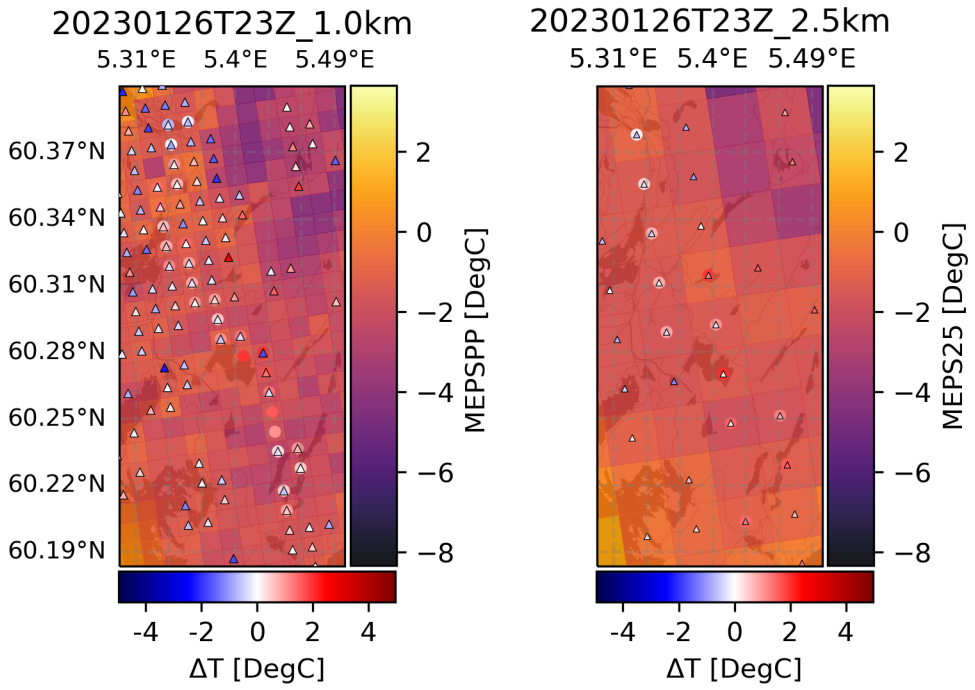

Figure 4.16: Model bias from iMet(points) and Netatmo(triangles) to the MEPS 1km post-processed model (left), and MEPS 2,5km model (right), represented by mesh grids over a map tile, all observations are averaged by grid cell, time: 26.01.2023 23Z. Map tiles by Stamen Design, under CC BY 3.0. Data by OpenStreetMap, under ODbL.

4.1.10 Bergen 27.02.2023 11:00 UTC

The remaining car measurements were influenced by a prolonged weather situation associated with a sudden stratospheric warming, caused by a disruption of the polar vortex, that occurred at the end of February 2023 (*Liberto*, 2023), causing cold and stable weather for the remainder of the observing period. Nevertheless, the evening of February 27^{th}, 2023 (figs: 4.17 & 4.18), features a robust and cold model bias for both Netatmo and iMet observations in the 2.5km model. It persists in the 1.0km model with a diminished but significant magnitude, except for the Netatmo readings, which now include positive biases in several locations over the entire domain.

Note the pronounced warm zone in the northwestern corner of the 1.0km model domain (fig: 4.17), covering Danmarksplass, Solheimsviken, Møllendal, and Nygård, among others. The area experiences large amounts of traffic and experiences great heating on warm, clear days, and likely some heat exchange with Store Lungegårdsvann and Damsgårdssundet on cold days (the area in the northwestern corner in fig 4.17, obscured by the positive bias markers from the car observations. Both iMet and Netatmo measurements suggest a correction due to the warm bias, albeit lesser in magnitude than the cold bias in the 2.5km model.

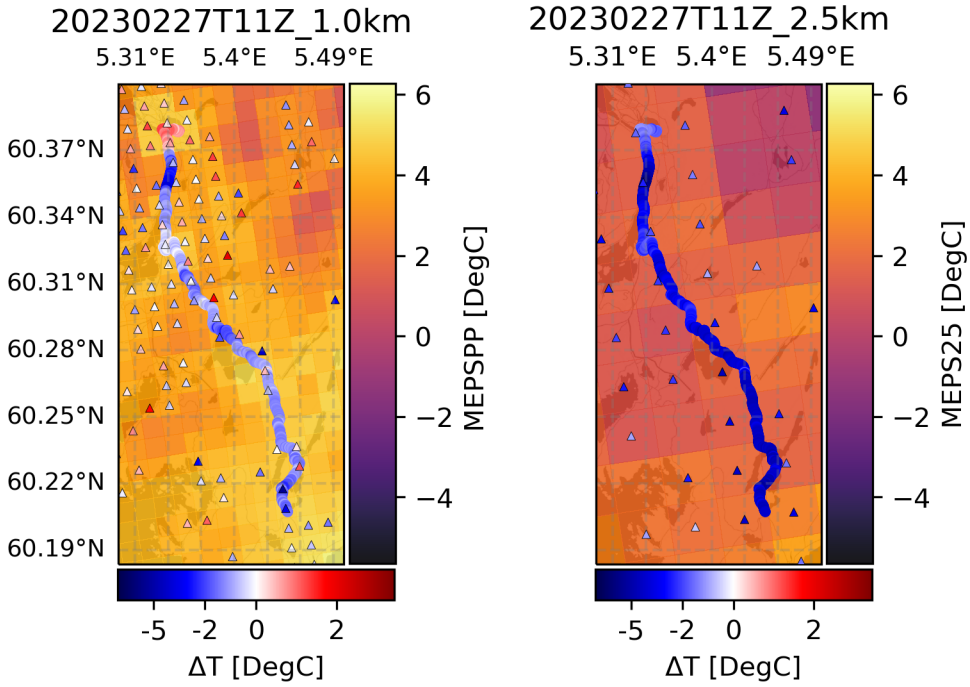

Figure 4.17: Model bias from iMet(points) and Netatmo(triangles) to the MEPS 1km post-processed model (left), and MEPS 2,5km model (right), represented by mesh grids over a map tile, Netatmo observations are averaged by grid cell, time: 27.02.2023 11Z. Map tiles by Stamen Design, under CC BY 3.0. Data by OpenStreetMap, under ODbL.

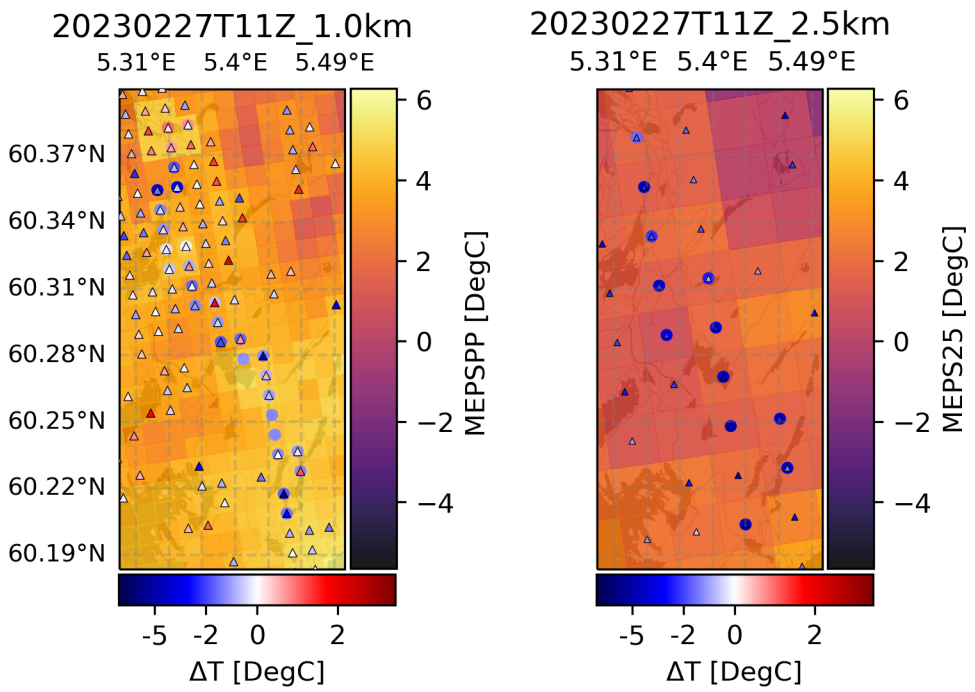

Figure 4.18: Model bias from iMet(points) and Netatmo(triangles) to the MEPS 1km post-processed model (left), and MEPS 2,5km model (right), represented by mesh grids over a map tile, all observations are averaged by grid cell, time: 27.02.2023 11Z. Map tiles by Stamen Design, under CC BY 3.0. Data by OpenStreetMap, under ODbL.

4.1.11 Bergen 27.02.2023 23:00 UTC

On February 27^{th}, 2023, there is again an evening bias (figs: 4.19 & 4.20), as shown before on 20.01.2022 23:00 UTC (sections: 4.1.7 & 4.1.9). The bias is weak overall but has some problems for RWF, such as the areas with temperatures between $0°C$ and $4°C$ with warm biases indicating actual temperatures of below $0°C$, that are not forecasted. Forecast errors at these temperatures potentially result in reduced readiness among road maintenance workers and perhaps a lack of preventative measures for slippery conditions.

The 1.0km forecast shows limited correction, likely due to the Netatmo observations showing little to no bias in the 2.5km model, except for the southernmost section, which has a warm bias in both observation sets.

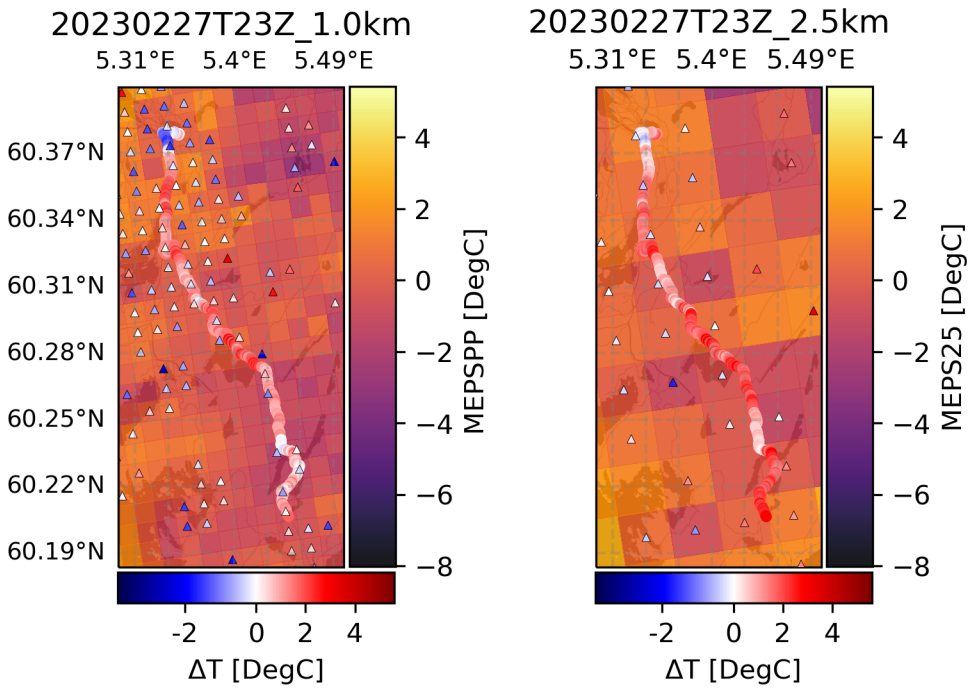

Figure 4.19: Model bias from iMet(points) and Netatmo(triangles) to the MEPS 1km post-processed model (left), and MEPS 2,5km model (right), represented by mesh grids over a map tile, Netatmo observations are averaged by grid cell, time: 27.02.2023 23Z. Map tiles by Stamen Design, under CC BY 3.0. Data by OpenStreetMap, under ODbL.

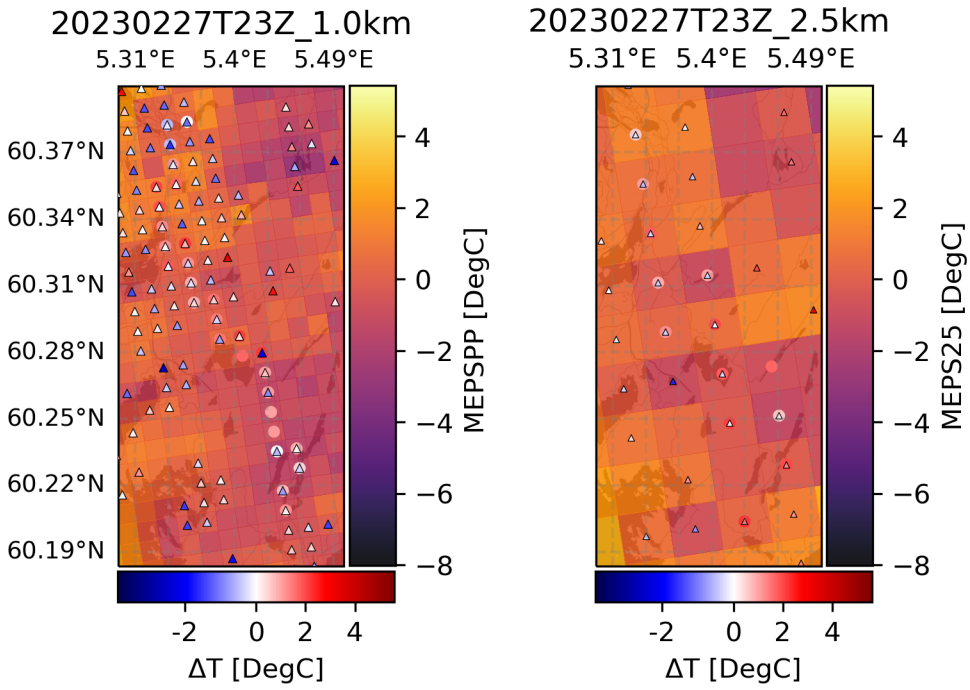

Figure 4.20: Model bias from iMet(points) and Netatmo(triangles) to the MEPS 1km post-processed model (left), and MEPS 2,5km model (right), represented by mesh grids over a map tile, all observations are averaged by grid cell, time: 27.02.2023 23Z. Map tiles by Stamen Design, under CC BY 3.0. Data by OpenStreetMap, under ODbL.

4.1.12 Bergen 28.02.2023 11:00 UTC

Daytime measurements on February 28^{th}, 2023, follow the patterns of the previous day described in section 4.1.10, with a strong cold bias in the 2.5km model for both observation sets (figs: 4.21 & 4.22), and a reduced, yet significant cold bias in the 1.0km model for the car observations. Biases with respect to Netatmo observation are mixed in the 1.0km model, with a negative tendency across the domain.

The warm section in the northwestern corner, covering the Bergen city center on 27.02.2022, 11:00 UTC (fig: 4.17 has returned and is more pronounced. Again, the iMet and Netatmo data give strong warm model biases, indicating another potential overcorrection. It is interesting, as it is the only large area with a consistently strong warm bias.

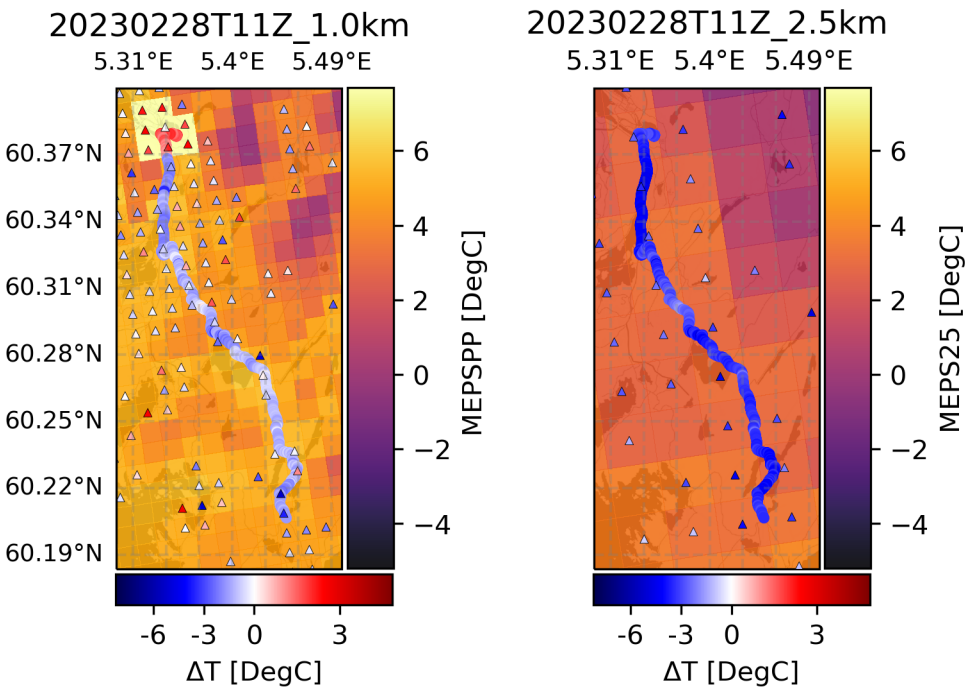

Figure 4.21: Model bias from iMet(points) and Netatmo(triangles) to the MEPS 1km post-processed model (left), and MEPS 2,5km model (right), represented by mesh grids over a map tile, Netatmo observations are averaged by grid cell, time: 28.02.2023 11Z. Map tiles by Stamen Design, under CC BY 3.0. Data by OpenStreetMap, under ODbL.

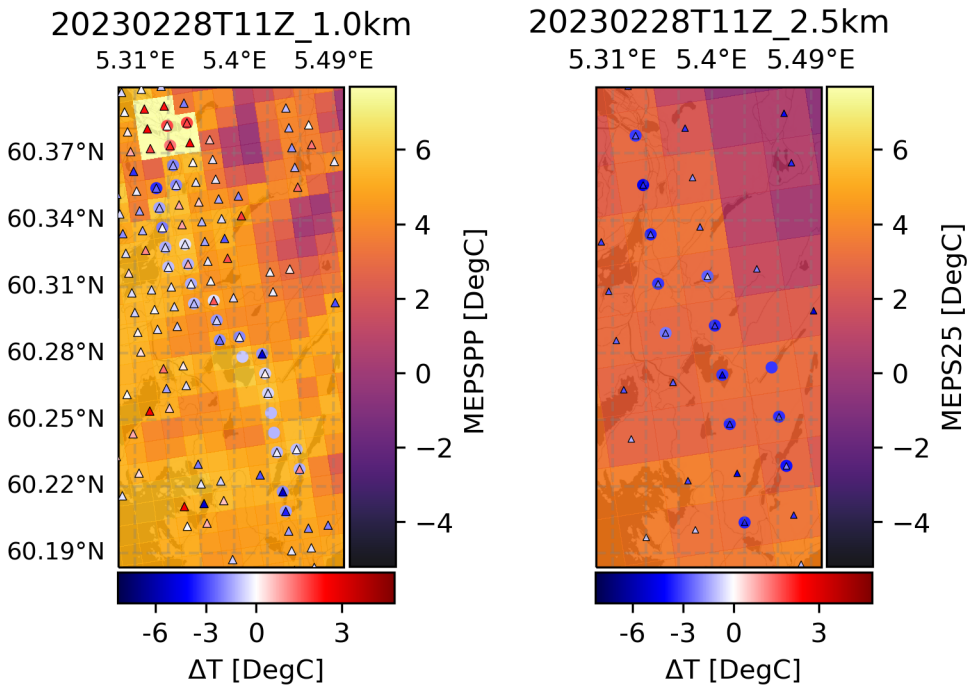

Figure 4.22: Model bias from iMet(points) and Netatmo(triangles) to the MEPS 1km post-processed model (left), and MEPS 2,5km model (right), represented by mesh grids over a map tile, all observations are averaged by grid cell, time: 28.02.2023 11Z. Map tiles by Stamen Design, under CC BY 3.0. Data by OpenStreetMap, under ODbL.

4.1.13 Bergen 28.02.2023 23:00 UTC

The evening of February 28^{th}, 2023 (figs: 4.23 & 4.24), diverges from the previous evening/nighttime by having a lightly mixed bias for Netatmo and iMet readings on both models. The mean biases are lower than $0.45°C$ in magnitude for both the iMet and Netatmo data (table 4.2). There are some outliers, with the stronger ones found in the Netatmo data next to bodies of water, potentially influencing the temperature through heat exchange, causing temperatures to be higher than forecast, resulting in a cold bias.

The low biases in the 2.5km model and 1.0km model might be caused by a more uniform temperature distribution both vertically and horizontally, as the mountaintops are not as pronounced as on previous days (figs: 4.11,4.15, & 4.19), and there is less variation in temperature along the road and domain in general. Resulting in an accurate forecast according to the observations, especially for the grid averaged observations (fig: 4.24).

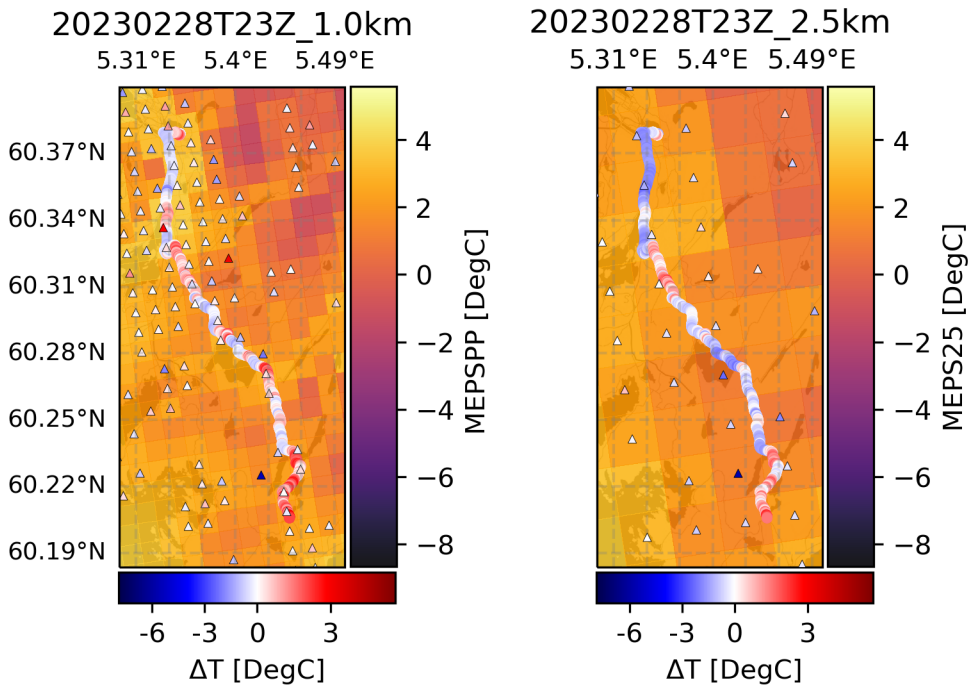

Figure 4.23: Model bias from iMet(points) and Netatmo(triangles) to the MEPS 1km post-processed model (left), and MEPS 2,5km model (right), represented by mesh grids over a map tile, Netatmo observations are averaged by grid cell, time: 28.02.2023 23Z. Map tiles by Stamen Design, under CC BY 3.0. Data by OpenStreetMap, under ODbL.

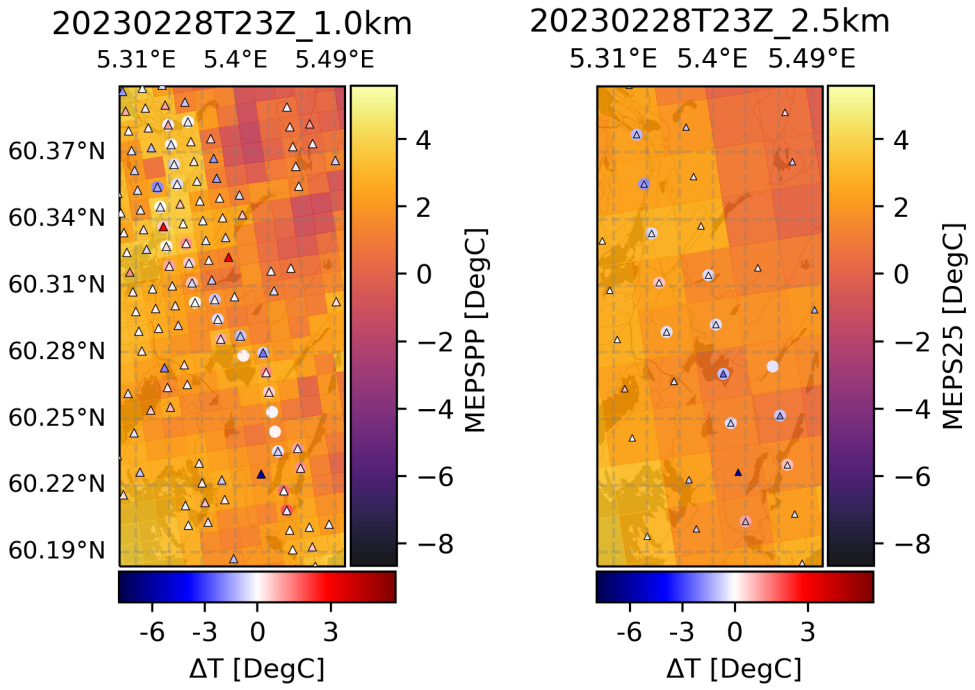

Figure 4.24: Model bias from iMet(points) and Netatmo(triangles) to the MEPS 1km post-processed model (left), and MEPS 2,5km model (right), represented by mesh grids over a map tile, All observations are averaged by grid cell, time: 28.02.2023 23Z. Map tiles by Stamen Design, under CC BY 3.0. Data by OpenStreetMap, under ODbL.

4.1.14 Bergen 01.03.2023 11:00 UTC

Measurements taken during the day on March 1^{st}, 2023 (figs: 4.25 & 4.26) repeat the bias patterns of the previous days described in sections: 4.1.8, 4.1.10, & 4.1.12, with a magnitude on a similar scale as the previous two days. The iMet bias is entirely negative for the 2.5km model, with the Netatmo obs having a max positive bias of $1.4°C$ on the figure border (not visible).

The warm zone at the northwestern corner has returned with the same behavior and size described in sections: 4.1.10, 4.1.12, & 4.1.12.

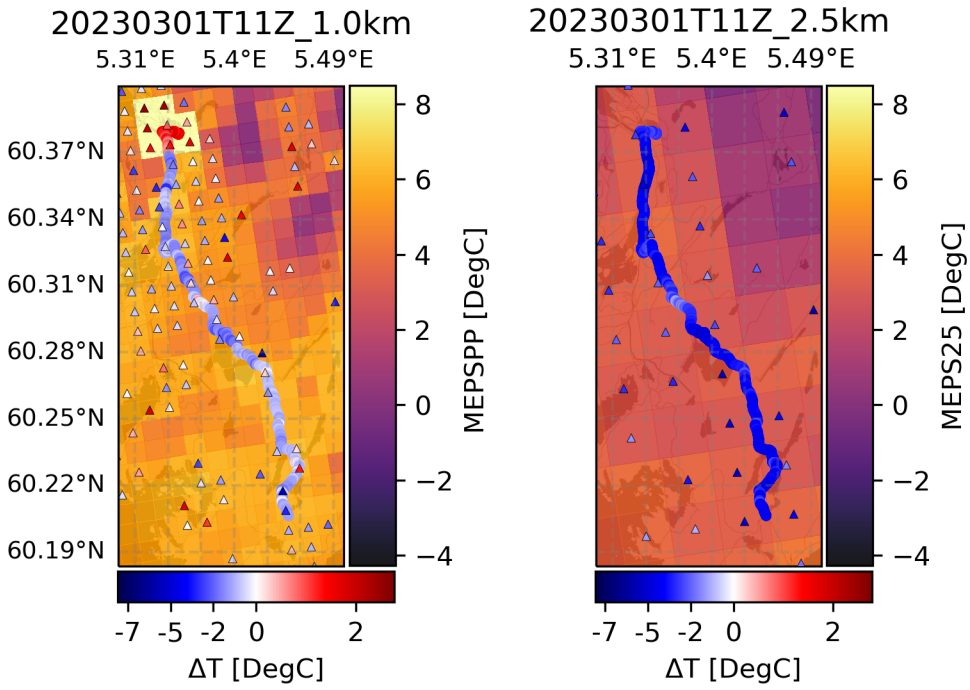

Figure 4.25: Model bias from iMet(points) and Netatmo(triangles) to the MEPS 1km post-processed model (left), and MEPS 2,5km model (right), represented by mesh grids over a map tile, Netatmo observations are averaged by grid cell, time: 01.03.2023 11Z. Map tiles by Stamen Design, under CC BY 3.0. Data by OpenStreetMap, under ODbL.

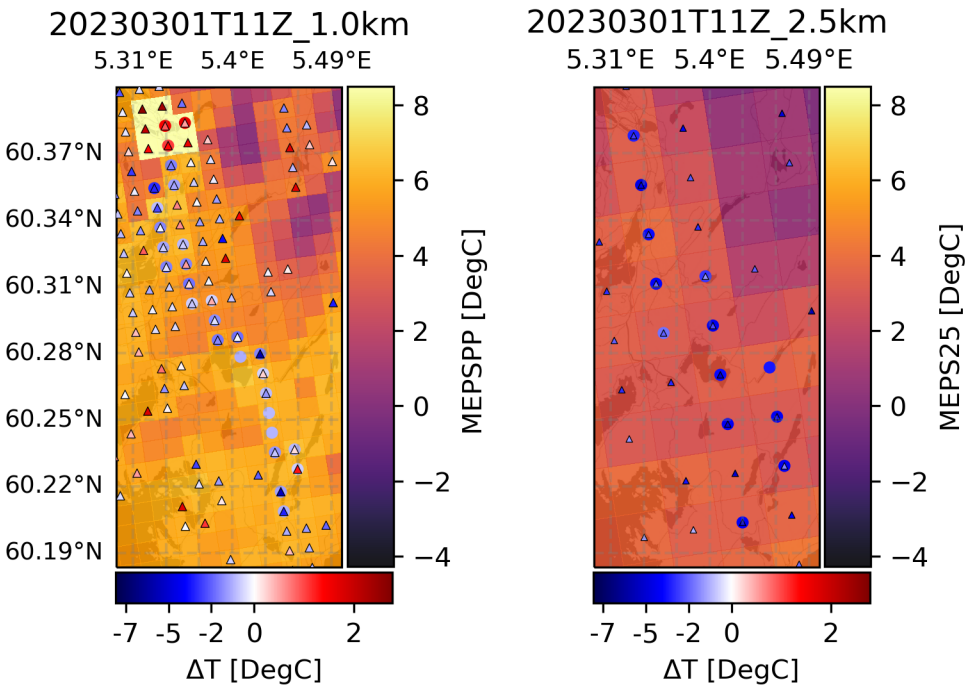

Figure 4.26: Model bias from iMet(points) and Netatmo(triangles) to the MEPS 1km post-processed model (left), and MEPS 2,5km model (right), represented by mesh grids over a map tile, all observations are averaged by grid cell, time: 01.03.2023 11Z. Map tiles by Stamen Design, under CC BY 3.0. Data by OpenStreetMap, under ODbL.

4.1.15 Bergen 01.03.2023 23:00 UTC

Measurements taken during the evening on March 1st, 2023 (figs: 4.27 & 4.28), are similar to the patterns found in previous evening runs, with a strong positive bias on the iMet measurements, for both models and Netatmo observation close to the road with little to no bias on the 2.5km, except for the southernmost section which has a pronounced warm bias. The 1.0km model still produces mixed biases with a tendency toward a cold bias compared with Netatmo data.

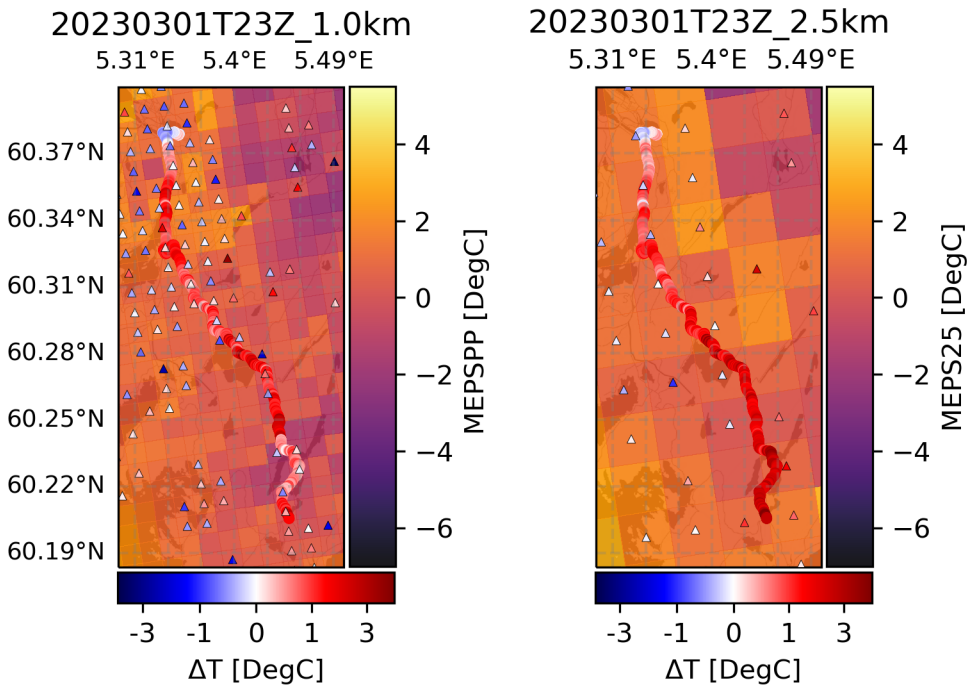

Figure 4.27: Model bias from iMet(points) and Netatmo(triangles) to the MEPS 1km post-processed model (left), and MEPS 2,5km model (right), represented by mesh grids over a map tile, Netatmo observations are averaged by grid cell, time: 01.03.2023 23Z. Map tiles by Stamen Design, under CC BY 3.0. Data by OpenStreetMap, under ODbL.

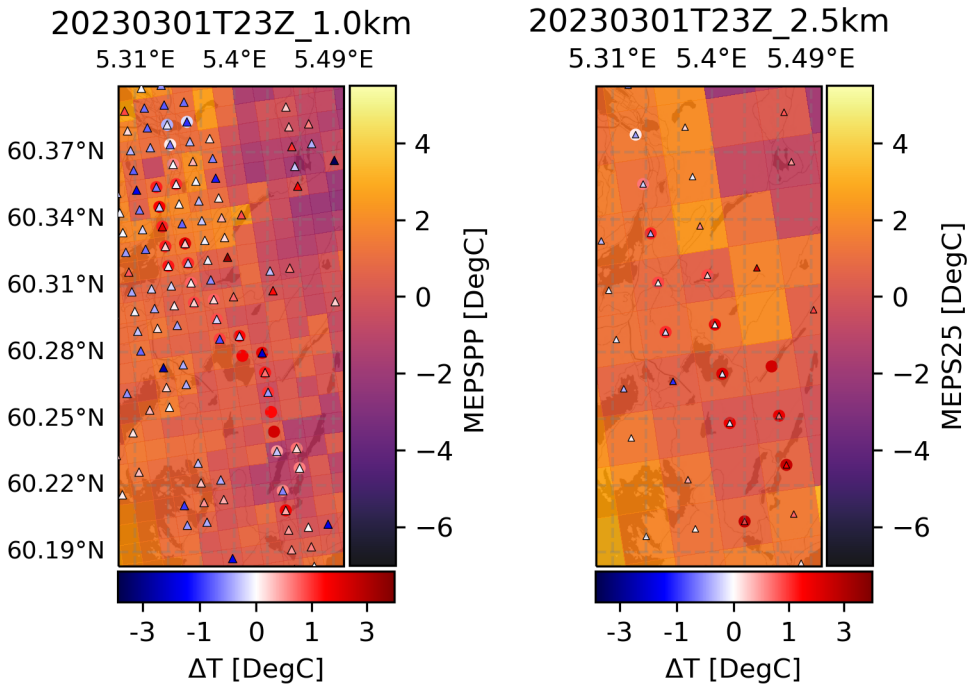

Figure 4.28: Model bias from iMet(points) and Netatmo(triangles) to the MEPS 1km post-processed model (left), and MEPS 2,5km model (right), represented by mesh grids over a map tile, all observations are averaged by grid cell, time: 01.03.2023 23Z. Map tiles by Stamen Design, under CC BY 3.0. Data by OpenStreetMap, under ODbL.

4.1.16 Bergen statistics

Based on the iMet measurements, it appears that the models used have distinct biases during the day and night. During the night, the model temperatures are warmer than the observations, causing warm biases. Conversely, during the day, the model temperatures are colder than the observations, resulting in cold biases. It's possible that the models react slowly to temperature changes caused by the diurnal cycle and advected air masses, especially in areas close to the road. For the 1.0 km model, the mean bias is positive for all evening runs, but negative for the daytime runs. The 2.5 km model follows the same pattern, except for the evening of February 28th, where there is a negative bias of -0.391$°C$.

Netatmo mean bias is negative during all car runs but is of greater magnitude during the daytime runs for both 1.0km and 2.5km models. Remember that these are not the plotted values; they were grid averaged to not obscure the plots. The grid averaged Netatmo-related mean bias is still negative for all but two runs for the 1.0km and three runs for the 2.5km, where the positive mean biases are from night observations (table 4.3). Still, the positive biases are more than a degree colder than those corresponding to the iMet observations, suggesting a significant difference in temperature, and questioning whether the Netatmo observations are representative of road conditions.

Further investigation shows that the mean daytime bias related to the iMets is twice that of those related to the Netatmo observations in the 1.0km model, with values of $-0.82°C$ and $-0.41°C$ respectively. The mean nighttime bias shows the biggest discrepancy with bias values of $1.01°C$ for the 1.0km iMet-related bias, and $-0.12°C$ for the 1.0km Netatmo-related bias. Interestingly, the difference in bias in relation to the iMet and Netatmo observations doubles at nighttime.

It appears that the 1.0km model is generating warmer temperatures compared to the iMet observations. This discrepancy could be attributed to the incorporation of Netatmo data during the model's post-processing. It's essential to acknowledge that Netatmo readings may be affected by heat emissions from their surroundings. These sensors are typically situated on structures like residential buildings, leaving them susceptible to external factors, such as heat emanating from vents, open windows, and poor insulation. If the Netatmo stations are affected by these variables and report higher temperatures than the model, it would result in a cold bias, which could potentially alter the model output.

All minimums are negative, meaning no positive biases. However, not all maximums are positive; daytime runs in February/March have negative maximums for the car observations, implying a cold tendency in the model at noon, local time. As this is a recurring observation, over varying non-precipitating conditions, observed in relation to both iMet and Netatmo observations, it is likely caused by the models' radiation schemes and the ability of the surface to absorb and emit shortwave/longwave radiation. Resulting in the model bias related to the iMet measurements being entirely negatively biased, meaning the model is too cold for the entire period according to the car observations.

Minimums are not all negative for the grid-averaged iMet measurements, with the 2.5km model showing positive values for 4/5 nighttime observations. Still, the maximums retain their sign, having positive values for all nighttime observations, resulting in the runs at Jan 20^{th}, Jan 26^{th}, Feb 23^{rd}, and Mar 1^{st} for the 2.5km model being entirely positively biased. Leading to an overestimation of temperature along the road according

to the iMet observations, which could prove problematic if the temperature is close to the freezing point.

The 1.0km model has a maximum standard deviation of $1.35°C$, while the 2.5km model has a maximum of $1.85°C$, in relation to the iMet observations (tab: 4.2). In contrast, the Netatmo observations have a higher maximum standard deviation of $1.99°C$ and $2.08°C$, respectively (tab: 4.2). On average, the Netatmo observations exhibit higher values, which can be attributed to a larger variation in station placement, particularly in terms of verticality. This includes remote data from mountainsides, coastal areas, and everything in between.

The standard deviation of iMet-related data has an average of $1.0°C$ for the 1.0km model and $0.9°C$ for the 2.5km model(tab: 4.2). In comparison, Netatmo observations show a standard deviation of $1.5°C$ and $1.6°C$ for the 1.0km and 2.5km models, respectively (tab: 4.2). The iMet-related mean standard deviation is likely smaller due to the consistent road surface and lack of frequent large altitude changes during observations, unlike the Netatmo data. Grid-averaged standard deviation values follow the same pattern but have slightly lower values due to the averaging out of some of the extreme values (tab: 4.3).

The 1.0km model shows little variation in RMSE in relation to the iMet observations between day and nighttime for the full dataset, with only a $0.01°C$ difference in mean RMSE. In contrast, the Netatmo-related RMSE is lower than the corresponding iMet-related RMSE for nighttime observations, but higher during the day with a difference of nearly $0.5°C$. The 2.5km model has a higher RMSE for both observation sets, with an especially high error during the day, likely due to varying solar insolation due to cloud cover, and sun angle affecting heat absorption in conjunction with vegetation and local topography.

Interestingly when grid averaging the Netatmo observations there is an increase in nighttime error, and a decrease in the daytime error, indicating that a substantial portion of the daytime error is linked to outliers in the datasets related to heating. The grid averaging of the iMet observations does not produce a large difference in RMSE during the day, likely because the instrument is actively cooled by a constant flow of fresh air, reducing the impact of insolation, and heating emitted by the car.

Table 4.2: Temperature anomaly statistics between iMet and Netatmo observations to the MEPS 1.0km post-processed product, and MEPS 2.5km model for the Bergen route

MEPS - iMet											
Datetime	Min	Min	Max	Max	Bias	Bias	Stdev	Stdev	MSE	MSE	RMSE	RMSE
	1.0km	2.5km	1.0km	2.5km	1.0km	2.5km	1.0km	2.5km	1.0km	2.5km	1.0km	2.5km
20230120T23Z	-1.216	-0.543	6.372	9.205	1.618	3.048	1.345	1.849	4.424	12.709	2.103	3.565
20230121T11Z	-2.082	-3.258	2.927	1.520	-0.135	-1.186	0.855	0.748	0.750	1.966	0.866	1.402
20230126T23Z	-1.090	-0.630	3.209	3.358	0.850	1.004	0.693	0.675	1.202	1.462	1.096	1.209
20230227T11Z	-4.272	-5.826	1.690	-1.291	-1.145	-3.683	1.151	1.007	2.635	14.578	1.623	3.818
20230227T23Z	-1.570	-0.525	3.580	3.773	0.992	1.407	0.782	0.729	1.596	2.510	1.263	1.584
20230228T11Z	-3.511	-5.179	2.110	-1.471	-0.991	-3.468	1.108	0.585	2.209	12.370	1.486	3.517
20230228T23Z	-2.170	-2.399	3.114	2.542	0.301	-0.391	0.970	1.089	1.031	1.339	1.015	1.157
20230301T11Z	-3.536	-5.782	2.330	-1.136	-1.024	-4.000	1.291	0.644	2.715	16.413	1.648	4.051
20230301T23Z	-1.050	-0.679	3.579	3.996	1.298	1.709	0.786	0.869	2.303	3.674	1.517	1.917

MEPS - Netatmo											
Datetime	Min	Min	Max	Max	Bias	Bias	Stdev	Stdev	MSE	MSE	RMSE	RMSE
	1.0km	2.5km	1.0km	2.5km	1.0km	2.5km	1.0km	2.5km	1.0km	2.5km	1.0km	2.5km
20230120T23Z	-5.511	-5.250	13.454	13.191	-0.057	-0.008	1.750	2.084	3.065	4.344	1.751	2.084
20230121T11Z	-5.672	-7.089	7.773	7.425	-0.081	-0.937	1.203	1.330	1.455	2.646	1.206	1.627
20230126T23Z	-4.672	-4.963	6.346	7.282	-0.162	-0.059	1.223	1.376	1.521	1.896	1.233	1.377
20230227T11Z	-8.041	-10.059	4.300	2.505	-0.553	-2.705	1.899	1.926	3.913	11.030	1.978	3.321
20230227T23Z	-4.418	-4.913	7.577	7.345	-0.117	-0.024	1.232	1.484	1.532	2.201	1.238	1.484
20230228T11Z	-7.385	-10.385	5.400	3.014	-0.421	-2.719	1.804	1.840	3.431	10.779	1.852	3.283
20230228T23Z	-6.528	-7.909	6.551	6.177	-0.051	-0.441	1.026	1.147	1.055	1.510	1.027	1.229
20230301T11Z	-7.468	-10.279	7.100	2.783	-0.577	-3.413	1.993	2.006	4.305	15.672	2.075	3.959
20230301T23Z	-4.061	-4.292	6.900	7.271	-0.206	-0.157	1.288	1.449	1.702	2.125	1.305	1.458

Table 4.3: Temperature anomaly statistics between grid averaged iMet and Netatmo observations to the MEPS 1.0km post-processed product, and MEPS 2.5km model for the Bergen route

MEPS - grid averaged iMet										
Datetime	Min 1.0km	Min 2.5km	Max 1.0km	Max 2.5km	Bias 1.0km	Bias 2.5km	Stdev 1.0km	Stdev 2.5km	MSE 1.0km	MSE 2.5km	RMSE 1.0km	RMSE 2.5km
20230120T23Z	-0.131	1.511	4.746	7.036	1.890	3.476	1.296	1.895	5.254	15.674	2.292	3.959
20230121T11Z	-1.330	-1.794	2.116	-0.268	-0.108	-1.124	0.664	0.444	0.453	1.462	0.673	1.209
20230126T23Z	-0.660	0.156	2.018	2.055	0.965	1.167	0.602	0.557	1.294	1.672	1.138	1.293
20230227T11Z	-4.083	-4.575	1.287	-1.961	-1.350	-3.813	1.109	0.789	3.055	15.165	1.748	3.894
20230227T23Z	-0.525	0.603	2.212	2.208	1.156	1.463	0.725	0.554	1.862	2.447	1.364	1.564
20230228T11Z	-3.436	-4.364	1.796	-2.206	-1.083	-3.329	1.084	0.501	2.348	11.336	1.532	3.367
20230228T23Z	-1.827	-1.685	1.908	1.015	0.211	-0.393	0.842	0.749	0.754	0.716	0.868	0.846
20230301T11Z	-3.397	-4.586	2.038	-2.233	-1.199	-3.865	1.155	0.593	2.772	15.288	1.665	3.910
20230301T23Z	-0.545	0.157	2.543	2.766	1.375	1.828	0.695	0.719	2.373	3.858	1.540	1.964
MEPS - grid averaged Netatmo												
Datetime	Min 1.0km	Min 2.5km	Max 1.0km	Max 2.5km	Bias 1.0km	Bias 2.5km	Stdev 1.0km	Stdev 2.5km	MSE 1.0km	MSE 2.5km	RMSE 1.0km	RMSE 2.5km
20230120T23Z	-3.816	-5.250	10.299	6.664	0.072	-0.044	1.481	1.915	2.198	3.671	1.483	1.916
20230121T11Z	-5.672	-7.089	7.773	2.058	-0.101	-1.002	1.068	1.426	1.152	3.036	1.073	1.742
20230126T23Z	-4.672	-4.963	4.965	3.225	-0.077	0.289	0.947	1.173	0.902	1.460	0.950	1.208
20230227T11Z	-6.734	-6.749	4.294	1.538	-0.576	-2.699	1.359	1.252	2.180	8.855	1.477	2.976
20230227T23Z	-3.260	-3.863	5.604	3.237	0.018	0.265	0.937	1.284	0.879	1.720	0.938	1.311
20230228T11Z	-7.385	-8.235	4.862	2.071	-0.512	-2.752	1.399	1.446	2.218	9.665	1.489	3.109
20230228T23Z	-6.528	-7.909	5.669	3.049	-0.069	-0.432	0.904	1.149	0.821	1.508	0.906	1.228
20230301T11Z	-6.946	-8.077	3.472	1.416	-0.674	-3.505	1.443	1.334	2.537	14.062	1.593	3.750
20230301T23Z	-3.529	-3.648	3.748	3.327	-0.124	0.071	0.940	1.136	0.900	1.295	0.949	1.138

4.2 Forecast validation

4.2.1 Haugesund forecasts for 28.09.2022 22:00 UTC

4 Hour lead time

Starting with the forecast from 18:00 with a four-hour lead time, there is a warm bias throughout the domain for both the 1.0km and the 2.5km models, with a single grid cell having a cold bias relative to the Netatmo temperature(fig: 4.29). The southern half of the domain has lower bias but higher differences between the Netatmo and iMet observations. Compared to the analysis in figure 4.2 (section 4.1.1), the model temperature is substantially different, with the forecast temperature mainly in the $12 - 14°C$ range. In contrast, the analysis stays mainly within the $8 - 12°C$, showing a lower in model temperature for both models.

The grid-averaged iMet-related mean bias is $3.60°C$ for the 1.0km model and $4.13°C$ for the 2.5km model (tab: 4.7). Similarly, the grid-averaged Netatmo-related mean biases are $2.12°C$ and $2.35°C$, respectively (tab: 4.9). These results suggest a consistent temperature difference between the iMet and Netatmo observations, which raises concerns about the representability of Netatmo observations for road conditions.

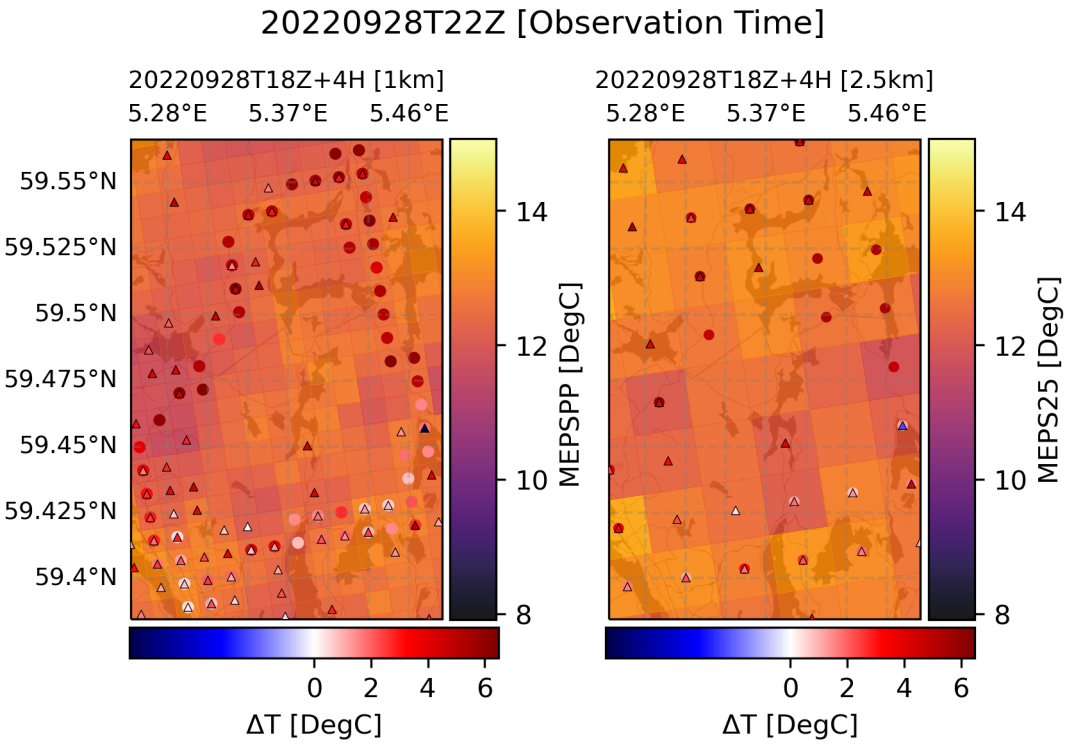

Figure 4.29: Model bias from iMet(points) and Netatmo(triangles) to the MEPS 1km post-processed model (left), and MEPS 2,5km model (right), represented by mesh grids over a map tile, observations are averaged by grid cell, time: 28.09.2022 18Z+4H. Map tiles by Stamen Design, under CC BY 3.0. Data by OpenStreetMap, under ODbL.

10 Hour lead time

Moving on to the forecast from 12:00 with a 10-hour lead time, there is a further increase in model temperature for both models, resulting in a warm bias for the entire domain, with an increase of around $2°C$ (fig: 4.30). The increasing temperature, when looking back to the previous forecast, suggests there might have been a shift in the weather situation, with colder air being advected through the domain.

As expected, mean model bias related to the grid-averaged iMet observations is higher with $6.17°C$ for the 1.0km model and $6.25°C$ for the 2.5km model (tab: 4.7), with Netatmo- related biases of $4.75°C$ and $4.42°C$ (tab: 4.9), respectively. There is a slight difference between the datasets caused by changes in temperature in grid cells that do not have corresponding iMet data. This is noteworthy because the closest Netatmo observation could be in a neighboring grid cell due to the observations being averaged to the model grid.

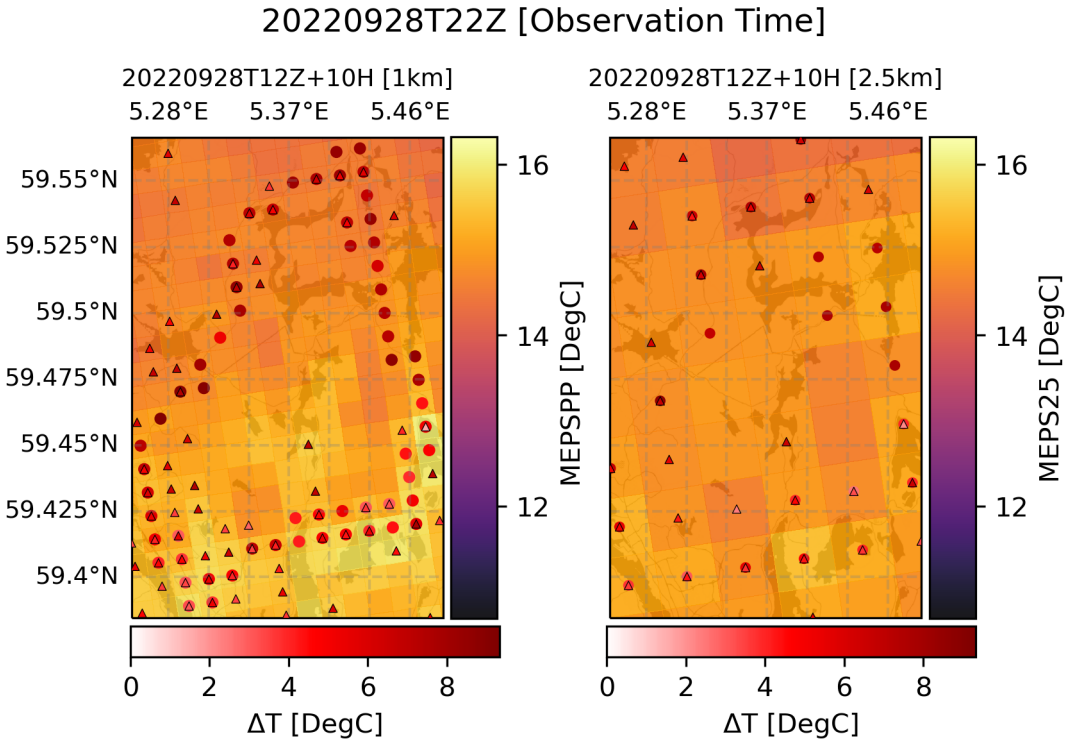

Figure 4.30: Model bias from iMet(points) and Netatmo(triangles) to the MEPS 1km post-processed model (left), and MEPS 2,5km model (right), represented by mesh grid over a map tile, observations are averaged by grid cell, time: 28.09.2022 12Z+10H. Map tiles by Stamen Design, under CC BY 3.0. Data by OpenStreetMap, under ODbL.

16 Hour lead time

The forecast from 06:00 with a 16-hour lead time (fig: 4.31) shows a much better result, with mean bias values of $1.243°C$ (1.0km) and $2.538°C$ (2.5km)(table: 4.7), and bias/temperature distribution mimicking that of the analysis (fig: 4.2, section 4.1.1),

with warmer model biases in the northern domain, with cold spots to the west, southwest, south, and east for the 1.0km model. The 2.5km is more uniform but retains some cold bias spots in the southern domain.

The 1.0km model forecast shows significant variation between the bias related to the iMet and Netatmo, with a greater amount of diverging grid-cell in the southern domain, but also some notable differences in the northern domain around $59.525 - 59.55°N$(fig: 4.31). Indicating varying degrees of representability when considering Netatmo observations for road conditions, once again highlighting the issues when comparing to neighboring grid cells, as these do not have a consistent difference in bias between the datasets.

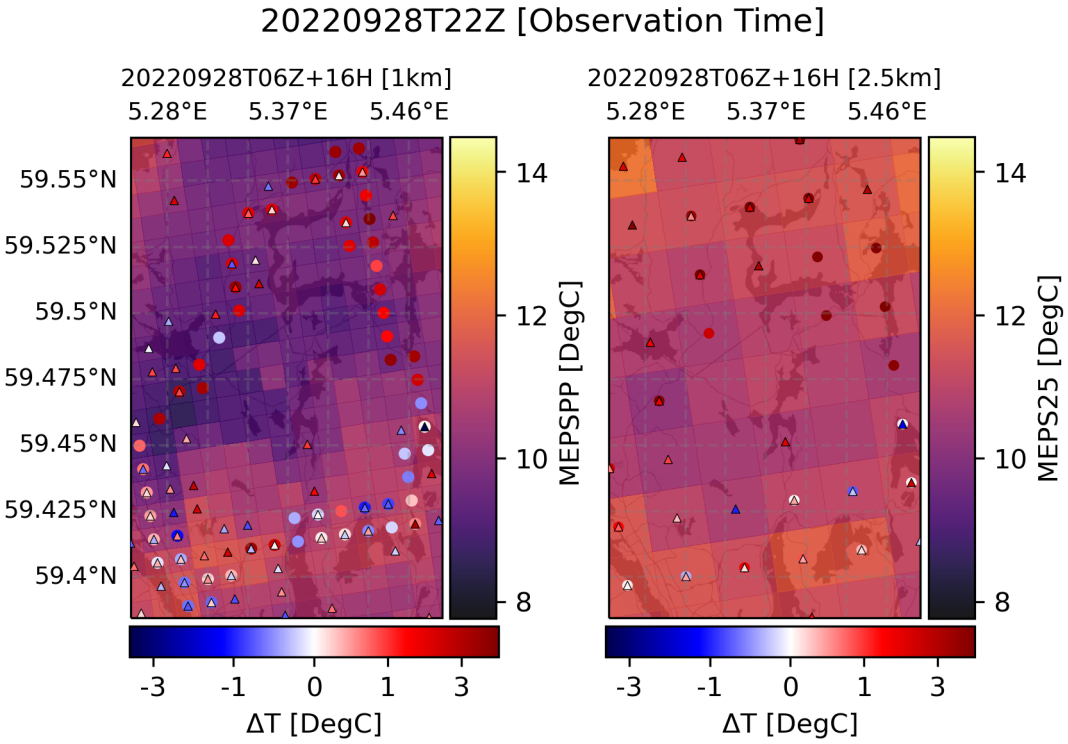

Figure 4.31: Model bias from iMet(points) and Netatmo(triangles) to the MEPS 1km post-processed model (left), and MEPS 2,5km model (right), represented by mesh grid over a map tile, observations are averaged by grid cell, time: 28.09.2022 06Z+16H. Map tiles by Stamen Design, under CC BY 3.0. Data by OpenStreetMap, under ODbL.

22 Hour lead time

For the last forecast initiated at 00:00 with a 22-hour lead time (fig: 4.36), the pattern from 06:00 grows in magnitude, with the cold bias in the southern section expanding, and the northern area retaining its warm bias, resulting in a lower mean bias of just 0.892(1.0km) & 1.586 (2.5km)(table: 4.7). Remember that the mean bias is low due to near equally divided temperature biases between the cold and warm sides and is still significant on the northern and southern sides.

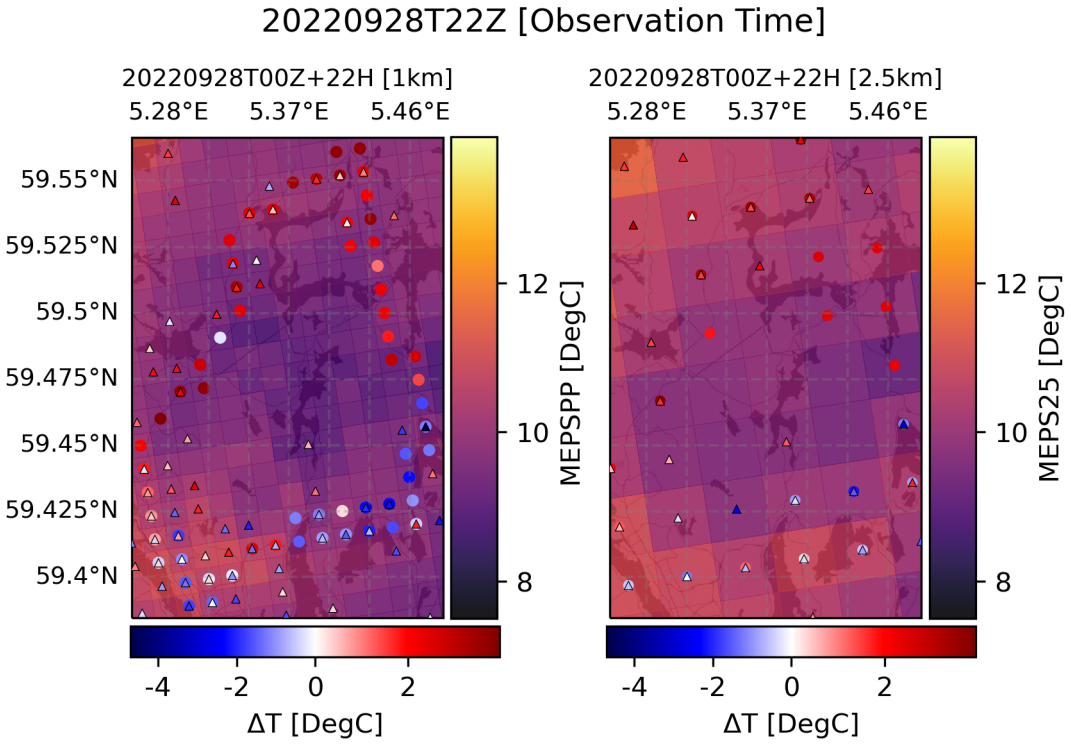

Figure 4.32: Model bias from iMet(points) and Netatmo(triangles) to the MEPS 1km post-processed model (left), and MEPS 2,5km model (right), represented by mesh grid over a map tile, observations are averaged by grid cell, time: 28.09.2022 00Z+22H. Map tiles by Stamen Design, under CC BY 3.0. Data by OpenStreetMap, under ODbL.

4.2.2 Haugesund Forecasts for 29.09.2022 10:00 UTC

4 Hour lead time

The forecast from 06:00 with a four-hour lead time (fig: 4.33) shows a similar temperature distribution to the analysis (fig: 4.6, section 4.1.1), albeit without any of the warm biases. Making the forecast entirely cold-biased for both the 1.0km model and the 2.5km model. With temperature ranges from the models lowered by $4°C$, resulting in a substantial increase in cold bias magnitude for both models.

The pronounced cold bias could have implications for temperature-dependent activities, like road maintenance, and could be caused by inaccurate initial conditions in the models, or an unexpected development in the weather situation. Additionally, it could indicate that the model is too slow to react to heating, as 10:00 UTC was noon local time, which is relatively early in the day.

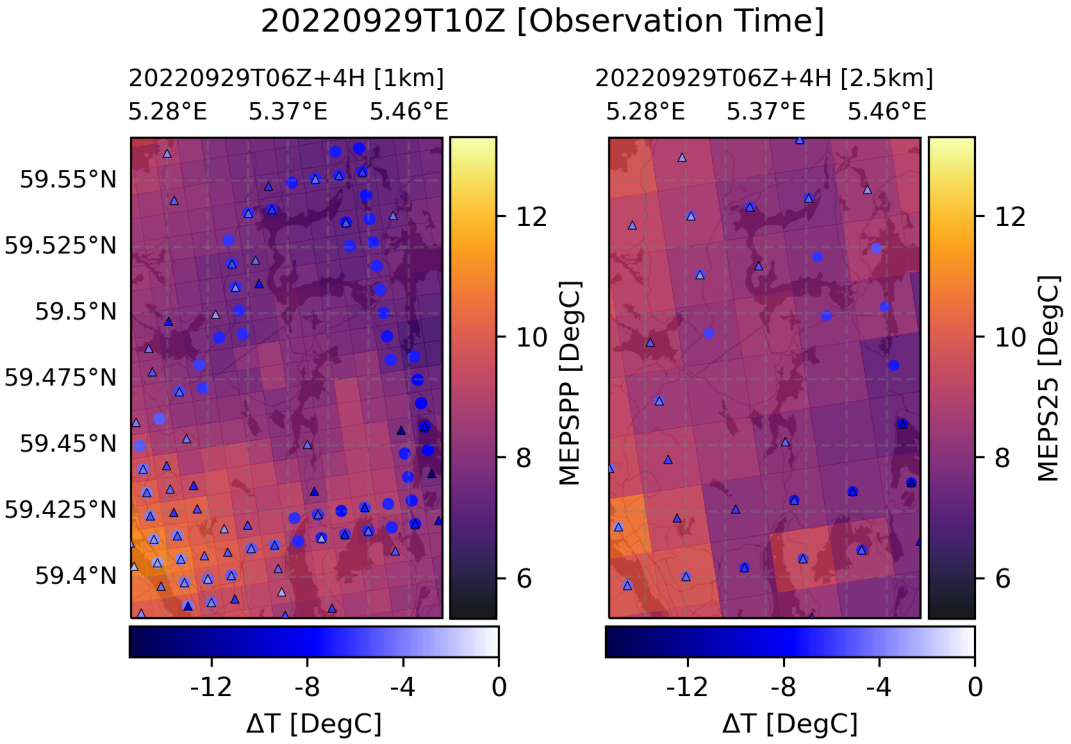

Figure 4.33: Model bias from iMet(points) and Netatmo(triangles) to the MEPS 1km post-processed model (left), and MEPS 2,5km model (right), represented by mesh grid over a map tile, observations are averaged by grid cell, time: 29.09.2022 06Z+4H. Map tiles by Stamen Design, under CC BY 3.0. Data by OpenStreetMap, under ODbL.

10 Hour lead time

The 00:00 forecast with a 10-hour lead time (fig: 4.34) is mostly unchanged from 06:00, but the cold bias in Haugesund has reduced in magnitude across most of the city. Model temperature distribution has changed slightly for both models, with higher temperatures in the northwestern and southwestern corners. The mean model bias from the iMet data is reduced by $\sim 1°C$(table: 4.7). In contrast, the 2.5km bias remains unaffected, with a comparable drop in the model bias relating to Netatmo data (table: 4.9). Resulting in the same implications as in the previous section.

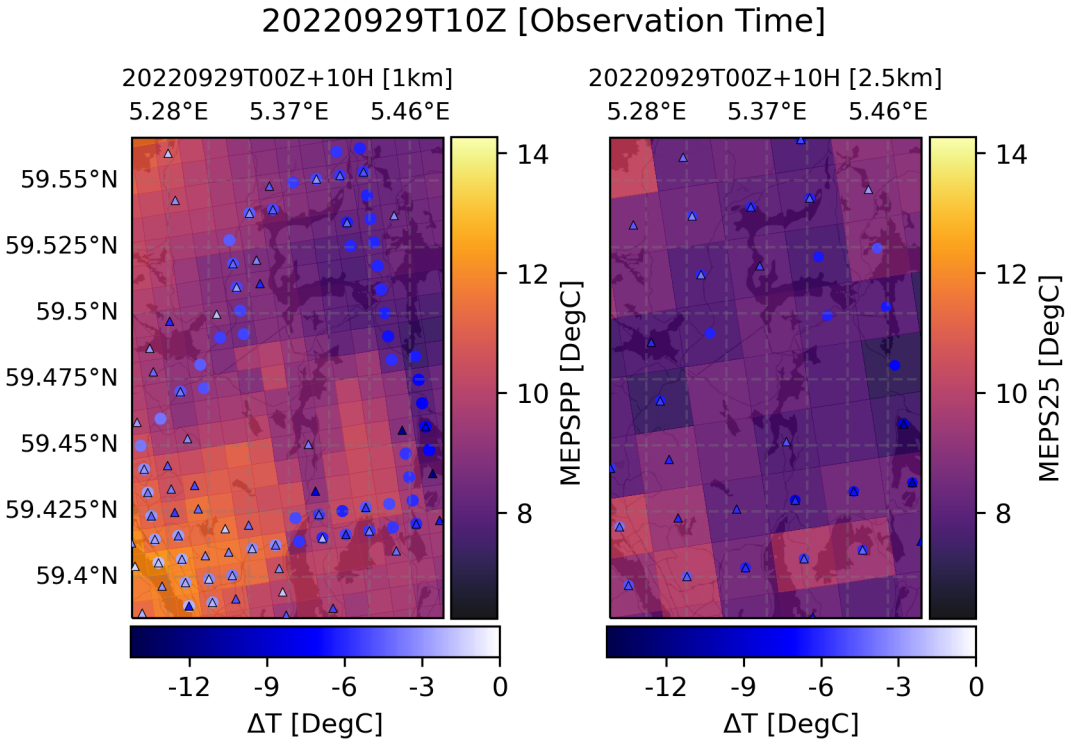

Figure 4.34: Model bias from iMet(points) and Netatmo(triangles) to the MEPS 1km post-processed model (left), and MEPS 2,5km model (right), represented by mesh grid over a map tile, observations are averaged by grid cell, time: 29.09.2022 00Z+10H. Map tiles by Stamen Design, under CC BY 3.0. Data by OpenStreetMap, under ODbL.

16 Hour lead time

Moving further back to 28.09, 18:00 with a 16-hour lead time (fig: 4.35), there is a significant decrease in bias, with the mean biases being more than halved for both 1.0km and 2.5km models concerning iMet and Netatmo observations(tables: 4.7 & 4.9). Resulting in an accurate forecast according to the observations, mainly as biases are almost entirely negative, meaning the local biases are small.

The reduction in bias magnitude reveals a reemergence of the bias difference pattern observed between the iMet and Netatmo observations noted in section 4.2.1. It is intriguing that the bias induced by the Netatmo observations, which lack corresponding iMet observations, appears to be lower or entirely gone for several areas. This difference in bias is likely also affected by the uncertainty in the NWP model, especially the data assimilation and initial conditions. As there are fewer stations when moving away from the city and major roadways.

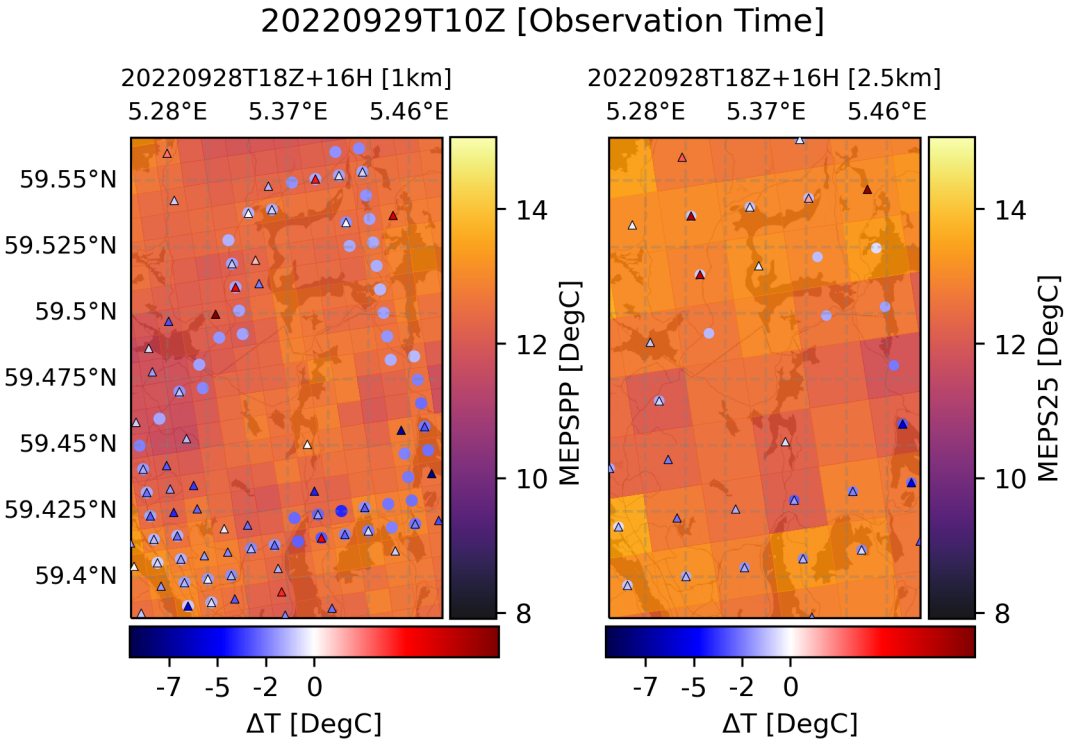

Figure 4.35: Model bias from iMet(points) and Netatmo(triangles) to the MEPS 1km post-processed model (left), and MEPS 2,5km model (right), represented by mesh grid over a map tile, observations are averaged by grid cell, time: 28.09.2022 18Z+16H. Map tiles by Stamen Design, under CC BY 3.0. Data by OpenStreetMap, under ODbL.

22 Hour lead time

Finally, the forecast from 28.09, 12:00 with a 22-hour lead time (fig: 4.36) flips the bias from cold to warm and improves the mean bias for both models and all observations, with all mean bias values below $1°C$ (table: 4.7 & 4.9).

Again, notice that biases are mixed, pushing down the mean bias but retaining high local biases. That being said, the model biases relating to iMet data have improved for most areas, except Haugesund, which has stronger warm biases. Interestingly, the Netatmo-related model biases have greater magnitudes than the iMet-related biases, which are also most pronounced outside of Haugesund.

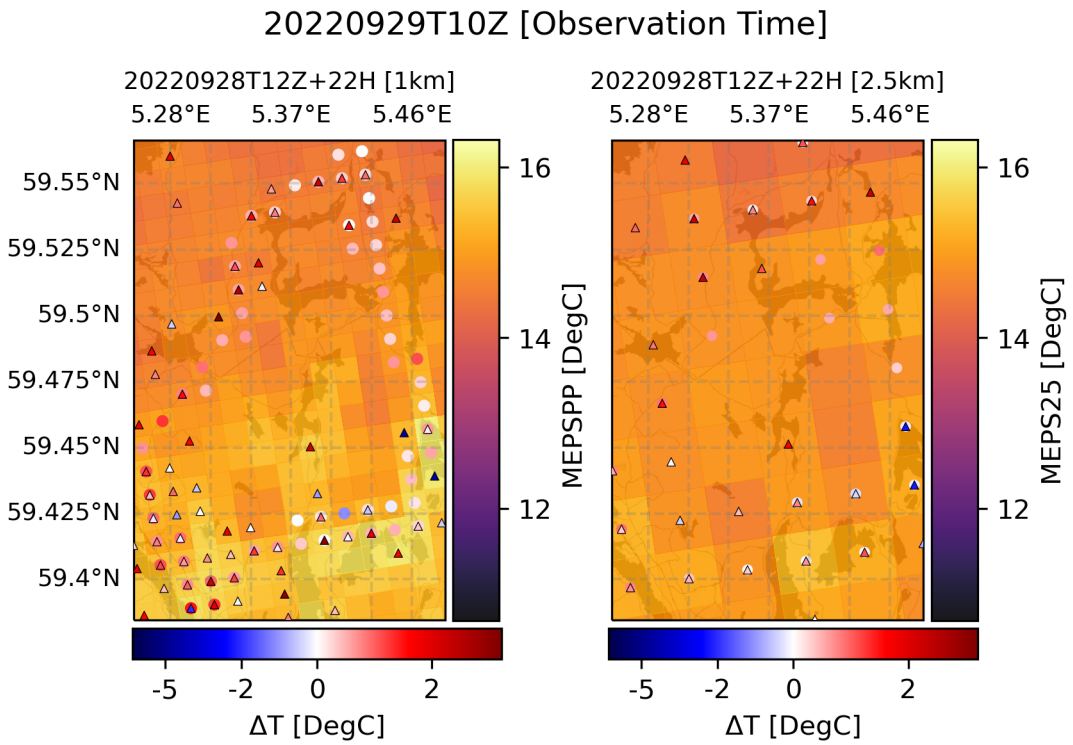

Figure 4.36: Model bias from iMet(points) and Netatmo(triangles) to the MEPS 1km post-processed model (left), and MEPS 2,5km model (right), represented by mesh grid over a map tile, observations are averaged by grid cell, time: 28.09.2022 12Z+22H. Map tiles by Stamen Design, under CC BY 3.0. Data by OpenStreetMap, under ODbL.

4.2.3 Forecast Results Haugesund

Minimum and maximum bias values are consistent between the 1.0km and 2.0km models with differences of less than $1.5°C$ for the un-gridded iMet (table: 4.6), and less then $2.7°C$ for the gridded models (table: 4.7), with the biggest differences found in the maximums. However, there is no discernable tendency between the size of the difference and the lead time of the models, which also applies to the mean model biases. Biases tend to vary by tenths of a degree but can vary by up to $1.3°C$ between the models(tab: 4.6, 4.7, & 4.4).

The mean standard deviation relating to the iMet observations is consistent between 1.0km and 2.0km models, with a variation of $\pm 0.1°C$ (tab: 4.4). Showing less variation in forecasts with longer lead times, referring to lead times of more than 10 hours.

The mean RMSE follows the same pattern as the standard deviation with smaller errors for the longer lead times, which is surprising as the shortest lead time has the second-highest error. Indicating that the short-range forecast, 4-10 hours in this case, performs worse than those with longer lead times, according to the observations. The error is consistent between the 1.0km and 2.5km models, with a maximum difference of $0.4°C$ (tab: 4.4).

Table 4.4: Averaged MEPS-iMet values from tables: 4.6 & 4.7 separated into lead time averages, and total averages

MEPS - iMet						
Leadtime	MAE 1.0	MAE 2.5	Stdev 1.0	Stdev 2.5	RMSE 1.0	RMSE 2.5
4H	3.248	2.897	1.546	1.555	3.721	3.427
10H	4.357	4.662	1.630	1.509	4.659	4.927
16H	2.824	3.247	1.365	1.486	3.263	3.664
22H	0.707	1.030	1.377	1.439	1.578	1.802
all	2.784	2.959	1.479	1.497	3.305	3.455
MEPS - grid averaged iMet						
Leadtime	MAE 1.0	MAE 2.5	Stdev 1.0	Stdev 2.5	RMSE 1.0	RMSE 2.5
4H	3.473	3.058	1.372	1.322	3.836	3.525
10H	4.595	4.967	1.466	1.202	4.833	5.137
16H	2.987	3.511	1.186	1.219	3.302	3.769
22H	0.857	1.320	1.219	1.183	1.514	1.790
all	2.978	3.214	1.311	1.231	3.371	3.555

The Netatmo results show larger gaps in minimum and maximum bias values between the 1.0km and 2.0km models, with the bias being comparable for both the gridded and un-gridded data (table: 4.8 & 4.9). However, the difference between standard deviations for the models tends to be smaller, with values frequently below $0.1°C$ (tab: 4.5).

Table 4.5: Averaged MEPS-Netatmo values from tables: 4.8 & 4.9 separated into lead time averages, and total averages

MEPS - Netatmo						
Leadtime	MAE 1.0	MAE 2.5	Stdev 1.0	Stdev 2.5	RMSE 1.0	RMSE 2.5
4H	2.280	2.209	1.541	1.618	2.890	2.894
10H	4.097	4.268	1.638	1.625	4.429	4.572
16H	2.710	2.973	1.588	1.627	3.373	3.579
22H	0.808	0.724	1.552	1.559	1.777	1.782
all	2.474	2.544	1.580	1.607	3.117	3.207
MEPS - grid averaged Netatmo						
Leadtime	MAE 1.0	MAE 2.5	Stdev 1.0	Stdev 2.5	RMSE 1.0	RMSE 2.5
4H	2.295	2.144	1.362	1.344	2.821	2.741
10H	4.173	4.408	1.459	1.354	4.430	4.612
16H	2.731	3.058	1.404	1.378	3.284	3.499
22H	0.806	0.781	1.319	1.233	1.574	1.550
all	2.501	2.598	1.386	1.327	3.027	3.100

The Netatmo-related RMSE is more consistent than the iMet-related errors, with a lower average RMSE for both the standard and grid-averaged observations (tab: 4.4 & 4.5). Much of the difference is likely due to the Netatmo observations being used in the data assimilation and post-processing of the models leading to overall lower bias.

Table 4.6: Temperature anomaly statistics between iMet observations to the forecasts from MEPS 1.0km model, and MEPS 2.5km model for the Haugesund route

MEPS - iMet											
Datetime	Min	Min	Max	Max	Bias	Bias	Stdev	Stdev	MSE	MSE	RMSE	RMSE
	1.0km	2.5km	1.0km	2.5km	1.0km	2.5km	1.0km	2.5km	1.0km	2.5km	1.0km	2.5km
20220928T18Z+4H	-1.570	-1.727	7.737	8.335	3.280	3.500	2.160	2.318	15.428	17.620	3.928	4.198
20220928T12Z+10H	1.444	1.042	10.356	10.082	5.943	5.702	2.077	2.251	39.635	37.585	6.296	6.131
20220928T06Z+16H	-3.292	-2.882	5.189	6.853	1.002	1.917	1.814	2.231	4.295	8.654	2.072	2.942
20220928T00Z+22H	-4.221	-3.843	5.177	5.709	0.669	1.007	2.188	2.222	5.236	5.950	2.288	2.439
20220929T00Z+4H	-3.166	-4.464	4.175	3.024	0.573	-0.647	1.275	1.398	1.954	2.372	1.398	1.540
20220928T18Z+10H	-0.130	-0.287	7.317	7.945	3.388	3.615	1.712	1.779	14.408	16.236	3.796	4.029
20220928T12Z+16H	2.516	2.342	9.480	9.575	6.064	5.818	1.606	1.737	39.349	36.864	6.273	6.072
20220928T06Z+22H	-2.721	-1.442	4.538	6.463	1.115	2.028	1.437	1.744	3.306	7.156	1.818	2.675
20220929T06Z+4H	-9.646	-10.346	-2.656	-2.759	-5.807	-5.774	1.459	1.316	35.853	35.068	5.988	5.922
20220929T00Z+10H	-8.716	-10.161	-0.980	-3.135	-4.678	-5.913	1.581	1.181	24.380	36.362	4.938	6.030
20220928T18Z+16H	-7.130	-7.018	0.645	0.784	-1.958	-1.691	0.771	0.938	4.427	3.739	2.104	1.934
20220928T12Z+22H	-4.501	-5.008	3.496	3.472	0.697	0.467	0.765	0.818	1.070	0.888	1.034	0.942
20220929T12Z+4H	1.018	-1.078	7.120	5.035	3.331	1.668	1.289	1.186	12.755	4.190	3.571	2.047
20220929T06Z+10H	-6.109	-6.727	-0.066	-0.666	-3.417	-3.419	1.148	0.826	12.994	12.373	3.605	3.517
20220929T00Z+16H	-5.227	-6.874	1.395	-0.481	-2.271	-3.560	1.268	1.039	6.766	13.753	2.601	3.708
20220928T18Z+22H	-2.540	-2.697	3.772	3.626	0.348	0.619	1.119	0.972	1.373	1.328	1.172	1.152
20221118T18Z+5H	-1.966	-2.347	5.527	4.677	0.972	0.982	1.177	1.051	2.330	2.069	1.526	1.439
20221118T12Z+11H	1.507	1.042	9.274	9.548	4.536	4.473	1.150	1.275	21.896	21.637	4.679	4.652
20221118T06Z+17H	-0.662	-1.427	5.959	7.069	2.253	2.172	1.106	1.268	6.301	6.327	2.510	2.515
20221118T00Z+23H	-0.452	-1.674	6.618	6.181	2.798	2.371	1.140	1.222	9.130	7.117	3.022	2.668

Table 4.7: Temperature anomaly statistics between grid averaged iMet observations to the forecasts from MEPS 1.0km model, and MEPS 2.5km model for the Haugesund route

MEPS - Grid Averaged iMet												
Datetime	Min 1.0km	Min 2.5km	Max 1.0km	Max 2.5km	Bias 1.0km	Bias 2.5km	Stdev 1.0km	Stdev 2.5km	MSE 1.0km	MSE 2.5km	RMSE 1.0km	RMSE 2.5km
20220928T18Z+4H	0.375	0.672	6.487	6.661	3.552	4.131	1.987	1.967	16.565	20.932	4.070	4.575
20220928T12Z+10H	2.976	2.568	9.337	8.869	6.169	6.245	1.825	1.881	41.385	42.532	6.433	6.522
20220928T06Z+16H	-1.641	-1.116	3.757	5.255	1.243	2.538	1.590	1.910	4.074	10.090	2.018	3.177
20220928T00Z+22H	-2.520	-2.186	3.959	4.264	0.892	1.568	1.996	1.879	4.777	5.990	2.186	2.447
20220929T00Z+4H	-1.507	-2.925	2.800	2.399	0.657	-0.238	1.091	1.332	1.621	1.831	1.273	1.353
20220928T18Z+10H	0.250	0.912	6.428	6.456	3.655	4.115	1.686	1.654	16.199	19.666	4.025	4.435
20220928T12Z+16H	2.851	2.944	8.713	8.137	6.272	6.229	1.518	1.553	41.637	41.208	6.453	6.419
20220928T06Z+22H	-1.766	-0.649	3.620	5.050	1.345	2.522	1.365	1.630	3.674	9.018	1.917	3.003
20220929T06Z+4H	-7.792	-7.739	-3.089	-3.544	-6.123	-5.911	1.211	1.034	38.960	36.012	6.242	6.001
20220929T00Z+10H	-7.271	-7.650	-1.863	-3.907	-5.004	-6.035	1.360	0.824	26.884	37.098	5.185	6.091
20220928T18Z+16H	-4.076	-3.078	-0.912	-0.589	-1.998	-1.682	0.545	0.660	4.288	3.265	2.071	1.807
20220928T12Z+22H	-1.361	-0.398	1.869	1.149	0.619	0.432	0.523	0.517	0.656	0.454	0.810	0.674
20220929T12Z+4H	1.463	-0.148	6.435	3.681	3.561	1.952	1.200	0.954	14.119	4.719	3.758	2.172
20220929T06Z+10H	-5.202	-4.300	-1.564	-2.476	-3.553	-3.471	0.992	0.448	13.604	12.247	3.688	3.500
20220929T00Z+16H	-4.189	-5.023	0.201	-2.446	-2.433	-3.594	1.090	0.751	7.108	13.483	2.666	3.672
20220928T18Z+22H	-1.286	-0.722	2.958	2.053	0.573	0.759	0.991	0.705	1.310	1.073	1.144	1.036
20221118T18Z+5H	-0.694	-0.557	3.870	2.737	1.010	0.919	1.058	0.737	2.139	1.388	1.463	1.178
20221118T12Z+11H	2.908	2.763	7.661	7.969	4.572	4.645	1.035	1.175	21.977	22.955	4.688	4.791
20221118T06Z+17H	0.684	0.293	4.939	4.170	2.292	2.312	0.933	0.982	6.122	6.308	2.474	2.512
20221118T00Z+23H	0.979	0.461	5.424	3.994	2.830	2.286	0.980	0.964	8.968	6.153	2.995	2.480

Table 4.8: Temperature anomaly statistics between Netatmo observations to the forecasts from MEPS 1.0km model, and MEPS 2.5km model for the Haugesund route

MEPS - Netatmo											
Datetime	Min	Min	Max	Max	Bias	Bias	Stdev	Stdev	MSE	MSE	RMSE	RMSE
	1.0km	2.5km	1.0km	2.5km	1.0km	2.5km	1.0km	2.5km	1.0km	2.5km	1.0km	2.5km
20220928T18Z+4H	-4.173	-3.737	6.358	6.595	2.078	2.159	1.379	1.501	6.222	6.915	2.494	2.630
20220928T12Z+10H	-1.296	-1.633	9.111	8.552	4.751	4.274	1.407	1.500	24.555	20.522	4.955	4.530
20220928T06Z+16H	-6.379	-5.485	5.072	5.190	0.100	0.602	1.304	1.488	1.711	2.576	1.308	1.605
20220928T00Z+22H	-6.259	-6.274	4.272	4.232	-0.467	-0.197	1.429	1.474	2.260	2.212	1.503	1.487
20220929T00Z+4H	-3.165	-4.309	6.293	4.639	0.162	-1.002	1.169	1.351	1.392	2.829	1.180	1.682
20220928T18Z+10H	-0.737	0.040	7.597	7.781	2.500	2.578	1.287	1.253	7.906	8.215	2.812	2.866
20220928T12Z+16H	2.086	2.066	10.350	9.792	5.167	4.690	1.298	1.268	28.384	23.608	5.328	4.859
20220928T06Z+22H	-2.983	-1.809	6.311	6.216	0.516	1.023	1.344	1.296	2.072	2.724	1.440	1.651
20220929T06Z+4H	-15.424	-14.244	0.607	1.051	-5.359	-5.333	2.150	2.144	33.335	33.038	5.774	5.748
20220929T00Z+10H	-14.290	-14.471	1.725	1.450	-4.139	-5.307	2.198	2.124	21.961	32.677	4.686	5.716
20220928T18Z+16H	-9.552	-9.675	4.351	4.918	-1.802	-1.735	2.010	2.078	7.284	7.330	2.699	2.707
20220928T12Z+22H	-6.077	-6.778	7.382	7.094	0.865	0.384	1.964	2.007	4.607	4.174	2.146	2.043
20220929T12Z+4H	-2.589	-4.195	5.487	3.681	1.519	-0.343	1.464	1.476	4.451	2.296	2.110	1.515
20220929T06Z+10H	-9.364	-9.711	-0.683	-0.391	-4.996	-4.914	1.658	1.623	27.710	26.786	5.264	5.176
20220929T00Z+16H	-8.211	-9.858	0.508	-0.231	-3.772	-4.864	1.740	1.672	17.260	26.456	4.155	5.143
20220928T18Z+22H	-5.597	-5.681	2.288	2.565	-1.383	-1.291	1.471	1.459	4.078	3.795	2.019	1.948
20221118T18Z+5H	-4.747	-3.901	5.798	5.977	1.060	1.147	1.218	1.259	2.609	2.901	1.615	1.703
20221118T12Z+11H	-0.952	-1.181	8.772	8.863	4.141	4.107	1.135	1.158	18.439	18.209	4.294	4.267
20221118T06Z+17H	-3.304	-3.594	6.118	6.170	1.760	1.937	1.114	1.205	4.340	5.202	2.083	2.281
20221118T00Z+23H	-2.677	-2.538	7.151	7.200	2.438	2.583	1.119	1.272	7.195	8.290	2.682	2.879

Table 4.9: Temperature anomaly statistics between grid averaged Netatmo observations to the forecasts from MEPS 1.0km model, and MEPS 2.5km model for the Haugesund route

MEPS - Grid Averaged Netatmo												
Datetime	Min 1.0km	Min 2.5km	Max 1.0km	Max 2.5km	Bias 1.0km	Bias 2.5km	Stdev 1.0km	Stdev 2.5km	MSE 1.0km	MSE 2.5km	RMSE 1.0km	RMSE 2.5km
20220928T18Z+4H	-1.741	-0.622	6.129	5.398	2.119	2.345	1.296	1.318	6.169	7.235	2.484	2.690
20220928T12Z+10H	1.596	1.932	8.264	7.039	4.754	4.418	1.321	1.301	24.349	21.214	4.934	4.606
20220928T06Z+16H	-3.436	-1.891	3.207	4.046	0.102	0.820	1.182	1.348	1.408	2.490	1.187	1.578
20220928T00Z+22H	-4.702	-3.380	3.673	3.444	-0.466	-0.074	1.356	1.356	2.057	1.844	1.434	1.358
20220929T00Z+4H	-3.165	-3.653	2.861	2.413	0.077	-0.787	1.053	1.190	1.115	2.035	1.056	1.427
20220928T18Z+10H	0.163	0.887	5.605	5.278	2.594	2.918	1.107	1.019	7.952	9.550	2.820	3.090
20220928T12Z+16H	2.640	2.672	8.915	7.217	5.223	4.991	1.138	1.020	28.578	25.949	5.346	5.094
20220928T06Z+22H	-2.283	-0.962	4.303	4.077	0.569	1.392	1.122	1.060	1.583	3.062	1.258	1.750
20220929T06Z+4H	-15.424	-10.359	-2.125	-0.410	-5.493	-5.435	1.848	1.725	33.588	32.517	5.795	5.702
20220929T00Z+10H	-14.290	-10.270	-0.883	0.190	-4.273	-5.273	1.900	1.645	21.866	30.509	4.676	5.524
20220928T18Z+16H	-9.552	-5.613	1.414	2.306	-1.756	-1.570	1.699	1.578	5.968	4.953	2.443	2.226
20220928T12Z+22H	-6.077	-2.922	4.020	3.124	0.880	0.515	1.608	1.408	3.361	2.249	1.833	1.500
20220929T12Z+4H	-1.890	-3.197	5.487	3.110	1.491	0.008	1.252	1.144	3.793	1.308	1.948	1.144
20220929T06Z+10H	-9.364	-9.369	-1.249	-1.957	-5.071	-5.023	1.508	1.451	27.990	27.341	5.291	5.229
20220929T00Z+16H	-8.141	-9.148	-0.334	-0.231	-3.842	-4.852	1.598	1.565	17.313	25.991	4.161	5.098
20220928T18Z+22H	-4.746	-4.817	1.851	1.916	-1.310	-1.141	1.190	1.107	3.132	2.527	1.770	1.590
20221118T18Z+5H	-2.466	-1.566	5.798	3.382	1.128	1.143	1.104	1.142	2.492	2.612	1.578	1.616
20221118T12Z+11H	1.230	2.441	8.772	7.863	4.166	4.350	1.097	1.015	18.557	19.948	4.308	4.466
20221118T06Z+17H	-1.376	0.313	6.035	5.031	1.793	2.208	1.008	1.019	4.230	5.916	2.057	2.432
20221118T00Z+23H	-0.272	0.065	7.151	5.296	2.482	2.595	0.999	1.186	7.160	8.143	2.676	2.854

4.2.4 Forecasts for Bergen 20.01.2023 23:00 UTC

5 Hour lead time

The forecast from 18:00, with a five-hour lead time (fig: 4.37) is quite similar to the analysis (fig: 4.11), with a general warm bias in most of the domain, but warmer in the southern half close to the road for the 1.0km model. The 2.5km model sees a reduction in magnitude for Netatmo-related cold bias but remains essentially unchanged through the rest of the domain, having a weak warm bias in the western half of the domain, with a more substantial warm bias on the eastern side, which holds for iMet-related bias as well. Overall the forecast is almost identical to the analysis, with only minor changes in the magnitude of the biases. Netatmo-related mean biases are $0.77°C$ & $0.24°C$ (table: 4.13), and iMet-related mean biases are $3.35°C$ & $4.01°C$ (table: 4.12), for the 1.0km and 2.5km models respectively.

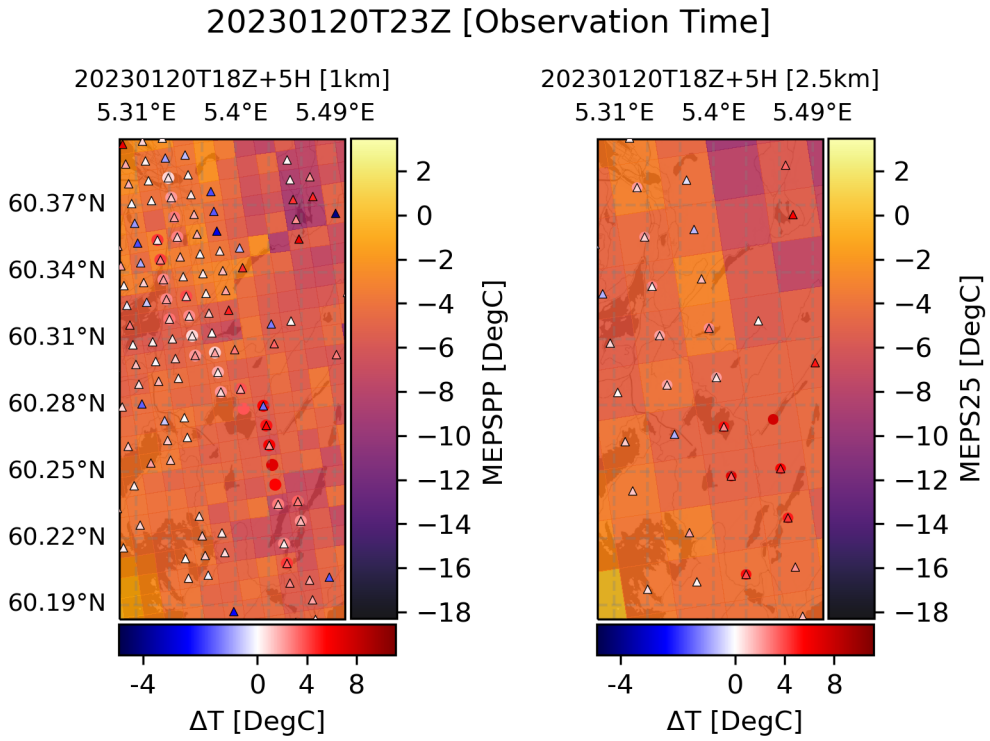

Figure 4.37: Model bias from iMet(points) and Netatmo(triangles) to the MEPS 1km post-processed model (left), and MEPS 2,5km model (right), represented by mesh grids over a map tile, observations are averaged by grid cell, time: 20.01.2023 18Z+5H. Map tiles by Stamen Design, under CC BY 3.0. Data by OpenStreetMap, under ODbL.

11 Hour lead time

Moving further back to the forecast from 12:00, with an 11-hour lead time (fig: 4.38), the model temperature has increased for both models, completely removing the cold bias from the 2.5km model, and removing all but the most substantial cold biases from the 1.0km model. Increasing the temperature also increases the existing warm bias throughout the domain of both models, with a mean temperature increase of around $2 - 3°C$ for large portions of the domain. Netatmo-related mean biases are $2.17°C$ &

2.97°C (table: 4.13), and iMet-related mean biases are 4.73°C & 6.51°C (table: 4.12), for the 1.0km and 2.5km models respectively.

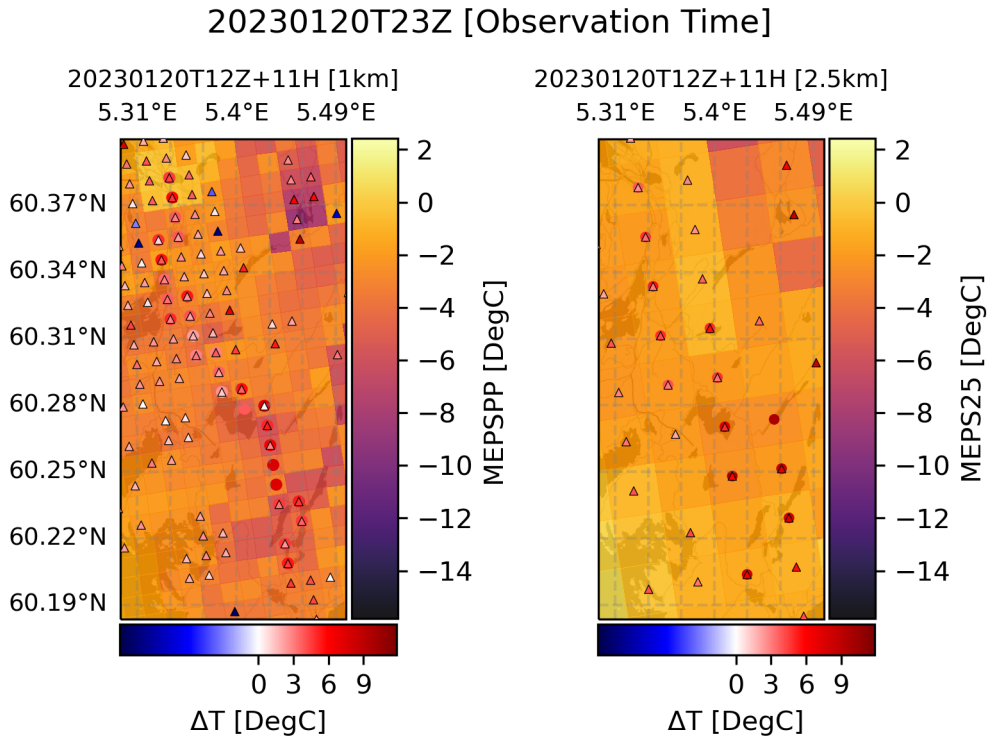

Figure 4.38: Model bias from iMet(points) and Netatmo(triangles) to the MEPS 1km post-processed model (left), and MEPS 2,5km model (right), represented by mesh grids over a map tile, observations are averaged by grid cell, time: 20.01.2023 12Z+11H. Map tiles by Stamen Design, under CC BY 3.0. Data by OpenStreetMap, under ODbL.

17 Hour lead time

Receding to the 06:00 forecast, with a 17-hour lead time (fig: 4.39), both model temperatures get colder, resulting in a distribution closer to that of the forecast from 18:00, and the analysis (figs: 4.37, 4.11), but with colder Netatmo-related temperature biases along the mountains surrounding Bergen city center and southwards. The iMet-related temperature biases are low through most of the domain, except the area around 60.25°N, which has a strong warm bias. Netatmo-related mean biases are -0.27°C & -0.74°C (table: 4.13), and iMet-related mean biases are 2.00°C & 2.56°C (table: 4.12), for the 1.0km and 2.5km models respectively.

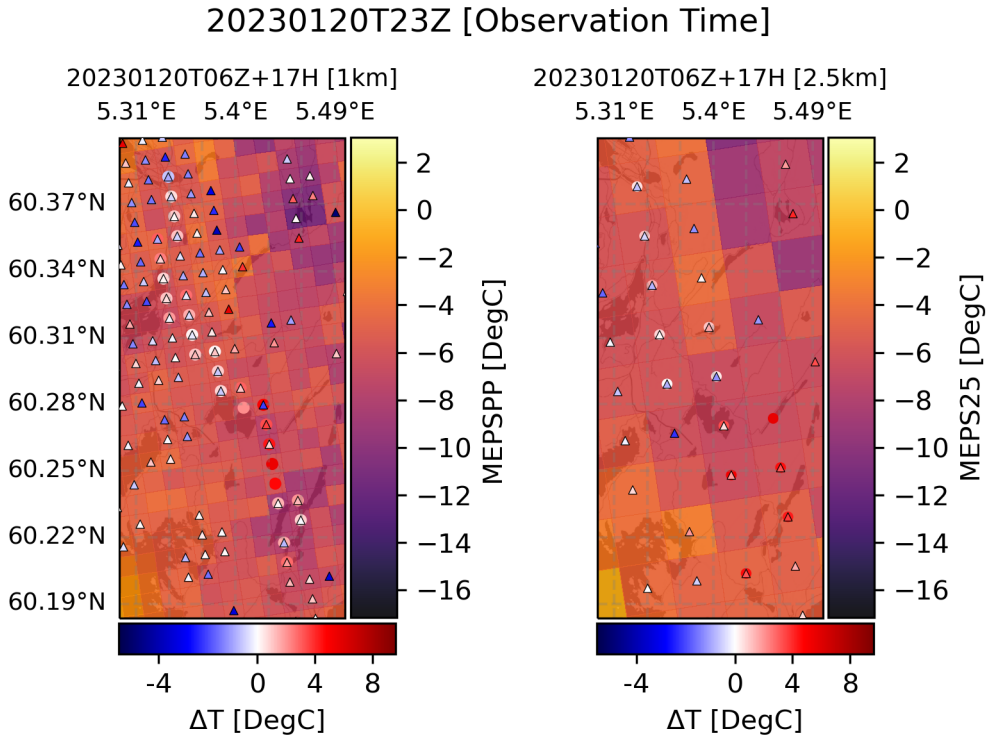

Figure 4.39: Model bias from iMet(points) and Netatmo(triangles) to the MEPS 1km post-processed model (left), and MEPS 2,5km model (right), represented by mesh grids over a map tile, observations are averaged by grid cell, time: 20.01.2023 6Z+17H. Map tiles by Stamen Design, under CC BY 3.0. Data by OpenStreetMap, under ODbL.

23 Hour lead time

Finally, the forecast from 00:00, with a 23-hour lead time (4.40) is similar to the 06:00 forecast (fig: 4.39), but has increased temperature in the colder mountainous regions, and valleys. The temperature distribution stays essentially the same, with some heating in the domain's southern part and the mountains surrounding Bergen in the northwestern quadrant. Netatmo-related mean biases are $0.56°C$ & $0.43°C$ (table: 4.13), and iMet-related mean biases are $3.10°C$ & $4.02°C$ (table: 4.12), for the 1.0km and 2.5km models respectively.

It is noteworthy how little variation there is between the iMet and Netatmo data within the grid cells, with only a single area having a sizeable, consistent difference at $60.28°N$ for the 1.0km model and no significant differences within the 2.5km model. This observation applies to all of the forecasts described in this section.

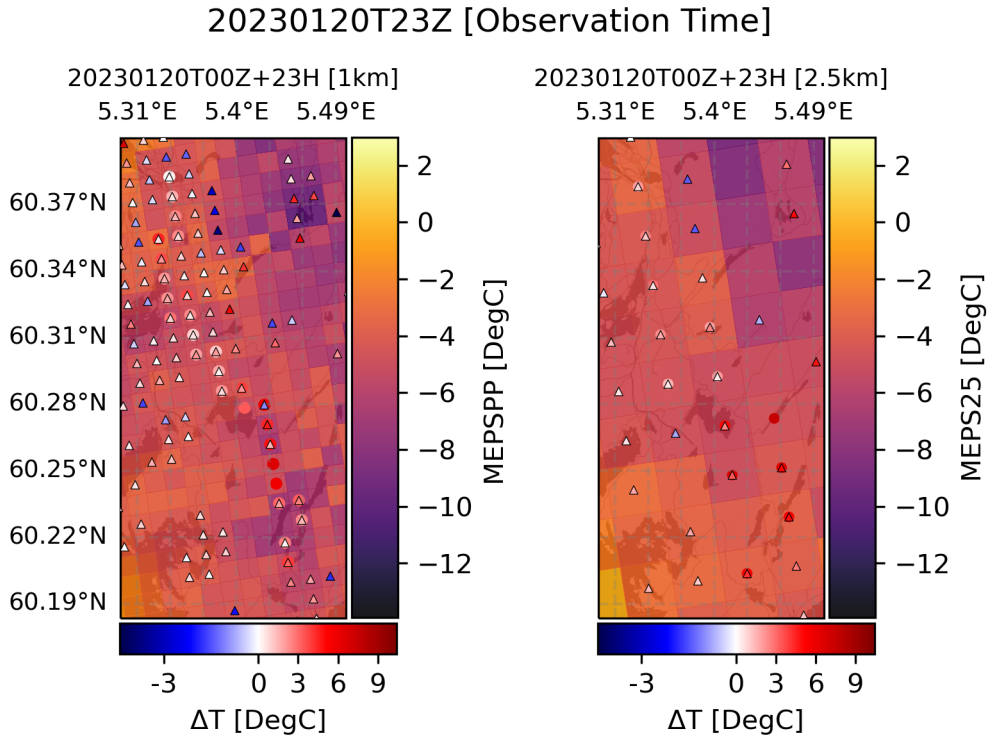

Figure 4.40: Model bias from iMet(points) and Netatmo(triangles) to the MEPS 1km post-processed model (left), and MEPS 2,5km model (right), represented by mesh grids over a map tile, observations are averaged by grid cell, time: 20.01.2023 00Z+23H. Map tiles by Stamen Design, under CC BY 3.0. Data by OpenStreetMap, under ODbL.

4.2.5 Forecasts for Bergen 21.01.2023 11:00 UTC

5 Hour lead time

The forecast from 06:00, with a lead time of 5 hours (fig: 4.41) is around $2 - 4°C$ colder than the analysis (fig: 4.14) for most areas, with some regions being substantially colder, like the southern section of the road (in the lower half of the domain), and the northeastern corner(around $60.37°N$, $5.49°E$), for the 1.0km model. Additionally, the northwestern corner around Bergen now has a weak cold bias instead of being neutral with a warm tendency. The 2.5km model is also warmer but lacks the cold peaks in the 1.0km model. As a result of the lower temperatures, both forecasts have strong cold biases through most of the domain, with weaker biases near the coast. Netatmo-related mean biases are $-2.99°C$ & $-2.37°C$ (table: 4.13), and iMet-related mean biases are $-4.12°C$ & $-2.45°C$ (table: 4.12), for the 1.0km and 2.5km models respectively.

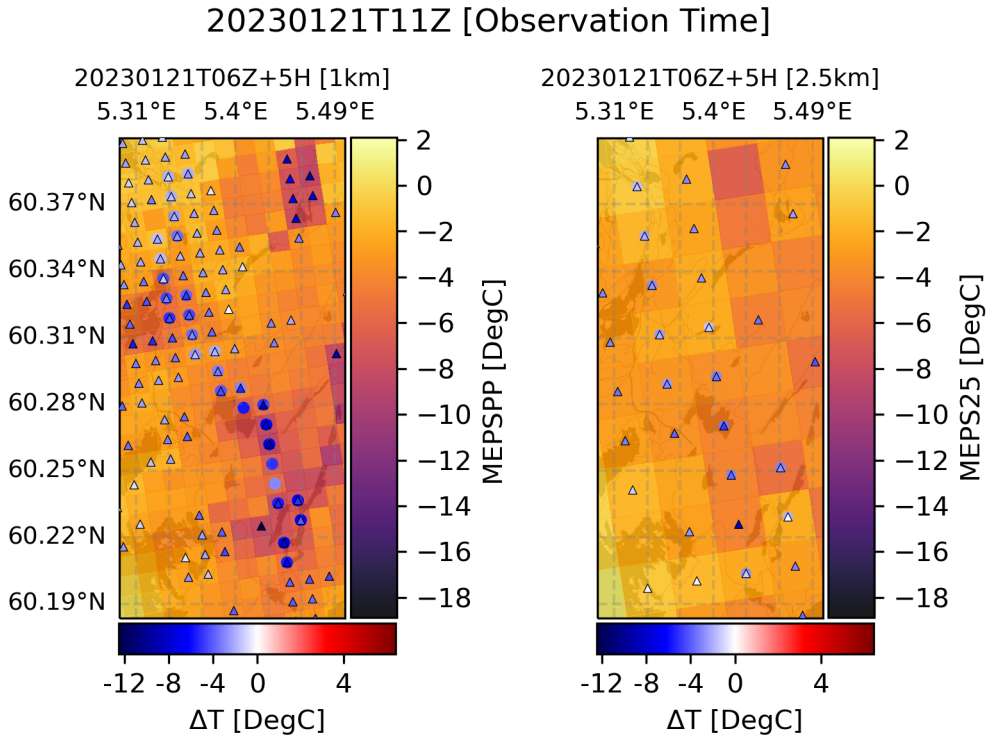

Figure 4.41: Model bias from iMet(points) and Netatmo(triangles) to the MEPS 1km post-processed model (left), and MEPS 2,5km model (right), represented by mesh grids over a map tile, observations are averaged by grid cell, time: 21.01.2023 06Z+5H. Map tiles by Stamen Design, under CC BY 3.0. Data by OpenStreetMap, under ODbL.

11 Hour lead time

Earlier, the forecast from 00:00, with a lead time of 11 hours (fig: 4.42), shows even colder model temperatures than that of the forecast from 06:00 (fig: 4.41). The cold regions are still present, but the surrounding areas have gotten colder as well, with the change visible in both the 1.0km model and the 2.5km model. They result in increased cold bias in relation to both iMet and Netatmo observations, especially for the previously warmer areas. Netatmo-related mean biases are $-4.86°C$ & $-5.04°C$ (table: 4.13), and iMet-related mean biases are $-5.93°C$ & $-4,55°C$ (table: 4.12), for the 1.0km and 2.5km models respectively.

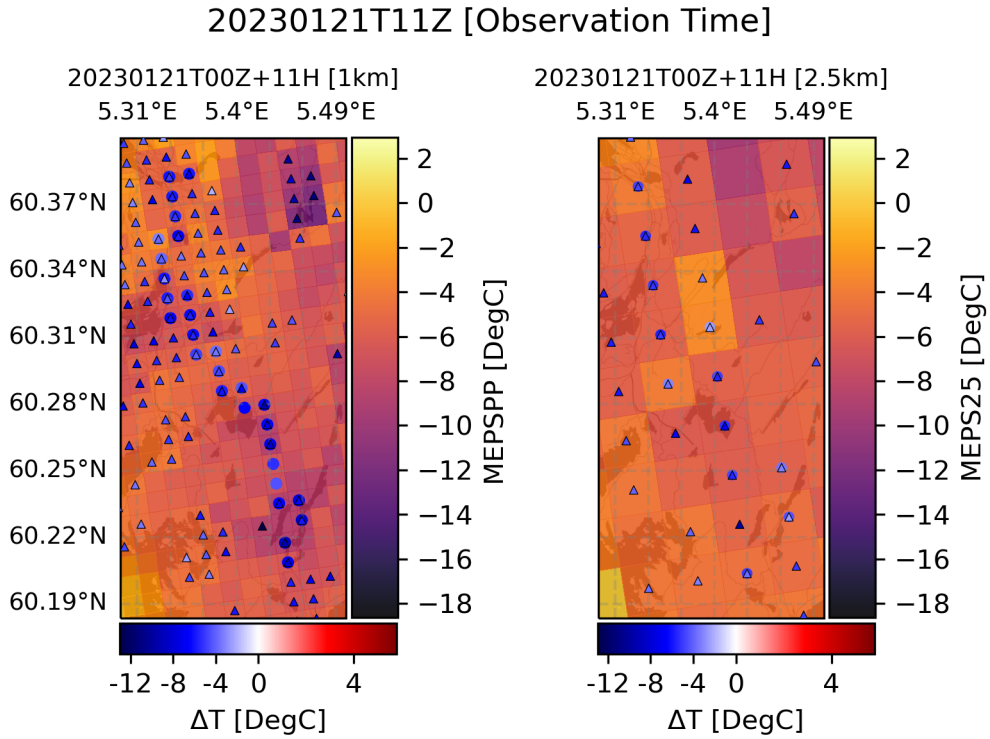

Figure 4.42: Model bias from iMet(points) and Netatmo(triangles) to the MEPS 1km post-processed model (left), and MEPS 2,5km model (right), represented by mesh grids over a map tile, observations are averaged by grid cell, time: 21.01.2023 00Z+11H. Map tiles by Stamen Design, under CC BY 3.0. Data by OpenStreetMap, under ODbL.

17 Hour lead time

The forecast from the previous day at 18:00, with a lead time of 17 hours (fig: 4.43) retains the temperature distribution from the previous forecast but has higher model temperatures. On average, the temperature has increased by around $2°C$, placing the temperatures in the range between the two first forecasts. Leading to Netatmo-related mean biases of $-4.19°C$ & $-4.65°C$ (table: 4.13), and iMet-related mean biases of $-4.44°C$ & $-3.84°C$ (table: 4.12), for the 1.0km and 2.5km models, respectively.

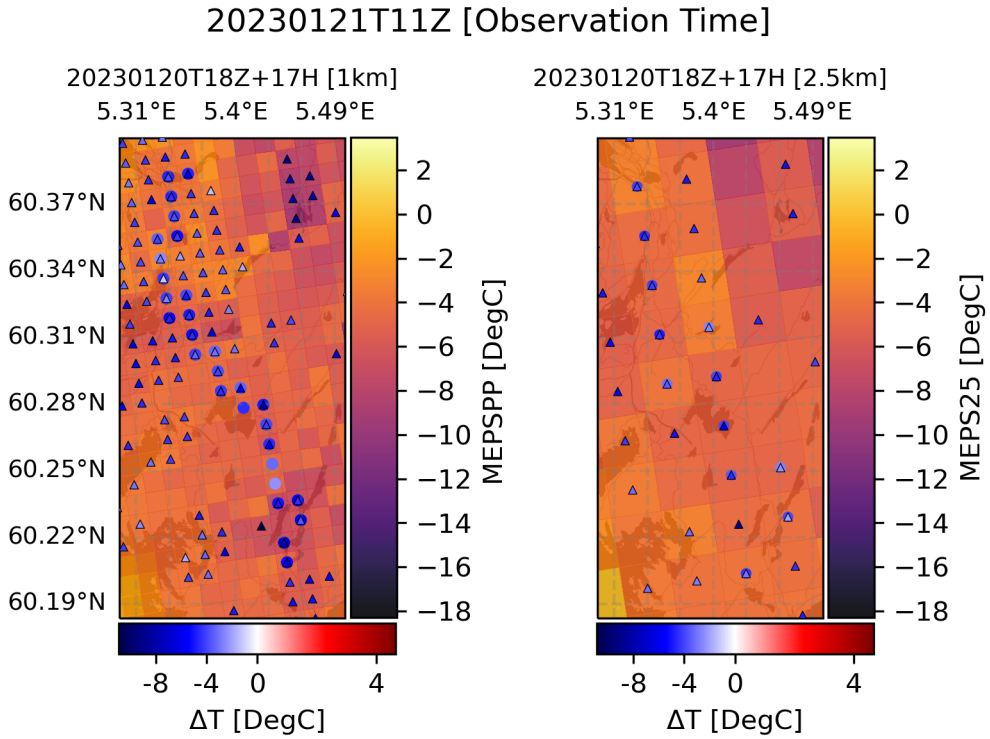

Figure 4.43: Model bias from iMet(points) and Netatmo(triangles) to the MEPS 1km post-processed model (left), and MEPS 2,5km model (right), represented by mesh grids over a map tile, observations are averaged by grid cell, time: 20.01.2023 18Z+17H. Map tiles by Stamen Design, under CC BY 3.0. Data by OpenStreetMap, under ODbL.

23 Hour lead time

Lastly, the forecast from 20.01.2022, 12:00 (fig: 4.44), loses several of the cold areas from the previous forecast (fig: 4.43), only retaining the most pronounced cold spots in the south and northeast, with the 2.5km model only keeping the cold spot in the northeastern corner of the domain. The 2.5km model has the most substantial temperature increase with most temperatures in the range of $-2°C$ to $2°C$, in contrast to the 1.0km models $-6°C$ to $2°C$. Resulting in lower model biases for both models as the forecasted values are closer to the observations. Netatmo-related mean biases are $-2.80°C$ & $-1.93°C$ (table: 4.13), and iMet-related mean biases are $-2.99°C$ & $-1.32°C$ (table: 4.12), for the 1.0km and 2.5km models respectively.

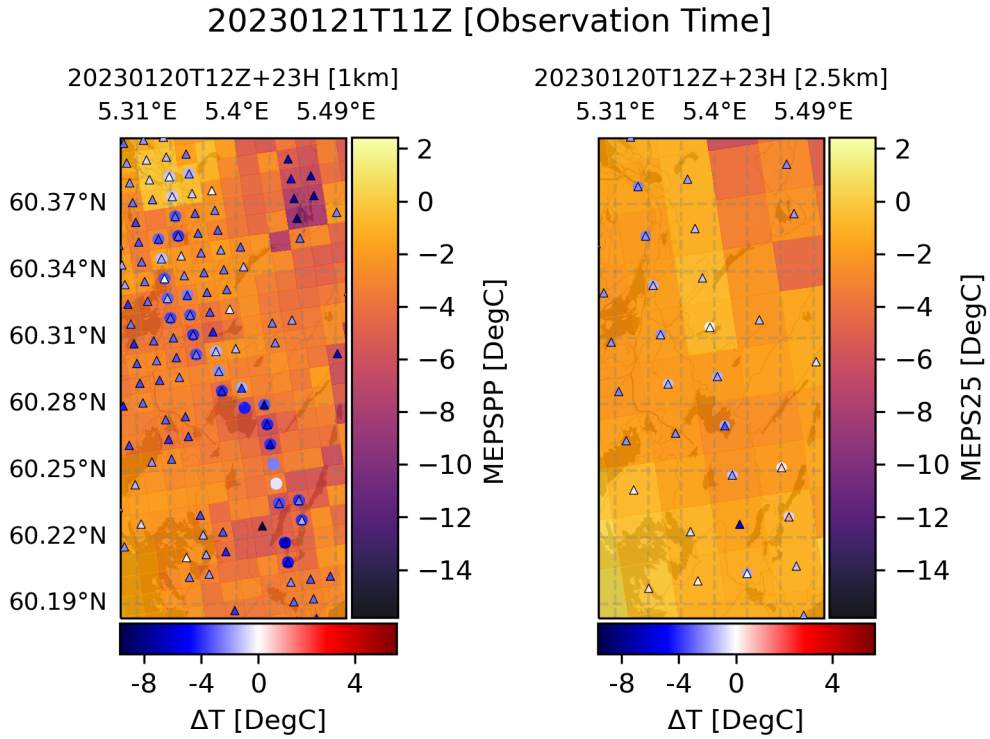

Figure 4.44: Model bias from iMet(points) and Netatmo(triangles) to the MEPS 1km post-processed model (left), and MEPS 2,5km model (right), represented by mesh grids over a map tile, observations are averaged by grid cell, time: 20.01.2023 12Z+23H. Map tiles by Stamen Design, under CC BY 3.0. Data by OpenStreetMap, under ODbL.

4.2.6 Forecast Results Bergen

The results from the forecasting section have been summarized in tables: 4.10 & 4.11, which include both grids averaged and complete observation sets. The summary tables are a compacted version of the main result tables (tables: 4.12-4.17), created by taking the mean of each lead time bracket and calculating the mean for selected error statistics, MAE, standard deviation, and RMSE. Note that the mean bias has been changed to the mean of the absolute mean bias (MAE), with the absolute mean bias referring to the values from the table, not raw data.

Interestingly, the summary tables (tabs: 4.10 & 4.11) show that the 17H & 23H lead times produce the best results, with lower MAE, standard deviations, and RMSE, both in relation to the iMet and Netatmo data. Furthermore, the 11-hour lead time is the worst, with MAE and RMSE of more than $1°C$ higher than its closest neighbor in relation to the iMet data and around $0.7 - 0.8°]C$ for the Netatmo(1k.m model) with outliers of $2 - 3°C$ for the Netatmo-related and iMet related data (2.5km model), respectfully.

Table 4.10: Averaged MEPS-iMet values from tables: 4.12, 4.14, & 4.17 separated into lead time averages, and total averages

MEPS - iMet						
Leadtime	MAE 1.0	MAE 2.5	Stdev 1.0	Stdev 2.5	RMSE 1.0	RMSE 2.5
5H	4.739	3.938	1.279	1.108	4.937	4.146
11H	5.785	5.954	1.147	1.154	5.911	6.082
17H	2.660	2.914	0.993	1.032	2.901	3.158
23H	2.560	2.217	0.989	0.980	2.837	2.492
all	3.936	3.756	1.102	1.068	4.146	3.970
MEPS - gridded iMet						
Leadtime	MAE 1.0	MAE 2.5	Stdev 1.0	Stdev 2.5	RMSE 1.0	RMSE 2.5
5H	4.801	4.070	1.188	0.963	4.973	4.218
11H	5.820	6.061	1.071	1.039	5.930	6.164
17H	2.751	2.959	0.879	0.919	2.935	3.152
23H	2.655	2.238	0.897	0.862	2.879	2.478
All	4.007	3.832	1.008	0.946	4.179	4.003

Finally, when including all lead times, the table shows that the 1.0km model is worse than the 2.5km model in all categories in relation to the iMet observations. In contrast, the opposite is true for the Netatmo observations, where the error data relating to Netatmo observations are better for the 1.0km model. As mentioned in previous sections, it is unsurprising as the Netatmo data is used in the post-processing for the 1.0km model, which would lower the bias and thereby lower the errors.

Table 4.11: Averaged MEPS-Netatmo values from tables: 4.13, 4.16, & 4.17 separated into lead time averages, and total averages

MEPS - Netatmo						
Leadtime	MAE 1.0	MAE 2.5	Stdev 1.0	Stdev 2.5	RMSE 1.0	RMSE 2.5
5H	3.290	2.703	1.653	1.706	3.746	3.335
11H	4.086	4.518	1.669	1.682	4.453	4.844
17H	1.738	2.299	1.601	1.687	2.602	2.967
23H	1.553	1.320	1.585	1.650	2.507	2.455
All	2.667	2.710	1.627	1.681	3.327	3.400
MEPS - gridded Netatmo						
Leadtime	MAE 1.0	MAE 2.5	Stdev 1.0	Stdev 2.5	RMSE 1.0	RMSE 2.5
5H	3.306	2.774	1.407	1.447	3.657	3.278
11H	4.081	4.507	1.438	1.381	4.358	4.732
17H	1.775	2.306	1.364	1.429	2.444	2.825
23H	1.561	1.302	1.323	1.353	2.295	2.176
All	2.681	2.722	1.383	1.403	3.189	3.253

Table 4.12: Temperature anomaly statistics between gridded and un-gridded iMet observations to the forecasts from MEPS 1.0km model, and MEPS 2.5km model for January, Bergen

	MEPS - iMet									
Datetime	Min	Min	Max	Max	Bias	Bias	Stdev	Stdev	MSE	MSE	RMSE	RMSE
	1.0km	2.5km	1.0km	2.5km	1.0km	2.5km	1.0km	2.5km	1.0km	2.5km	1.0km	2.5km
20230120T18Z+5H	-0.354	-0.018	8.843	9.979	3.125	3.584	1.624	1.836	12.401	16.217	3.521	4.027
20230120T12Z+11H	0.937	2.257	9.460	12.549	4.585	6.140	1.519	1.987	23.332	41.649	4.830	6.454
20230120T06Z+17H	-1.573	-1.568	7.440	8.438	1.741	2.209	1.602	1.984	5.598	8.819	2.366	2.970
20230120T00Z+23H	-0.623	-0.226	8.137	9.954	2.838	3.702	1.618	1.966	10.672	17.568	3.267	4.191
20230121T06Z+5H	-7.931	-4.742	-0.583	-0.038	-4.225	-2.506	1.751	0.808	20.915	6.934	4.573	2.633
20230121T00Z+11H	-9.524	-6.481	-2.056	-2.082	-6.071	-4.895	1.286	0.928	38.510	24.820	6.206	4.982
20230120T18Z+17H	-7.572	-5.628	-0.992	-1.240	-4.519	-4.066	1.103	0.860	21.641	17.269	4.652	4.156
20230120T12Z+23H	-5.645	-3.103	0.850	1.513	-3.025	-1.515	1.323	0.970	10.899	3.236	3.301	1.799
20230126T18Z+5H	1.469	0.341	5.615	4.545	3.184	2.077	0.600	0.672	10.501	4.764	3.240	2.183
20230126T12Z+11H	4.139	3.376	8.394	7.927	5.880	5.445	0.704	0.780	35.070	30.257	5.922	5.501
20230126T06Z+17H	3.392	2.450	6.811	7.087	4.614	4.265	0.508	0.707	21.551	18.691	4.642	4.323
20230126T00Z+23H	5.533	3.936	9.310	8.504	6.953	5.919	0.587	0.734	48.685	35.567	6.977	5.964

	MEPS - gridded iMet									
Datetime	Min	Min	Max	Max	Bias	Bias	Stdev	Stdev	MSE	MSE	RMSE	RMSE
	1.0km	2.5km	1.0km	2.5km	1.0km	2.5km	1.0km	2.5km	1.0km	2.5km	1.0km	2.5km
20230120T18Z+5H	0.893	2.036	6.955	7.575	3.345	4.010	1.509	1.909	13.462	19.720	3.669	4.441
20230120T12Z+11H	2.223	3.867	7.726	9.778	4.734	6.507	1.390	2.032	24.342	46.470	4.934	6.817
20230120T06Z+17H	-0.645	0.058	5.493	5.704	1.995	2.560	1.510	2.006	6.261	10.577	2.502	3.252
20230120T00Z+23H	0.306	1.400	6.624	7.539	3.102	4.021	1.525	2.081	11.949	20.497	3.457	4.527
20230121T06Z+5H	-7.225	-3.229	-1.495	-1.430	-4.117	-2.452	1.724	0.565	19.924	6.330	4.464	2.516
20230121T00Z+11H	-8.772	-5.588	-3.161	-2.454	-5.931	-4.551	1.288	0.970	36.838	21.649	6.069	4.653
20230120T18Z+17H	-6.819	-4.828	-2.327	-2.614	-4.444	-3.842	0.996	0.691	20.738	15.237	4.554	3.903
20230120T12Z+23H	-4.892	-2.422	-0.501	0.248	-2.985	-1.320	1.187	0.788	10.318	2.363	3.212	1.537
20230126T18Z+5H	2.358	1.126	4.298	3.161	3.250	2.219	0.499	0.513	10.809	5.188	3.288	2.278
20230126T12Z+11H	4.681	4.162	6.893	6.527	5.921	5.584	0.594	0.619	35.415	31.561	5.951	5.618
20230126T06Z+17H	3.919	3.235	5.656	5.389	4.686	4.426	0.385	0.571	22.104	19.918	4.702	4.463
20230126T00Z+23H	6.013	4.721	8.173	6.931	7.023	6.047	0.509	0.567	49.579	36.886	7.041	6.073

Table 4.13: Temperature anomaly statistics between gridded and un-gridded Netatmo observations to the forecasts from MEPS 1.0km model, and MEPS 2.5km model for January, Bergen

MEPS - Netatmo										
Datetime	Min	Min	Max	Max	Bias	Bias	Stdev	Stdev	MSE	MSE	RMSE	RMSE
	1.0km	2.5km	1.0km	2.5km	1.0km	2.5km	1.0km	2.5km	1.0km	2.5km	1.0km	2.5km
20230120T18Z+5H	-4.249	-4.835	14.126	13.442	0.760	0.329	1.789	2.076	3.776	4.419	1.943	2.102
20230120T12Z+11H	-2.176	-1.467	15.518	15.330	2.208	2.975	1.882	2.081	8.419	13.182	2.901	3.631
20230120T06Z+17H	-5.538	-5.964	13.784	11.814	-0.304	-0.820	1.813	2.067	3.379	4.945	1.838	2.224
20230120T00Z+23H	-4.416	-4.951	14.232	13.159	0.547	0.421	1.811	2.055	3.578	4.401	1.892	2.098
20230121T06Z+5H	-12.501	-9.262	6.429	6.615	-3.060	-2.359	1.749	1.533	12.425	7.918	3.525	2.814
20230121T00Z+11H	-12.987	-10.743	5.798	3.252	-5.037	-5.114	1.679	1.508	28.186	28.430	5.309	5.332
20230120T18Z+17H	-10.919	-10.872	4.654	3.794	-4.227	-4.663	1.434	1.431	19.922	23.786	4.463	4.877
20230120T12Z+23H	-9.702	-8.287	5.727	6.339	-2.781	-2.025	1.430	1.403	9.781	6.069	3.128	2.464
20230126T18Z+5H	-3.803	-4.159	9.137	8.427	2.061	1.157	1.266	1.454	5.850	3.454	2.419	1.859
20230126T12Z+11H	-0.710	-0.453	11.926	11.576	4.513	4.396	1.340	1.396	22.163	21.270	4.708	4.612
20230126T06Z+17H	-0.542	-0.786	10.340	10.290	3.702	3.320	1.260	1.365	15.293	12.887	3.911	3.590
20230126T00Z+23H	0.760	0.494	11.618	11.868	5.481	4.989	1.305	1.384	31.743	26.811	5.634	5.178

MEPS - gridded Netatmo										
Datetime	Min	Min	Max	Max	Bias	Bias	Stdev	Stdev	MSE	MSE	RMSE	RMSE
	1.0km	2.5km	1.0km	2.5km	1.0km	2.5km	1.0km	2.5km	1.0km	2.5km	1.0km	2.5km
20230120T18Z+5H	-4.036	-4.835	11.190	6.794	0.771	0.244	1.584	1.904	3.104	3.685	1.762	1.920
20230120T12Z+11H	-1.375	-1.467	11.846	10.007	2.174	2.965	1.687	1.874	7.574	12.302	2.752	3.507
20230120T06Z+17H	-4.984	-5.611	9.629	6.484	-0.272	-0.740	1.600	1.872	2.632	4.054	1.622	2.013
20230120T00Z+23H	-4.401	-3.814	10.428	6.916	0.555	0.425	1.622	1.838	2.939	3.558	1.714	1.886
20230121T06Z+5H	-12.501	-8.948	6.429	1.248	-2.990	-2.373	1.705	1.672	11.850	8.426	3.442	2.903
20230121T00Z+11H	-12.987	-10.743	5.798	0.726	-4.857	-5.039	1.700	1.619	26.476	28.013	5.145	5.293
20230120T18Z+17H	-10.919	-10.872	4.654	0.554	-4.186	-4.646	1.359	1.560	19.365	24.019	4.401	4.901
20230120T12Z+23H	-9.702	-8.287	5.727	2.657	-2.804	-1.933	1.329	1.487	9.626	5.948	3.103	2.439
20230126T18Z+5H	-3.803	-4.159	6.908	4.587	2.110	1.466	1.024	1.296	5.501	3.828	2.346	1.956
20230126T12Z+11H	-0.710	-0.167	9.332	7.609	4.548	4.476	1.088	1.114	21.873	21.278	4.677	4.613
20230126T06Z+17H	-0.542	-0.128	8.640	6.521	3.776	3.592	1.007	0.982	15.273	13.870	3.908	3.724
20230126T00Z+23H	0.760	1.216	9.567	8.338	5.448	5.205	1.068	1.006	30.819	28.101	5.551	5.301

Table 4.14: Temperature anomaly statistics between iMet observations to the forecasts from MEPS 1.0km model, and MEPS 2.5km model for Feb-March, Bergen

	MEPS - iMet									
Datetime	Min	Min	Max	Max	Bias	Bias	Stdev	Stdev	MSE	MSE	RMSE	RMSE
	1.0km	2.5km	1.0km	2.5km	1.0km	2.5km	1.0km	2.5km	1.0km	2.5km	1.0km	2.5km
20230227T06Z+5H	-9.351	-8.779	-2.078	-1.626	-5.492	-5.723	1.746	1.914	33.211	36.423	5.763	6.035
20230227T00Z+11H	-7.927	-7.668	-2.031	-1.890	-4.646	-5.281	1.423	1.491	23.615	30.114	4.860	5.488
20230226T18Z+17H	-3.946	-6.341	1.417	-0.056	-1.517	-3.195	1.326	1.554	4.060	12.623	2.015	3.553
20230226T12Z+23H	-3.871	-3.220	0.731	1.371	-1.157	-0.963	0.836	1.041	2.037	2.010	1.427	1.418
20230227T18Z+5H	2.548	1.475	7.327	6.182	4.984	3.853	0.846	0.880	25.558	15.620	5.056	3.952
20230227T12Z+11H	4.487	3.905	9.787	10.291	6.970	7.452	1.173	1.309	49.958	57.240	7.068	7.566
20230227T06Z+17H	-1.263	-1.703	3.408	2.608	0.997	0.748	0.773	0.699	1.593	1.049	1.262	1.024
20230227T00Z+23H	-0.918	-0.750	4.311	2.997	1.880	1.241	0.813	0.610	4.195	1.912	2.048	1.383
20230228T06Z+5H	-10.362	-9.412	-4.462	-4.263	-7.455	-6.490	1.430	0.968	57.621	43.056	7.591	6.562
20230228T00Z+11H	-9.113	-9.217	-4.812	-5.290	-6.897	-7.333	0.868	0.793	48.327	54.407	6.952	7.376
20230227T18Z+17H	-4.968	-6.173	-0.746	-1.494	-2.673	-3.862	0.886	0.710	7.931	15.420	2.816	3.927
20230227T12Z+23H	-3.738	-2.082	1.047	1.551	-0.785	-0.305	0.798	0.707	1.253	0.593	1.119	0.770
20230228T18Z+5H	-0.761	-1.390	5.218	4.322	2.359	0.964	1.126	1.178	6.832	2.318	2.614	1.522
20230228T12Z+11H	0.786	1.155	7.620	7.279	4.338	3.733	1.227	1.253	20.324	15.505	4.508	3.938
20230228T06Z+17H	-6.617	-4.648	-0.033	1.366	-3.300	-2.299	1.156	1.257	12.229	6.865	3.497	2.620
20230228T00Z+23H	-4.783	-5.596	-0.169	0.674	-2.765	-3.152	0.945	1.244	8.536	11.481	2.922	3.388
20230301T06Z+5H	-9.679	-8.447	-3.032	-3.646	-5.952	-6.464	1.438	0.775	37.491	42.384	6.123	6.510
20230301T00Z+11H	-6.889	-7.916	-2.249	-3.284	-4.937	-6.141	0.908	0.734	25.197	38.251	5.020	6.185
20230228T18Z+17H	-4.552	-5.716	-0.026	-1.031	-2.601	-4.020	0.706	0.674	7.263	16.615	2.695	4.076
20230228T12Z+23H	-2.774	-3.115	2.530	1.740	-0.573	-1.268	1.167	0.662	1.690	2.047	1.300	1.431
20230301T18Z+5H	3.339	1.270	8.292	6.356	5.873	3.777	0.951	0.937	35.391	15.141	5.949	3.891
20230301T12Z+11H	4.562	4.251	10.292	9.801	7.740	7.165	1.218	1.109	61.392	52.561	7.835	7.250
20230301T06Z+17H	-0.026	-0.898	4.715	3.602	1.981	1.562	0.876	0.843	4.690	3.150	2.166	1.775
20230301T00Z+23H	0.863	-0.584	5.432	4.116	3.061	1.889	0.816	0.883	10.035	4.348	3.168	2.085

Table 4.15: Temperature anomaly statistics between grid averaged iMet observations to the forecasts from MEPS 1.0km model, and MEPS 2.5km model for Feb-March, Bergen

	MEPS - gridded iMet									
Datetime	Min	Min	Max	Max	Bias	Bias	Stdev	Stdev	MSE	MSE	RMSE	RMSE
	1.0km	2.5km	1.0km	2.5km	1.0km	2.5km	1.0km	2.5km	1.0km	2.5km	1.0km	2.5km
20230227T06Z+5H	-8.501	-8.165	-2.481	-2.295	-5.782	-6.187	1.576	1.648	35.921	40.998	5.993	6.403
20230227T00Z+11H	-7.077	-6.970	-2.434	-2.559	-4.882	-5.545	1.312	1.292	25.558	32.419	5.056	5.694
20230226T18Z+17H	-3.424	-5.466	1.014	-0.725	-1.796	-3.472	1.203	1.419	4.671	14.067	2.161	3.751
20230226T12Z+23H	-3.682	-2.125	0.189	0.702	-1.345	-1.071	0.814	0.847	2.471	1.865	1.572	1.366
20230227T18Z+5H	3.644	2.603	6.429	5.305	5.086	4.047	0.771	0.795	26.462	17.009	5.144	4.124
20230227T12Z+11H	4.839	5.033	8.799	9.000	7.009	7.780	1.113	1.206	50.368	61.989	7.097	7.873
20230227T06Z+17H	-0.151	-0.289	2.115	1.539	1.099	0.697	0.679	0.542	1.669	0.779	1.292	0.883
20230227T00Z+23H	0.154	0.378	2.971	2.048	1.999	1.320	0.708	0.440	4.497	1.936	2.121	1.392
20230228T06Z+5H	-9.660	-8.232	-4.802	-4.998	-7.406	-6.365	1.362	0.839	56.699	41.218	7.530	6.420
20230228T00Z+11H	-8.451	-8.025	-5.524	-5.823	-6.927	-7.330	0.824	0.664	48.663	54.165	6.976	7.360
20230227T18Z+17H	-4.266	-4.667	-1.207	-2.230	-2.738	-3.785	0.842	0.626	8.204	14.716	2.864	3.836
20230227T12Z+23H	-3.662	-1.615	0.432	0.942	-0.814	-0.051	0.853	0.629	1.391	0.398	1.180	0.631
20230228T18Z+5H	-0.418	-0.677	4.013	2.795	2.244	1.027	1.052	0.853	6.145	1.782	2.479	1.335
20230228T12Z+11H	1.129	1.869	6.108	5.752	4.195	3.837	1.166	0.939	18.959	15.606	4.354	3.950
20230228T06Z+17H	-5.400	-3.655	-2.174	-0.161	-3.280	-2.198	0.858	1.029	11.493	5.890	3.390	2.427
20230228T00Z+23H	-4.197	-4.823	-1.375	-0.853	-2.801	-3.163	0.705	0.978	8.344	10.961	2.889	3.311
20230301T06Z+5H	-8.781	-7.637	-3.829	-4.743	-6.093	-6.370	1.334	0.733	38.901	41.110	6.237	6.412
20230301T00Z+11H	-6.250	-6.951	-3.244	-4.381	-5.044	-6.062	0.815	0.663	26.102	37.183	5.109	6.098
20230228T18Z+17H	-4.182	-4.566	-1.420	-2.128	-2.700	-3.918	0.652	0.640	7.716	15.763	2.778	3.970
20230228T12Z+23H	-2.635	-2.020	2.238	0.643	-0.749	-1.108	1.044	0.643	1.652	1.641	1.285	1.281
20230301T18Z+5H	3.844	2.106	6.939	5.126	5.887	3.949	0.864	0.812	35.399	16.253	5.950	4.031
20230301T12Z+11H	5.067	5.087	9.620	8.571	7.738	7.352	1.133	0.962	61.164	54.982	7.821	7.415
20230301T06Z+17H	0.510	-0.062	3.173	2.913	2.025	1.730	0.782	0.744	4.712	3.545	2.171	1.883
20230301T00Z+23H	1.595	0.252	4.144	3.223	3.074	2.038	0.726	0.788	9.975	4.773	3.158	2.185

Table 4.16: Temperature anomaly statistics between Netatmo observations to the forecasts from MEPS 1.0km model, and MEPS 2.5km model for Feb-March, Bergen

	MEPS - Netatmo											
Datetime	Min	Min	Max	Max	Bias	Bias	Stdev	Stdev	MSE	MSE	RMSE	RMSE
	1.0km	2.5km	1.0km	2.5km	1.0km	2.5km	1.0km	2.5km	1.0km	2.5km	1.0km	2.5km
20230227T06Z+5H	-11.756	-12.648	0.469	0.984	-4.120	-4.734	2.023	2.114	21.072	26.875	4.590	5.184
20230227T00Z+11H	-10.287	-11.298	2.182	1.287	-2.729	-3.888	2.005	2.000	11.467	19.115	3.386	4.372
20230226T18Z+17H	-7.578	-9.654	3.908	2.565	-0.449	-1.981	1.942	1.992	3.973	7.892	1.993	2.809
20230226T12Z+23H	-7.305	-6.435	4.135	4.455	-0.182	0.321	1.887	1.929	3.595	3.825	1.896	1.956
20230227T18Z+5H	-1.516	-2.426	10.536	9.345	3.390	2.289	1.381	1.480	13.399	7.432	3.660	2.726
20230227T12Z+11H	-0.327	0.402	12.354	11.775	4.183	5.007	1.598	1.584	20.054	27.583	4.478	5.252
20230227T06Z+17H	-5.606	-5.853	6.869	7.384	-0.785	-1.401	1.340	1.460	2.413	4.094	1.553	2.023
20230227T00Z+23H	-3.793	-4.721	7.938	7.120	0.601	-0.552	1.343	1.370	2.163	2.181	1.471	1.477
20230228T06Z+5H	-13.356	-14.086	-0.089	1.396	-5.759	-5.304	2.012	2.062	37.215	32.383	6.100	5.691
20230228T00Z+11H	-14.001	-13.129	0.137	0.093	-5.390	-6.135	1.863	1.923	32.521	41.340	5.703	6.430
20230227T18Z+17H	-8.956	-10.326	3.154	3.265	-1.552	-2.657	1.796	1.858	5.633	10.515	2.373	3.243
20230227T12Z+23H	-7.375	-6.603	4.915	6.341	-0.767	0.060	1.881	1.908	4.127	3.642	2.031	1.908
20230228T18Z+5H	-4.852	-6.518	8.415	7.367	1.806	0.720	1.153	1.144	4.591	1.828	2.143	1.352
20230228T12Z+11H	-2.471	-3.090	10.108	9.917	3.617	3.382	1.196	1.172	14.512	12.813	3.809	3.580
20230228T06Z+17H	-9.911	-11.241	3.727	5.196	-2.884	-2.431	1.369	1.504	10.190	8.170	3.192	2.858
20230228T00Z+23H	-8.958	-10.250	3.937	3.893	-2.515	-3.254	1.208	1.311	7.785	12.308	2.790	3.508
20230301T06Z+5H	-12.950	-13.211	1.681	0.553	-4.852	-5.483	2.044	2.039	27.717	34.220	5.265	5.850
20230301T00Z+11H	-11.614	-12.580	2.388	1.620	-3.868	-4.767	1.968	2.025	18.835	26.829	4.340	5.180
20230228T18Z+17H	-9.083	-9.607	3.867	3.441	-1.721	-2.809	2.009	1.992	7.000	11.861	2.646	3.444
20230228T12Z+23H	-6.899	-7.189	7.300	5.561	0.102	-0.148	1.995	1.989	3.990	3.978	1.997	1.995
20230301T18Z+5H	-0.274	-2.186	11.202	9.220	3.801	1.950	1.456	1.455	16.566	5.919	4.070	2.433
20230301T12Z+11H	0.259	0.723	12.528	12.336	5.233	5.000	1.489	1.446	29.607	27.095	5.441	5.205
20230301T06Z+17H	-5.104	-5.711	8.351	7.052	0.015	-0.613	1.450	1.513	2.104	2.666	1.451	1.633
20230301T00Z+23H	-4.114	-4.806	8.939	7.366	1.000	0.106	1.407	1.504	2.979	2.272	1.726	1.507

Table 4.17: Temperature anomaly statistics between grid averaged Netatmo observations to the forecasts from MEPS 1.0km model, and MEPS 2.5km model for Feb-March, Bergen

	MEPS - gridded Netatmo									
Datetime	Min	Min	Max	Max	Bias	Bias	Stdev	Stdev	MSE	MSE	RMSE	RMSE
	1.0km	2.5km	1.0km	2.5km	1.0km	2.5km	1.0km	2.5km	1.0km	2.5km	1.0km	2.5km
20230227T06Z+5H	-11.711	-9.660	0.161	0.102	-4.174	-5.000	1.582	1.449	19.923	27.100	4.463	5.206
20230227T00Z+11H	-10.287	-7.636	2.182	0.770	-2.685	-3.875	1.627	1.352	9.856	16.845	3.139	4.104
20230226T18Z+17H	-6.458	-5.547	3.318	2.171	-0.506	-2.133	1.489	1.377	2.472	6.445	1.572	2.539
20230226T12Z+23H	-5.751	-3.597	4.135	3.936	-0.179	0.202	1.414	1.305	2.031	1.743	1.425	1.320
20230227T18Z+5H	-0.389	-1.701	8.080	5.050	3.345	2.452	1.115	1.252	12.433	7.582	3.526	2.754
20230227T12Z+11H	0.525	1.986	9.339	8.234	4.269	5.073	1.416	1.276	20.228	27.363	4.498	5.231
20230227T06Z+17H	-4.348	-5.282	4.061	1.354	-0.749	-1.480	1.079	1.106	1.726	3.413	1.314	1.847
20230227T00Z+23H	-2.862	-3.112	6.082	2.004	0.731	-0.356	1.084	0.974	1.709	1.076	1.307	1.037
20230228T06Z+5H	-13.252	-11.936	-0.089	-1.538	-5.832	-5.128	1.729	1.841	37.005	29.685	6.083	5.448
20230228T00Z+11H	-12.003	-10.979	0.137	-1.173	-5.428	-6.093	1.563	1.526	31.902	39.447	5.648	6.281
20230227T18Z+17H	-7.871	-8.176	2.880	2.415	-1.732	-2.650	1.512	1.520	5.288	9.333	2.300	3.055
20230227T12Z+23H	-7.375	-5.007	4.139	4.603	-0.804	-0.019	1.584	1.545	3.156	2.386	1.776	1.545
20230228T18Z+5H	-4.852	-6.518	6.776	3.987	1.736	0.750	1.113	1.081	4.253	1.731	2.062	1.316
20230228T12Z+11H	-2.471	-3.090	9.517	7.328	3.571	3.364	1.084	1.112	13.925	12.557	3.732	3.544
20230228T06Z+17H	-9.911	-11.241	3.711	2.992	-2.877	-2.131	1.340	1.766	10.072	7.662	3.174	2.768
20230228T00Z+23H	-8.958	-10.250	3.937	1.018	-2.467	-3.065	1.133	1.384	7.368	11.312	2.714	3.363
20230301T06Z+5H	-12.869	-11.311	-1.173	-0.814	-5.010	-5.484	1.610	1.467	27.688	32.222	5.262	5.676
20230301T00Z+11H	-11.614	-10.406	-0.372	0.253	-3.922	-4.700	1.528	1.477	17.716	24.270	4.209	4.926
20230228T18Z+17H	-9.083	-7.581	3.315	2.068	-1.833	-2.868	1.649	1.379	6.079	10.127	2.466	3.182
20230228T12Z+23H	-6.032	-4.185	3.876	4.194	0.017	-0.242	1.501	1.373	2.254	1.944	1.501	1.394
20230301T18Z+5H	-0.274	-1.828	8.098	4.616	3.784	2.067	1.205	1.065	15.768	5.408	3.971	2.326
20230301T12Z+11H	0.259	1.262	9.905	7.617	5.278	4.976	1.253	1.080	29.428	25.932	5.425	5.092
20230301T06Z+17H	-5.104	-5.047	3.933	2.225	-0.043	-0.515	1.238	1.302	1.533	1.961	1.238	1.400
20230301T00Z+23H	-4.114	-4.116	4.584	3.000	1.043	0.275	1.169	1.269	2.454	1.686	1.566	1.298

5 Discussion

5.1 Benchmarking

There is a significant distinction between paved and unpaved roads when considering surface heating effects, and the effect on car temperature sensors as seen in section 3.2.1. The difference in heating is caused by differing albedo, roughness, and insulation in the surface material, with gravel having a less uniform surface, and particles insulated by air in the uncompacted surface layer, reducing internal heat transfer. While gravel roads are less common than asphalt roads, they still serve small rural communities, farms, and some reroute roads. These roads are generally much cheaper to build and can be equally durable as paved roads if built properly, not to mention cheaper to maintain. They are thus unlikely to disappear any time soon, requiring them to be included in any complete RWF product, with the difference in radiated surface heat accounted for observational products.

The difference in radiated surface heat can be lessened by avoiding having temperature sensors close to the ground, as seen in section 3.2.1 where the roof-mounted sensor is colder than the bottom-mounted counterpart. Traditionally, cars have had their temperature sensors in front of the engine compartment by the vents, which has the unfortunate effect of being susceptible to both engine heat(for combustion engines) and surface heat (*Bell et al.*, 2022). Some car manufacturers have caught on, and are using alternative mounting locations, with the door mirrors becoming a popular new location, providing a middle ground between the bottom and the roof of the car.

Still, filtering can be applied to remove data from stationary and slow-moving vehicles to remove the undesirable heating effects. Additionally, moving vehicles tend to have a much smaller temperature difference between sensor locations due to cooling provided by the constant supply of fresh air (fig: 3.7).

5.2 Analysis

After analyzing the data in section 4.1, it has been determined that both the Bergen and Haugesund routes have unresolved temperature variations. These variations follow a consistent diurnal pattern with warm biases during the night and cold biases during the day, particularly on the Bergen route. The models exhibit slow reaction times, taking too long to warm up during early to midday and too slow to cool down in the evening. This is influenced by various factors, including the radiation scheme, cloud cover, cloud microphysics, flora, topography, and available observations. The cause of the biases is likely a result of several of these factors, but assumptions in cloud microphysics have been known to impact the radiation scheme by increasing the outgoing longwave radiation, causing unrealistic cold biases (*Müller et al.*, 2017).

The city center of Bergen serves as an intriguing example of regional weather patterns that consistently deviate from the expected model output. During the day, temperatures in Bergen tend to be warmer than anticipated, while at night, they often drop below expectations, which is the opposite of the rest of the domain. This discrepancy

is likely caused by the urban microclimate and geographical influence of the surrounding mountains, making it less exposed to advection. However, note that the observed temperatures might be skewed as they are likely mounted closer to buildings than the official Met-Norway weather station at Florida, outside the geophysical institute.

It's crucial to recognize that observation stations, including privately-owned weather stations such as Netatmo stations, may not always provide accurate weather conditions experienced on the road. Though these stations offer valuable meteorological data, they may not fully capture localized microclimates and variations that can exist along roadways. Elevation changes, proximity to bodies of water, or urban heat islands can significantly impact the drivers' weather experiences and may not be adequately reflected in official or privately owned weather station data.

Depending solely on data from observation stations may not give a complete understanding of the real conditions on the road. This is especially true when it comes to temperature readings, as the heat absorption of the asphalt and the surrounding environment can cause temperature fluctuations that deviate from the readings obtained by fixed sensors. However, having access to several sources of data for the same area can make it easier to validate observations that would otherwise be flagged as inaccurate due to perceived excessive differences from model results. Effectively opening another pathway to improve operational forecasting by ensuring more reliable quality control among the observations.

The 2.5km model uses a sophisticated surface model that includes 1.0km high-resolution tiles for lakes, vegetation, and land types. In contrast, the 1.0km model uses high-resolution GIS data and not the downscaled land area fraction from the 2.5km, resulting in the removal of lake tiles (*Nypen*, 2023). Thus the 1.0km model only distinguishes between land and sea tiles, theoretically resulting in larger model biases near lakes. However, the 1.0km model compensates by having more observation points, enabling temperature corrections to mitigate the missing high-resolution surface model data, if observations are available.

There were some similarities and differences between the 2.5km and 1.0km models near lake tiles. In a few cases, the 2.5km model performed better than the 1.0km model, as seen near Haugesund (figs: 4.1 & 4.9), where there was a noticeable hot spot near the central southern area east of Haugesund, with a stronger warm bias in the 1.0km model. The western half of the hot spot was located on the bank of a small lake, which was hidden by the temperature markers. It is possible that the temperature corrections from the Netatmo observations caused this, as the model showed almost zero bias compared to the Netatmo measurements, indicating a difference in temperature between the residential areas and the road. The housing located in the vicinity of the lake is at varying altitudes from the road, mainly because of the steep slope on the eastern side. The central area lacks any housing, while the houses on the western side are situated in an offshoot valley.

5.3 Forecast

Evaluating the forecast in relation to car observations and Netatmo observations shows substantial increases in model bias for most of the forecast runs, often skewing the models to be near entirely warm or cold-biased. Some lead times for the forecasts make the model biases change sign, for example, the forecast for 29.09.2022 10:00 UTC with a lead time

of 22 hours (section 4.2.2) where the mean model bias switches from cold to warm and reduces in magnitude. The change in mean model bias between the forecast runs shows much variability between the different forecast reference times. With generally larger variability for the two shortest lead times (4-5H, & 10-11H), and less variability for the two longest lead times (16H, & 22H). Interestingly the longer lead times tend to be more accurate, at least for the period investigated, with the 16-17 hour and 22–23-hour lead times performing best on average.

After comparing the forecast with car and Netatmo observations, it was noticed that the model bias tends to lean towards either being warm or cold-biased. The degree of similarity to the analysis varies. While most of the forecast reference times produced slightly stronger or weaker biases than their neighbors, some instances showed a change in the bias's sign. These events indicate times/areas of great uncertainty within the models, which can pose problems for accurate RWF products. The short-range forecasting's average performance for the Bergen area, with lead times between 4-11 hours, was particularly worrying, performing worse than the longer-range forecasts with lead times between 16-23 hours. However, it's important to note that the testing period was relatively short and regionally confined, which may not be representative of other areas.

5.4 Future use of RWS and observation products

Although the current forecast state may not be ideal for predicting road conditions, there are various options available to enhance the forecast. The major challenge in achieving accurate forecasting lies in having an incomplete picture of current and past conditions. This becomes more apparent when examining the RWF from Statens Vegvesen (*Statens Vegvesen*, 2022), where data from official road weather stations (RWS) are used to approximate the conditions. To provide some context, when driving along the Haugesund route, I did not pass a single RWS for the entirety of the route, with only one station located nearby (eastern dot in figure 5.1). This often results in forecasts that are inaccurate and have a wide temperature range. At the time of writing the site is only available by a link, as it is not advertised on Statens Vegvesen's main web page, route planning page, or road condition page, with all references to weather going to individual RWS or to the forecast from yr.no, which is the state-owned official weather provider.

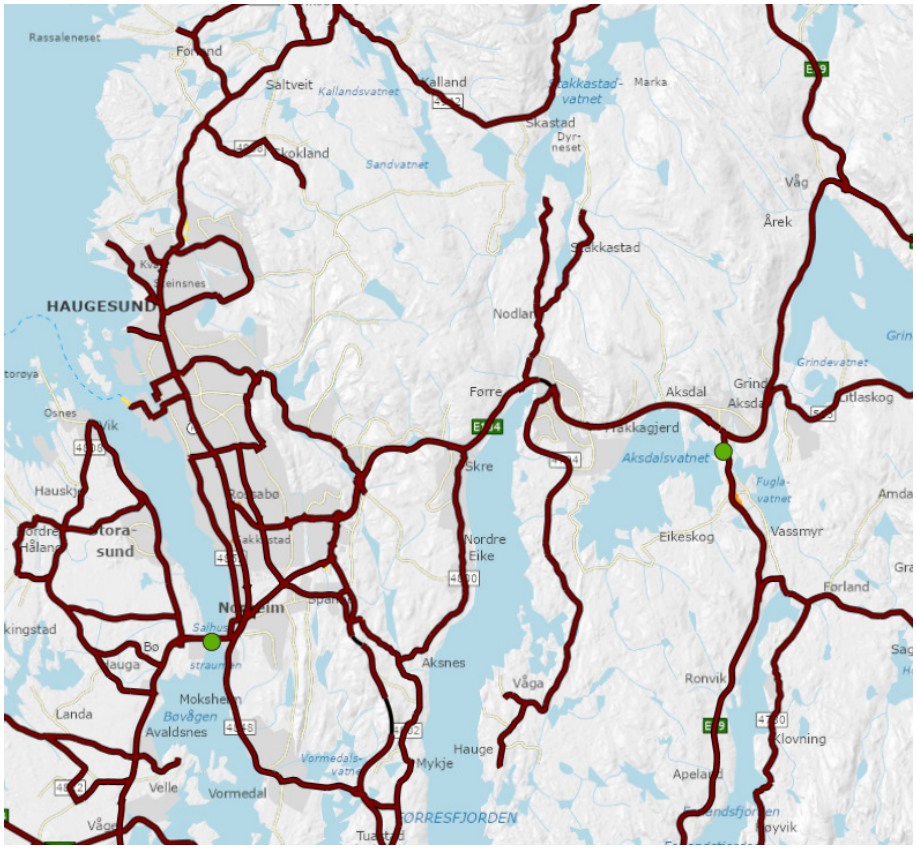

Figure 5.1: Snapshot from Vegær (RWF), green dots are observation stations, the color over the roads is the estimated temperature with red corresponding to $10°C$ *or higher, temperature ranges are divided into 7-degree intervals for values between* $-10°C$ *and* $10 \circ C$*, precise values for each section is given if click on Statens Vegvesen (2022).*

One potential solution for improving weather forecasts involves utilizing crowdsourced temperature data from vehicles. Many modern cars have internet connectivity for software updates and can easily upload data. However, establishing efficient data collection and distribution networks is essential to gather relevant information and disseminate it to the appropriate forecasting and road maintenance organizations. Collecting data can be challenging since both temperature and location data are required, which raises privacy concerns. To address this, data must be anonymized either by the car before uploading or by the receiving data center, including both car identifiers and GPS locations in low-traffic areas where routes can be inferred.

One way to improve privacy and reduce the load on collection servers is to store the model grid points in the vehicle and only upload a single value for each grid cell for a given time interval. This would ensure that the precise location of the car cannot be accurately determined and simultaneously reduce the load on network bandwidth and storage space. In addition, it is worth noting that many modern cars are equipped with GPS systems that remember the locations of the driver's home and workplace. This information can be used to filter out grid cells near those areas, further enhancing privacy and security. The GPS can also be used to determine if the car is moving in case the car does not have a digital velocity readout, which is useful for filtering out data from stationary cars to reduce the effect of heat radiating from the engine and road surface.

It is possible to use indirect measurements to gain insights into weather conditions. For instance, windscreen wiper usage and ABS and traction control data can help deduce rainfall, rain intensity, and road friction. This method allows for a more comprehensive understanding of the weather without requiring extra equipment. Road friction alerts are already in use in some cars, where the cars will upload safety-related traffic data to the cloud, sharing them with the road authorities and other nearby cars (*Volvo Cars*, 2017). Given appropriate privacy considerations these systems could likely also provide the location of the slippery sections through the car's navigation system. However, this might be unwanted as it could enable reckless driving when there are other undetected slippery sections nearby, as a car may be unable to detect the change in friction when there is no braking, acceleration, or turning.

Simply improving the RWF products is not sufficient if they remain unused. To address this issue, we must first identify the reasons why they are not being utilized. Some possible explanations include a lack of awareness about their existence, difficulty in locating or obtaining them, impracticality, or lack of forecast accuracy. However, even in areas where they are readily available, they are still not widely used, as in the example by *Nurmi et al.* (2013), as most people do not seem to alter their routes based on forecast information.

There are several steps that can be taken to remedy these problems, starting with increasing the reliability of the forecast through crowdsourced data as described earlier. Second, the forecast product needs to be available where it is most needed, in the car. If people won't actively look up the forecast it needs to be delivered to them in an unintrusive and useful way. Troublesome sections of the road should be highlighted on the car's navigation system, assuming it has one so that drivers are aware and can take appropriate precautions before approaching the area. Third, nearby road conditions should be available on the local weather apps, with options to add your daily commute, to include both your local road conditions and the conditions along your commute. Fourth, dangerous weather should be indicated in the different map apps if present along the route.

Finally, it is worth noting that the advancements in the field of deep learning show great potential in improving forecast products given large dense datasets, with ECMWF reporting a reduction in RMSE for T_{2m} by 13% for a 3-day lead time (*Kim et al.*, 2022). Deep learning in conjunction with car data has the potential to produce a better forecast by virtue of understanding temperature patterns and responses without needing the deep physical knowledge required by NWP models, with the quality of the model depending on the quality and abundance of the training material, i.e., previous observations. At the moment of writing, there is not much mention of deep learning used in conjunction with car data, but there are an increasing number of articles utilizing machine learning algorithms with car observations, such as *Yang et al.* (2019) and *Bojer* (2022), in addition to an official ECMWF machine learning roadmap for 2021-2030 (*Bauer et al.*, 2022).

6 Summary and Conclusion

The AROME-MetCoOp analysis (closest forecast for 2.5km) MEPS 2.5km model and the 1.0km post-processed product from Met-Norway (*Müller et al.*, 2017) showed promising results, with acceptable bias values for most car runs, for both routes. However, there is a clear indication of diurnal bias patterns, with warm bias around midnight and cold bias around noon (local time). Due to its consistency, this points to slow temperature response times in the model, indicating an inaccurate parametrization, likely related to the radiation, cloud microphysics, cloud cover, vegetation, or topography. The diurnal pattern is present for both models but tends to be most pronounced in the 2.5km model.

Similarly, the 2.5km model frequently has a higher mean bias than the 1.0km model, most likely due to the increased resolution in the 1.0km model grid, and the use of Netatmo weather stations for bias corrections (*Nipen et al.*, 2020).

The forecast products were less promising, with higher MBE, RMSE, and variability. Surprisingly the shorter lead times (4-5H, 10-11) performed the worst, which was interesting as the lead time was short, and thus the uncertainty should be lower. The amount of uncertainty shown by the changes in local model bias and mean model bias illustrates that the forecasts were not reliable as the temperature could vary by over $5°C$ (section: 4.2.1 & 4.2.2).

Netatmo data generally performed better than the iMet car data for both 1.0 and 2.5km models, both in terms of model bias and RMSE, which is unsurprising as parts of it are included in the observation product and used for post-processing(*Nipen et al.*, 2020). However, comparisons between the Netatmo and iMet data in both the analysis (sec: 4.1) and forecast sections (sec: 4.2) reveal that not all of the Netatmo observations are representable for the road conditions, with certain stations close to the road in the southern half of the Bergen route being particularly prone to significant differences. Still, the dense coverage of Netatmo stations in conjunction with the grid average, removed many of the largest outliers containing unrealistic temperature observations.

Adding car data to the observation network can enhance the density and provide observations from thinly populated areas. However, it calls for new quality control measures due to surface heat sensitivity in stationary vehicles (*Bell et al.*, 2022). This data is crucial for real-time road weather forecasting and sharing updates on road conditions via cloud-storage solutions between cars, benefitting both authorities and the public (*Volvo Cars*, 2017).

In conclusion, the AROME-MetCoOp model products are a decent starting point for RWF but leave something to be desired in small-scale variability, as confined small-scale differences have been found with more than $6°C$ difference between predicted and observed value for both the forecast and analysis. Netatmo observations generally correspond well with neighboring car observations but have several outliers, some of them consistent but others displaying significant variation. An expansion of the observation network is required to fully capture the small-scale variability present along roadways, improve observational products for weather forecasting, and create an accurate nowcasting product designed to seamlessly integrate into existing weather and mapping products,

even into cars. The seamless integration is essential as research shows that a significant portion of people does not check the forecast, even if readily available (*Nurmi et al.*, 2013), requiring the forecast to be integrated into services that are already in use.

Bibliography

Bauer, P., M. Buehner, A. Carrassi, C. Charette, M. Chevallier, L. Delle Monache, I. Dharssi, M. Drusch, I. Ebert-Uphoff, J. Fyfe, T. Haiden, T. M. Hamill, T. Hewson, T. Janjic, A. R. Karspeck, D. Klocke, V. Kumer, M. Leutbecher, Y. Liu, N. Lott, J.-F. Mahfouf, A. P. McNally, E. J. Mlawer, N. K. Nichols, T. J. O'Kane, T. N. Palmer, F. Pappenberger, R. W. Potthast, L. Raynaud, P. Ruggieri, I. C. Sandu, S. I. Seneviratne, and D. J. Stensrud (2022), Esa-ecmwf report on recent progress and research directions in machine learning for earth system observation and prediction, *npj Digital Earth*, *5*(1), 1–10, doi:10.1038/s41612-022-00269-z. 83

Bell, Z., S. L. Dance, and J. A. Waller (2022), Exploring the characteristics of a vehicle-based temperature dataset for kilometre-scale data assimilation, *Meteorological Applications*, *29*(3), e2058, doi:https://doi.org/10.1002/met.2058. 2, 79, 84

Bojer, C. S. (2022), Understanding machine learning-based forecasting methods: A decomposition framework and research opportunities, *International Journal of Forecasting*, *38*(4), 1555–1561, doi:https://doi.org/10.1016/j.ijforecast.2021.11.003, special Issue: M5 competition. 83

Chapman, L., and J. E. Thornes (2011), What spatial resolution do we need for a route-based road weather decision support system?, doi:10.1007/s00704-011-0433-9. 2

CNRM (2023), Surfex. iii, 12

Coney, J., B. Pickering, D. Dufton, M. Lukach, B. Brooks, and R. R. Neely III (2022), How useful are crowdsourced air temperature observations? an assessment of netatmo stations and quality control schemes over the united kingdom, *Meteorological Applications*, *29*(3), e2075, doi:https://doi.org/10.1002/met.2075. iii, 3

Crevier, L.-P., and Y. Delage (2001), Metro: A new model for road-condition forecasting in canada, *Journal of Applied Meteorology*, *40*(11), 2026 – 2037, doi:https://doi.org/10.1175/1520-0450(2001)040<2026:MANMFR>2.0.CO;2. 2

El Faouzi, N.-E., R. Billot, P. Nurmi, and B. Nowotny (2010), Effects of adverse weather on traffic and safety: state-of-the-art and a european initiative, *SIRWEC 2010: 15th International Road Weather Conference*. 1

Fisher, M. (2001), Assimilation techniques (3): 3dvar, Lecture, European Centre for Medium-Range Weather Forecasts. 12

Google Inc (n.d.a), Naf øvingsbane sotra, https://earth.google.com/web/@60.36918208,4.99076808,42.75366543a,492.27227767d,35y,0h,0t,0r, accessed: May 2, 2023. iii, 6

Google Inc (n.d.b), Haugesund-haukås-aksdal test route, https://www.google.com/maps/@59.4631134,5.4259855,24669m/data=!3m1!1e3, accessed: May 2, 2023. iii, 9, 10

Google Inc (n.d.c), Bergen-os test route, https://www.google.com/maps/@60.2969295,5.3488758,19654m/data=!3m1!1e3, accessed: May 2, 2023. iii, 10

Hintz, K. S., K. O'Boyle, S. L. Dance, S. Al-Ali, I. Ansper, D. Blaauboer, M. Clark, A. Cress, M. Dahoui, R. Darcy, J. Hyrkkanen, L. Isaksen, E. Kaas, U. S. Korsholm, M. Lavanant, G. Le Bloa, E. Mallet, C. McNicholas, J. Onvlee-Hooimeijer, B. Sass, V. Siirand, H. Vedel, J. A. Waller, and X. Yang (2019), Collecting and utilising crowdsourced data for numerical weather prediction: Propositions from the meeting held in copenhagen, 4–5 december 2018, *Atmospheric Science Letters*, *20*(7), e921, doi: https://doi.org/10.1002/asl.921. 2

InterMet International Met Systems (2021), imet-xq2 uav sensor, https://www.intermetsystems.com/products/imet-xq2-uav-sensor/, accessed: May 2, 2023. 4

Kangas, M., M. Heikinheimo, and M. Hippi (2015), RoadSurf: a modelling system for predicting road weather and road surface conditions, *Royal Meteorological Society*, *22*(3), 544–553, doi:10.1002/met.1486. iii, 1, 2

Karsisto, V., and L. Lovén (2019), Verification of road surface temperature forecasts assimilating data from mobile sensors, *Weather and Forecasting*, *34*(3), 539–558, doi: 10.1175/WAF-D-18-0167.1. 1

Karsisto, V., S. Tijm, and P. Nurmi (2017), Comparing the Performance of Two Road Weather Models in the Netherlands, *Weather and forecasting*, *32*(3), 991–1006, doi: 10.1175/WAF-D-16-0158.1. 1, 2

Kim, J., M. Kim, S. Kim, S. Kim, Y. Kim, D. Lee, J. Lee, J. Lee, S. Lee, S. Lee, et al. (2022), Ecmwf short-term prediction accuracy improvement by deep learning, *Scientific Reports*, *12*(1), 1–11. 83

Liberto, T. D. (2023), Disrupted polar vortex brings sudden stratospheric warming in february 2023, https://www.climate.gov/news-features/event-tracker/disrupted-polar-vortex-brings-sudden-stratospheric-warming-february. 38

Meteorologisk Institutt (2018), Private værstasjoner gir bedre temperaturvarsler på yr, https://www.met.no/nyhetsarkiv/private-vaerstasjoner-gir-bedre-temperaturvarsler-pa-yr, web Article. 24

Meteorologisk institutt (2021), Verification of operational weather prediction models march 2021 - may 2021, PDF. 12

Meteorologisk Institutt (n.d.), Metcoop, Norwegian Meteorological Institute, accessed: 2023-05-26. 11

Müller, M., M. Homleid, K. I. Ivarsson, M. A. Køltzow, M. Lindskog, K. H. Midtbø, U. Andrae, T. Aspelien, L. Berggren, D. Bjørge, P. Dahlgren, J. Kristiansen, R. Randriamampianina, M. Ridal, and O. Vignes (2017), AROME-MetCoOp: A nordic convective-scale operational weather prediction model, *Weather and Forecasting*, *32*(2), 609–627, doi:10.1175/WAF-D-16-0099.1. iii, 2, 3, 11, 12, 79, 84

Netatmo (), Smart weather station, https://www.netatmo.com/no-no/smart-weather-station, accessed on June 1, 2023. 3, 11

Nipen, T. N., I. A. Seierstad, C. Lussana, J. Kristiansen, and Øystein Hov (2020), Adopting citizen observations in operational weather prediction, *Bulletin of the American Meteorological Society*, *101*(1), E43 – E57, doi:https://doi.org/10.1175/BAMS-D-18-0237.1. 2, 11, 12, 84

Norwegian Meteorological Institute (n.d.), Met-Norway THREDDS Server, https://thredds.met.no/thredds/metno.html, accessed: May 3, 2023. 13

Nurmi, P., A. Perrels, and V. Nurmi (2013), Expected impacts and value of improvements in weather forecasting on the road transport sector, *Meteorological Applications*, *Volume 20*, pp.217–223, doi:10.1002/met.1399. 1, 2, 83, 85

Nypen, T. (2023), Surfex not used in meps 1.0km post-processed product, personal correspondence. 12, 80

Statens Vegvesen (2022), Vegvær, accessed: 31.05.2023. viii, 81, 82

UiB (2016), ITAS GFI Manual 20160518. 4

Volvo Cars (2017), Volvo cars ceo urges governments and car industry to share safety-related traffic data, *Volvo Cars Global Newsroom*. 83, 84

Yang, C. H., D. G. Yun, J. G. Kim, G. Lee, and S. B. Kim (2019), Machine Learning Approaches to Estimate Road Surface Temperature Variation along Road Section in Real-Time for Winter Operation, *International Journal of Intelligent Transportation Systems Research*, *18*(2), 343–355, doi:10.1007/s13177-019-00203-3. 83